



Anne-Catherin Zappe

---

Design and Analysis of  
fMRI Experiments  
Probing  
Brain Activity  
Induced by Event-Related  
Tactile Stimulation

Diplomarbeit

HD-KIP-03-01



# **Faculty of Physics and Astronomy**

University of Heidelberg

Diploma thesis

in Physics

submitted by

**Anne-Catherin Zappe**

born in Heidelberg

**January 2003**



**Design and Analysis of  
fMRI Experiments  
Probing  
Brain Activity  
Induced by Event-Related  
Tactile Stimulation**

**This diploma thesis has been carried out by *Anne-Catherin Zappe* at the**

**KIRCHHOFF-INSTITUTE OF PHYSICS**

**UNIVERSITY OF HEIDELBERG**

**under the supervision of**

**Prof. Dr. Karlheinz Meier**



## **Abstract**

This thesis presents the design and analysis of functional magnetic resonance imaging (fMRI) experiments on the processing of event-related stimulations in the human brain. For this purpose the relevant principles of neurology and fMRI are introduced. A pneumatically driven tactile display designed and built within the lab, is used to realize tactile stimulations. In order to compare the results with visual stimulation experiments an fMRI suited goggles system has been constructed. The different preprocessing steps could be simplified and thereby the evaluation time significantly reduced by the introduction of a Matlab based script.

The study includes six healthy subjects and has been analyzed with *SPM*, a statistical parametric mapping tool. The first experiment is optimized to model the individual hemodynamic response on visual and tactile stimuli. The second experiment probes for dependencies on the frequency of vibratory tactile stimulations. The activation due to vibratory tactile stimuli of the abdomen is localized in the primary and secondary somatosensory cortex whilst in the secondary cortex a larger area is activated than in the primary cortex. No conclusions on a frequency dependence are found within the examined domain. It is shown that the statistical power of the data is too low to determine variabilities of the hemodynamic response by fitting. Fourier analyzing an average of a significant cortical region does not yield differences in the hemodynamic response, but it proves to be suited to detect a hemodynamic activation.

## **Inhalt**

Diese Arbeit beinhaltet Design und Analyse von funktionellen Magnetresonanztomographie Experimenten zur Erforschung der Verarbeitung kurzer taktile Reize im menschlichen Gehirn. Die dazu notwendigen Grundlagen der Neurologie, sowie der fMRI werden erarbeitet. Zur taktilen Stimulation wird ein im Haus entworfenes und gefertigtes pneumatisches Anzeigegerät verwendet. Für Vergleichsuntersuchungen mit visueller Stimulation ist ein fMRI geeignetes Brillensystem entwickelt worden. Die einzelnen Analyse Schritte wurden durch die Zusammenfassung in ein Matlab Skript vereinfacht wodurch die Verarbeitungsgeschwindigkeit wesentlich erhöht werden konnte.

Die Studie beinhaltet Ergebnisse von sechs Probanden, die durch eine statistische Analyse (*SPM*) ausgewertet wurden. Das erste Experiment ist optimiert die individuelle Antwortfunktion des Gehirns auf visuelle und taktile Reize zu modellieren. Im zweiten Experiment wird die Abhängigkeit von der Frequenz taktile Reize untersucht. Die Analyse zeigt, daß eine taktile Reizung der Bauchoberfläche sowohl im primären, als auch im sekundären somatosensorischen Kortex repräsentiert ist, wobei die Aktivität im sekundären Kortex eine größere Fläche einnimmt. Es konnten keine Rückschlüsse auf eine Abhängigkeit der Gehirnaktivität auf dem untersuchten Frequenzbereich gefunden werden. Es wird gezeigt, daß die Signifikanz der Daten nicht ausreicht, um Veränderungen der individuellen Blut-Antwort Funktion mit der Methode der Kurvenanpassung zu bestimmen. Eine Fourier Analyse, gemittelt über einen kortikalen Bereich, konnte keine Unterschiede der Blut-Antwort Funktion erkennen, die Methode erweist sich als geeignet zur Aktivitätserkennung.



# Contents

<b>Introduction</b>	<b>1</b>
<b>1 The Somatosensory and Visual System</b>	<b>3</b>
1.1 The Mechanoreceptors for Tactile Perception . . . . .	3
1.2 The Somatosensory Pathways . . . . .	4
1.3 The Visual Pathways . . . . .	4
1.4 The Organization of the Human Brain . . . . .	5
1.4.1 Functional Anatomy in the Cerebral Cortex . . . . .	5
1.4.2 Details on the Somatosensory Cortex . . . . .	6
1.4.3 The Organization of the Visual System . . . . .	8
<b>2 Basics of functional Magnetic Resonance Imaging</b>	<b>10</b>
2.1 Principles of Magnetic Resonance Imaging . . . . .	11
2.2 Properties of the Signal . . . . .	11
2.2.1 Spatial Decoding . . . . .	12
2.2.2 Echo-Planar Imaging . . . . .	13
2.2.3 Signal-Variations and Noise . . . . .	13
2.2.4 Artifacts . . . . .	14
2.3 The Hemodynamic Response . . . . .	15
<b>3 Analyzing Methods</b>	<b>17</b>
3.1 Preprocessing . . . . .	17
3.1.1 Realignment . . . . .	18
3.1.2 Normalization . . . . .	18
3.1.3 Smoothing . . . . .	19
3.2 Statistical Analysis . . . . .	19
3.2.1 The Principles of <i>SPM</i> . . . . .	20
3.2.2 The Design Matrix . . . . .	20
3.2.3 Estimation . . . . .	20
3.2.4 Contrasting and the Students t-Test . . . . .	21
3.2.5 Thresholding . . . . .	22
<b>4 Devices and Developments for the fMRI Environment</b>	<b>23</b>
4.1 The Pneumatically Driven Tactile Display (PTD) . . . . .	23
4.1.1 Description of the System . . . . .	23
4.1.2 The Way from Pattern to Perception . . . . .	24

4.1.3	Specifications of the PTD . . . . .	24
4.2	Visual Stimulation Device . . . . .	25
4.2.1	Construction of a New Visual Stimulation Device . . . . .	26
4.3	Software . . . . .	27
4.3.1	Preprocessing with <i>SPM</i> . . . . .	27
4.3.2	The Script <i>Quickshot</i> . . . . .	28
<b>5</b>	<b>Experiments</b>	<b>31</b>
5.1	The fMRI-System in Strassbourg . . . . .	32
5.2	Experimental Setup . . . . .	32
5.3	The Design of the Experiments . . . . .	33
5.3.1	Event-related Stimulation . . . . .	33
5.3.2	Paradigm Design . . . . .	34
5.3.3	Experimental Procedures . . . . .	36
5.4	<i>SPM</i> Analysis . . . . .	36
5.4.1	Design Matrix for the Session: Modelling the <i>hrf</i> . . . . .	36
5.4.2	Design Matrix for the <i>Parametric</i> Session . . . . .	37
5.4.3	Contrasting . . . . .	37
<b>6</b>	<b>Results</b>	<b>39</b>
6.1	Localization of the Observed Activity . . . . .	39
6.1.1	Experiments in Literature . . . . .	39
6.1.2	Mapping the Activation on MNI Template . . . . .	39
6.1.3	Localization of the Activation . . . . .	46
6.1.4	Summary of the Activation Localization . . . . .	48
6.2	Dependencies on the Stimulation Frequency . . . . .	50
6.3	Modelling the Hemodynamic Response . . . . .	53
6.3.1	Procedures before Fitting . . . . .	53
6.3.2	The Fitting Function . . . . .	56
6.3.3	The Fitting Routine . . . . .	57
6.3.4	Results of the Fitting . . . . .	58
6.3.5	Characterization of the Fourier Spectrum . . . . .	60
6.3.6	The Fourier Coefficients . . . . .	60
6.3.7	Fault Assessment . . . . .	63
6.3.8	Summary of the Hemodynamic Model . . . . .	64
	<b>Discussion and Outlook</b>	<b>65</b>
<b>A</b>	<b>Glossary</b>	<b>67</b>
<b>B</b>	<b>Atlas for the Human Brain</b>	<b>69</b>
B.1	Brodman's Areas . . . . .	69
B.2	Directions and Planes . . . . .	70
B.3	Locations in the Human Brain . . . . .	71

<b>C</b>	<b>Ways of Presenting fMRI Data</b>	<b>72</b>
C.1	The Coordinate System of Talaraich and Tournaux . . . . .	72
C.2	The MNI Brain . . . . .	72
C.3	Orientation of the Data . . . . .	73
C.4	Results Presented with <i>SPM</i> . . . . .	74
C.5	Brain Maps of Tactile Activation . . . . .	75
<b>D</b>	<b>Technical Drawings</b>	<b>78</b>
D.1	Technical Drawing of the Prisms . . . . .	78
D.2	Circuit Diagram of Helper Electronics Added to the TIOTU . . . . .	79
D.3	Circuit Diagram for the TIOTU . . . . .	80
<b>E</b>	<b>Manual for <i>Quickshot</i></b>	<b>81</b>
	<b>List of Figures</b>	<b>86</b>
	<b>List of Abbreviations</b>	<b>88</b>
	<b>Bibliography</b>	<b>91</b>



# Introduction

The Electronic Vision(s) Group at the Kirchoff Institute for Physics developed and constructed in 1996 a new **Tactile Vision Substitution System**. The TVSS can process information from a high dynamic range CMOS<sup>1</sup> image sensor onto a **Virtual Tactile Display** [MMS00] with which a blind person can perceive images with its fingertips. The conducted experiments with the VTD concentrated on the presentation of simple 2-dimensional geometries of variable shapes and sizes to blind and blindfolded probands [MMS01]. The analysis of the results require a deeper understanding of the processing of tactile information during image exploration. In order to further examine this area with the help of brain imaging techniques a collaboration with other faculties in the frame of a European Union project called *SenSub* was initiated. Since the year 2000 physicians, psychologists, biologists, physicists and technicians from Strassbourg, Brussel and Heidelberg have been working together under the topic *Brain Plasticity and Sensory Substitution in Human Blindness*. To investigate this the following tasks were set up:

- To develop and optimize artificial sensory substitutions for the transfer of visual information into sensory or auditive information.
- To study the cortical and cognitive plasticity when tactile or auditive inputs are provided in the case of sensory deprivation (blindness).
- To analyze the brain responses induced by visual-like effects of auditory and tactile sensory substitution perceptions using brain imaging techniques.
- To study the relative virtues of a cross-check between **functional Magnetic Resonance Imaging** and **Positron Emission Tomography**.

Two devices were built and optimized for the realization of the project. The group around Claude Veraart in Brussels works mainly with PET and developed a **Prothesis for Substitution of Vision by Audition** [CTAV98]. The PSVA is based on a digital signal processor which is connected to a miniature head-mounted video camera and head phones. Each pixel of a captured image is assigned a sinusoidal tone with the frequency coding the location of the pixel in the camera's field of view. The image processing performs edge detection and achieves graded resolution. In practice a trained blind proband is given the chance to achieve visual-like information through audition and thus gain imaginations just like a sighted person does.

Parallel to this, the Electronic Vision(s) Group in Heidelberg developed a pneumatically driven display (PTD) which can be used for tactile stimulation in the fMRI environment as well as in a psychologists' lab for training purposes (see section 4.1 for detailed description). Meanwhile

---

<sup>1</sup>Complementary **Metal Oxide Semiconductor**

psychologists and biologists designed reasonable experiments to start investigations on the brain plasticity in human blindness.

The major questions asked in the context of *SenSub* aim at the understanding of the kind of perception generated by the sensory substitution devices. One hopes to find the modality which is activated in the brain of blind and blindfolded people and map possible differences in their signal processing. And possibly, there is even a new kind of perception or unexpected signal processing stimulated in the brain. The partners of *SenSub* expect in any case a deeper understanding of the processing of tactile perception.

This thesis emerged from the necessity to evaluate numerous fMRI experiments involving tactile stimulation within the *SenSub* project. Before using the fMRI data for a cross-check with PET, reference measurements have to be done with the additional goal to improve the method itself. The mapping of brain activity induced by complex tactile stimulation in previous fMRI-experiments has shown a low **S**ignal to **N**oise **R**atio.

This thesis concentrates on optimizing experimental paradigms and evaluation in order to improve and better understand tactile activation patterns. To be able to comprehend the signal processing in the brain a brief introduction into the somatosensory and visual system is given. Furthermore, the fundamentals of fMRI as the tool for data acquisition and *SPM* as the software for data analysis are acquired and introduced. The description of the fundamentals, which this work are based on, are completed with the specifications of the PTD. The following developments and results have been achieved by the author within the frame of this thesis.

To perform comparable measurements involving two different stimulation modalities a visual stimulation device that is well-suited for the fMRI environment was constructed. It is remarkably small and easy to handle. Software development emerged from the need to get a faster and work-flow optimized evaluation tool. For saving calculation time the various preprocessing steps have been combined within one Matlab script which furthermore improves the evaluation features.

One major challenge was to design two experiments which allow:

- (i) the characterizing of the hemodynamic response and
- (ii) to search for dependencies of the somatosensory system on tactile stimulation frequencies.

Both experiments involve event-related tactile and visual stimulation. The measurements have been analyzed and the activation in the brain is detailed examined. The position of the activation in the cortex was mapped with *SPM*. The statistical software is as well utilized to determine a frequency dependence of the neuronal response in the brain. For the investigation of the shape of the hemodynamic response two approaches have been traced with Mathematica. The first approach attempts to fit the fMRI signal, thereafter the Fourier spectrum of the data has been analyzed.

This work includes many biomedical expressions from neuroscience which are highlighted and explained in the glossary.

# Chapter 1

## The Somatosensory and Visual System

### 1.1 The Mechanoreceptors for Tactile Perception

Several different receptors in our skin are responsible for the sensation of touch. The non-hairy human skin contains three types of mechanoreceptors: slowly (SA), rapidly (RA) and very rapidly (PC) adapting. Slowly adapting receptors are *Merkel's* receptors in superficial skin and *Ruffini's* corpuscles in subcutaneous tissue. They respond to persistent stimuli as e. g. continuous pressure at the sole of the foot. They code the intensity of pressure through their discharge frequency. *Pacinian* corpuscles from the group of very rapidly adapting receptors (PC) only respond to changing stimuli. *Meissner's* corpuscles (RA sensors) are continuously active during short stimuli. Furthermore they code velocities in their discharge frequency (for a more detailed description [ST87]).

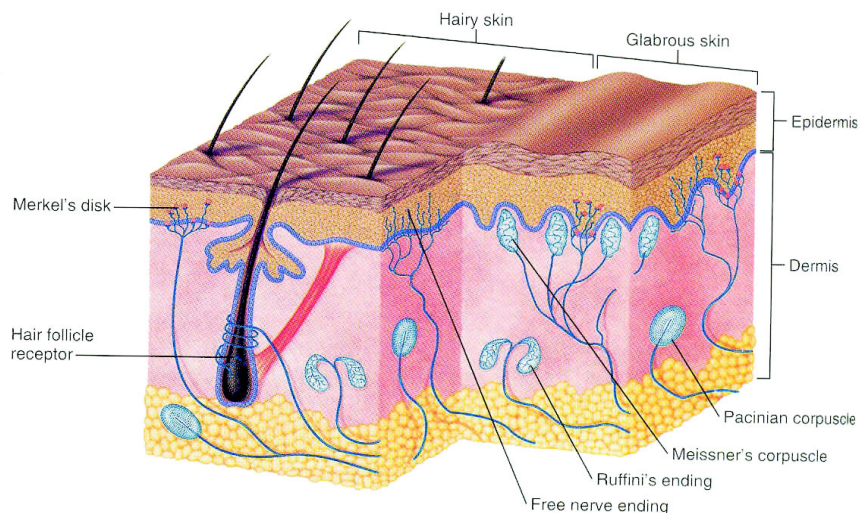


**Figure 1.1:** Histological section through the human's glabrous and hairy skin [GS02].

## 1.2 The Somatosensory Pathways

The processing of these peripheral signals includes three domains: afferent (uprising), integrative (processing) and efferent (down-leading). The afferent part contains the spinal cord, brain stem, thalamus and the somatosensory cortex (see figure 1.2). Starting at a peripheral sensory receptor the information is passed on to the spinal cord and transmitted through the brain stem. Sensory information that enters the spinal cord from the left side of the body crosses over to the right side of the central nervous system. The activity is projected to the cortex through the thalamus. The thalamus is considered to be the last relay station for all afferent information to the cortex. This gives a structural order of the peripheral signals in the central nervous system. The local order in the cortex is called somatotopy (see section 1.9).

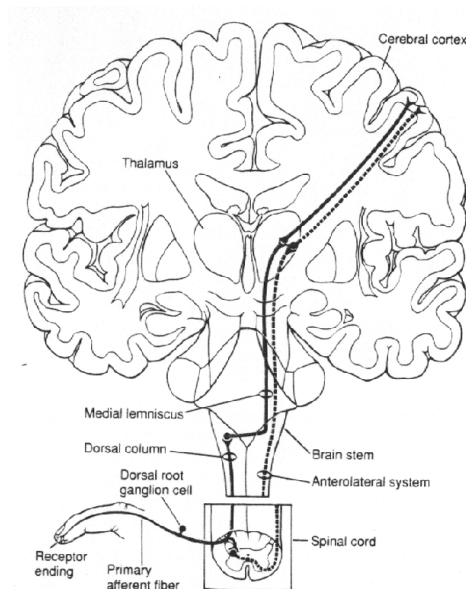


**Figure 1.2:** Illustration of the afferent system [Kan91].

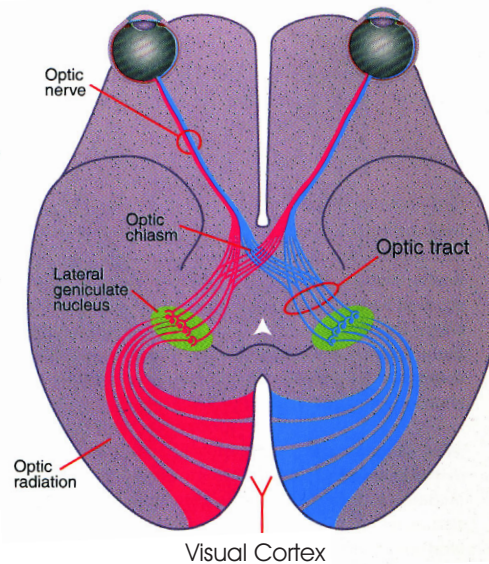


**Figure 1.3:** The optical pathways from visual world onto the visual cortex [ZBR<sup>+</sup>99].

## 1.3 The Visual Pathways

The signals leave the eyes by two nerve cords, the so-called optic nerves which are crossed at the optic chiasm (see figure 1.3) in the thalamus. Behind the chiasm the axons are called the optic tract. The optic tract wraps around the midbrain ending in the **Lateral Geniculate Nucleus**, where all the axons must synapse. The LGN axons which fan out towards the visual cortex are called the optic radiations. The optic radiations lead through the deep white matter of the brain.

The visual pathways are rather complex since the paths differ for the two hemifields of each eye. The visual information is obtained from the left and right eye simultaneously whereby some of the field of view overlaps. The image is projected onto the retina with the left part of the field of view mapped on the right half of the retina (the fovea defines the center) as shown in figure 1.4.

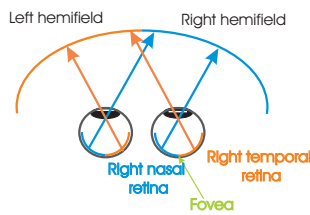


**Figure 1.4:** The projection of the visual world onto the retina of the eye [Mol97].

From here the information is relayed to the thalamus, where the information from the retina is distributed to the primary visual cortex. The nasal retina of the right hemifield is crossed with the nasal retina of the left hemifield in the optical chiasm (see figure 1.3). The temporal retinas do not cross since they are already positioned to see the contralateral side of the world.

This sophisticated system has practical consequences: Damage of the visual system before the chiasm affecting one eye will erase parts of both hemifields - analogous to closing one eye. On the contrary, damaging the pathway after the chiasm will alter the perception of both eyes but only one hemifield.

## 1.4 The Organization of the Human Brain

First insights into the functional organization of the brain were derived in the late 19th century. Progresses came from work involving electrical currents in the stimulation of the cortices of animals and later on humans. In the beginning of the 20th century Brodman pushed anatomical studies by microscopy to map the entire human cortex. He headed a school where a new method called cytoarchitectonic was introduced. By comparing the cellular and functional structure in the cortex Brodman described 52 areas, the Brodman areas (for the entire map see appendix B.1).

Simultaneously, the observation of patients with neurological disorders was carried out. A systematical loss of a defined psychological function was observed for subjects with lesions. This helped Kleist to create a map with localized brain areas naming their functions [ST87]. This confirms the concept of localization in the functional organization of the brain. The localization theory claims that every mental function, including emotion, is carried out by a single, precisely localized and specialized area of the brain. The results, however, contained many inconsistencies. Thus, the *aggregate field view* existed for a long time as a second opposing concept. Supporters believe that all parts of the brain especially the cerebral hemispheres participate in all mental functions.

In 1876 C. Wernicke introduced the idea of *distributed processing* [Kan91] that still dominates the present concept of brain functionality. He suggested that the most basic mental functions are localized in single cortical areas. Interconnection between functional domains make the progressing of more complex intellectual functions such as language or emotions possible. The current theory on brain functionality is a more elaborate version of Wernicke's *distributed processing*.

There are two fundamental principles: *functional integration* and *functional segregation*. Functional segregation implies the specialization of a cortical area for an aspects of perceptual or motor processing. This area is anatomically segregated in the cerebral cortex. In the means of integration the brain is treated as one unit. The opposite was proved by P. Broca, who discovered an area responsible for speech [ST87].

### 1.4.1 Functional Anatomy in the Cerebral Cortex

There are two main grooves (sulci or fissures) in the brain, located on the lateral surface. These are the lateral and the central sulcus (see figure B.5). They subdivide the cortex into four lobes: the frontal, the parietal, the temporal and the occipital lobes as illustrated in figure 1.5.

The different lobes are specialized for remarkably distinct functions. The frontal lobe extends from the central sulcus to the anterior limit of brain. It contains the motor cortex and prefrontal

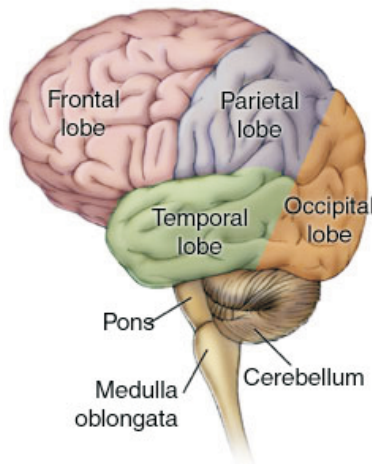


**Figure 1.5:** The division of the cerebral cortex into four lobes [Fou02].

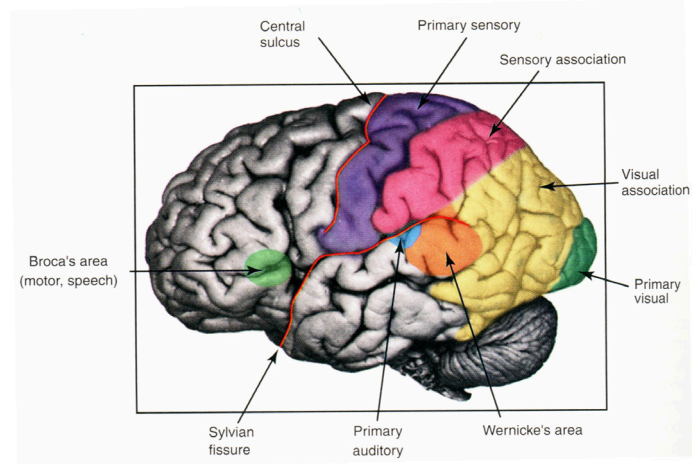


**Figure 1.6:** Illustration of the sensory primary areas in the cortex [ZBR<sup>+</sup>99].

cortex. The posterior part is called the precentral gyrus and is responsible for the control of fine movements.

The parietal lobe lies between the occipital lobe and central sulcus, one of the deepest grooves in the surface of the cortex. This region processes information on the position of the body (proprioception) including sensory perception. Posterior to the central sulcus the postcentral gyrus containing the primary somatosensory area (see figure 1.6) is located where the skin sense is processed.

The temporal lobe is located laterally in each hemisphere near the temples and is involved in more complex aspects of vision (perception of complex patterns such as faces).

In the posterior end of the cortex the occipital lobe is located. It is the main target for axons from thalamic nuclei that receive inputs from the visual pathways and contains the primary visual cortex (see figure 1.6). Elevated convolutions in the cortex are called gyri e. g. the postcentral gyrus between central sulcus and the postcentral sulcus.

### 1.4.2 Details on the Somatosensory Cortex

The somatosensory system can be divided into three cortical areas. The *primary somatosensory cortex (SI)* which receives direct projections from the thalamus. It then projects to the *secondary somatosensory cortex (SII)* and the *somatosensory association area*. The SI is located in the posterior bank of the central sulcus and on the crown of the postcentral gyrus (see figure 1.7). The SII is located in the superior bank and the depth of the lateral sulcus (parietal operculum) and on the most inferior aspect of the postcentral gyrus. It is hidden from a top view of the brain. The somatosensory association area can be found in the superior parietal lobe and extends further into the posterior part of the parietal cortex.

These areas are closely connected by their adjacent locations and their dense innervation. Some tasks are distributed between the areas and some are processed in close collaboration.

The primary somatosensory cortex is the most important part for sensory perception. Ablation of SI will result in the loss of all modalities of sensation in the immediate postoperative period. Pain

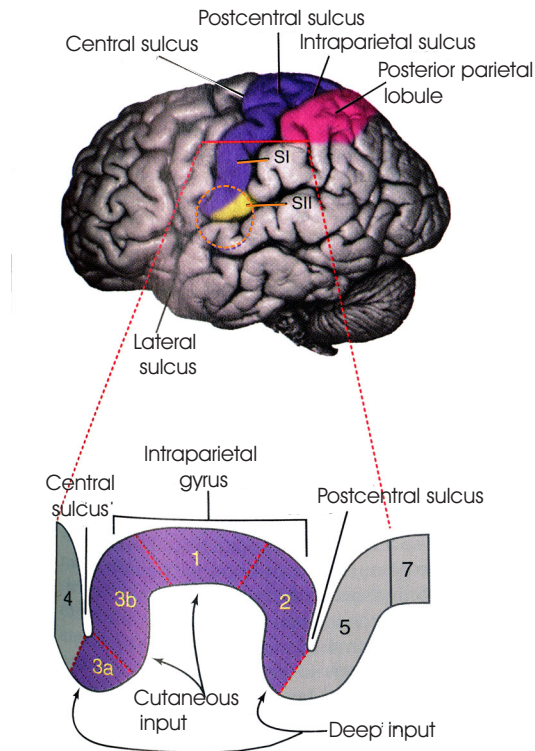


**Figure 1.7:** Functional organization of the somatosensory cortex with Brodman area 1-5 and 7 enlarged [ZBR<sup>+</sup>99].

and temperature sensation will return in form of a crude awareness, but discriminative touch and proprioception are lost forever. Removal of SII will cause severe impairment in the discrimination of both shape and texture. The secondary somatosensory cortex is also important for the conscious perception of noxious stimuli. In addition, there is some evidence that vibrational stimulation is primarily processed in SII [JM99]. The somatosensory association area is concerned with higher order processing.

### The Functional Structure

Modern studies have give raise to the assumption that SI can be divided into four physiological as well as anatomically distinct areas.

The postcentral sulcus corresponds to *Brodman areas* 1, 2 and 3. Area 3 is further divided into two parts: 3b on the posterior wall of the central sulcus and 3a in the depth of the central sulcus (see figure 1.7). Regions with different cytoarchitecture within the primary somatosensory cortex subserve different functions where interactions in the processing can occur.

*Brodman areas* 2 and 3a receive information from receptors located in deep structures, such as muscles and joints. Area 2 integrates positional information concerning edge detection and an object's 3-dimensional shape. Information from mechanoreceptors is transmitted to area 1 and 3b.

Area 1 is responsible for the processing of texture information from SA and RA receptors whilst 3b is a conduit for all cutaneous sensibility.

In each of these areas a separate representation of the body can be found (details in section 1.4.2). The representation in 1 and 3b is complete and highly detailed while it is more coarse in areas 2 and 3a. Concerning tactile stimulation areas 1 and 3b as well as areas 5 and 7 (posterior parietal cortex) are relevant.

### Somatotopy in the Somatosensory Cortex

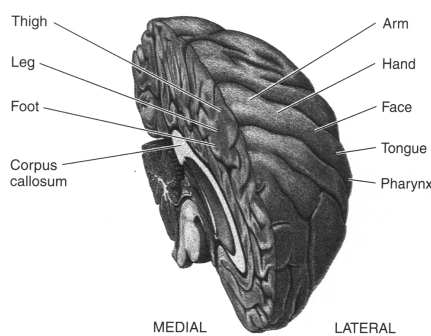


**Figure 1.8:** Medial slice through the human brain.

The signals from peripheral receptors are projected in such a way into the somatosensory cortex that a structural order is maintained. This phenomenon is called *somatotopic organization*, the body which is mapped on the cortex is referred to as the *Somatosensory Homunculus*.

Most striking in the somatotopic organization is the size of the area that is responsible for the different parts of the human body. The projection is more or less in a proper order, i. e. head  $\rightarrow$  arm  $\rightarrow$  leg. But the representations of the various body parts is not proportional to their size. They are instead related to their importance for the discriminative tactile tasks. The fingers cover a large area while the legs' portion is much smaller (see figure 1.9).

This distortion reflects differences in innervation density in different areas of the body. Especially, the face's representation with the tongue separately expanded covers a relatively large area of the lateral central sulcus. The secondary somatosensory cortex exhibits a similar somatotopic organization which is not as precise as that in the primary somatosensory cortex. Furthermore, it is often bilateral while the somatosensory homunculus of SI is mapped to the contralateral side of the body (except for the face representation which is also bilateral).

According to [Mar96] the *Somatosensory Homunculus* should neither be identical for everybody nor necessarily static during lifetime. Instead it is expected to adapt to the intensity of usage. If for example one body part is prevented from integration in tactile discrimination its cortical representation will diminish. The representation in the cortex is most likely to expand if one part is used extensively during a certain period of time. A blind person who accomplished reading Braille code is expected to exhibit a large representation of the index and middle finger.

### 1.4.3 The Organization of the Visual System

In early studies the visual cortex was identified as the three *Brodman areas* 17, 18 and 19, which are located in the occipital lobe see figure B.1. Area 17 is assigned to the primary cortex (V1) while area 18 and 19 serve as association areas (V2, V3 and V4). During the last decades 30 subdivision have been added due to their physiology, cytoarchitecture and connection with other areas. They are located in large regions of the temporal and parietal lobe. Each of these visual areas is thought to make unique contributions to the visual perception.

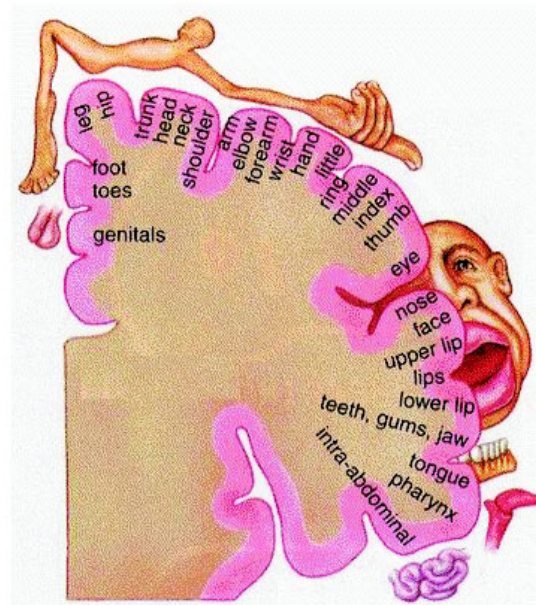


**Figure 1.9:** Functional organization of the somatosensory cortex [Mar96].

Hubel and Wiesel observed that cells responding to physiological response property were organized in an orderly fashion across the cortical surface [ZBR<sup>+</sup>99]. They found that cells in the visual cortex receive the input from the retina in a structural way. This was termed the *functional architecture* of the visual cortex.

The proposal that the neurons of the cortex are organized as vertical columns was confirmed by their observations of the line detection in an anaesthetized cat [LHW75]. In addition to this the progressing of orientation varies between neighbored columns mainly in a smooth way. This property was named ocular dominance, which so far has been confirmed by anatomical and physiological evidences [GNM02].

It has been demonstrated that for the projection from the retina to the visual cortex a structural order is maintained [TM41]. Receptive fields that are located nearby in the retina transmit their signal to roughly the same cortical column. Thus, nearby columns represent the visual space in an orderly and arranged manner. Regions of the brain (such as V1 or the LGN) that maintain the relations between adjacent retinal regions are said to have a retinotopic map.

## Chapter 2

# Basics of functional Magnetic Resonance Imaging

In 1980 Roy and Sherrington suggested that neural activity was accompanied by the increase of the cerebral blood flow. Until 1990 there was no non-invasive measuring method of the blood flow in cortical regions. Ogawa and Lee at Bell laboratories discovered that the oxygenation level of the haemoglobin acts as a contrast agent in *Magnetic Resonance Imaging*. They demonstrated that signals received from vessels were altered by drug-induced changes in blood flow from the brain [Sho]. Combined with the growing computational power this created a new technique: functional *Magnetic Resonance Imaging*. When interpreting fMRI results there are two facts to keep in mind: (i) images are only reconstructed and calculated signals, no direct ‘photographs’. (ii) they do not resemble the neural activity but illustrate local changes in the blood oxygenation level or other effects on hemodynamic level as discussed in section 2.3.

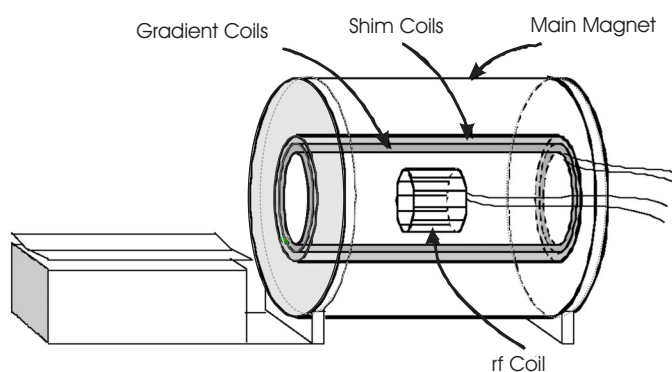


**Figure 2.1:** Schematic drawing of the fMRI system. The essential components include the magnet producing the magnetic field, shim coil, a set of gradient coils, r.f. coil, amplifiers and computer systems (not shown) for control of the scanner and data acquisition [BBD00].

## 2.1 Principles of Magnetic Resonance Imaging

The nucleus must have a non-zero spin quantum number to exhibit the properties of magnetic resonance. As far as medical applications are concerned, the proton ( $^1\text{H}$ ) is the nucleus of interest. In the MRI the nucleus is exposed to a strong magnetic field ( $B_0$ ) of 1.5 to 3 Tesla. The proton spin of  $\frac{1}{2}$  can occupy two energy levels due to the Zeemann interaction. The two energy levels can be interpreted as parallel ( $N^+$ ) or antiparallel ( $N^-$ ) alignment of the nucleus to the external magnetic field. The occupation of these states reaches a thermal equilibrium through perturbations, which is described by the Boltzmann distribution

$$\frac{N^-}{N^+} = e^{-\frac{\Delta E}{kT}}. \quad (2.1)$$

Where  $\Delta E$  is the Energy difference of the two states. Incidentally, the parallel orientation is inhibited due to the higher energy level, what causes a net magnetization of amplitude  $M_0$ .

A second, time-varying magnetic field which lies in the plane transverse to  $B_0$  is applied in form of a radio-frequency pulse by an r.f. coil. Transitions between the states are induced by photons of the Larmor-frequency:  $\omega = \gamma B$  (where  $\gamma$  is the gyromagnetic ratio). The duration and strength of the emitted r.f. pulse determines the angular orientation of  $M_0$  versus  $B_0$ . For a rotation from the z-axis into the xy plane the r.f. pulse is called '90°-pulse'. After the emission of a 90° pulse, the nuclei precess at a transient phase coherence towards the static magnetization  $B_0$ . Thus, a current is induced in the r.f. coil, which is responsible both for sending and detecting radio frequency pulses.

## 2.2 Properties of the Signal

Two fundamental temporal parameters are used to describe the MR signal. The longitudinal relaxation time,  $T_1$ , is the time at which the nuclei, once placed in a magnetic field, exponentially approaches thermal equilibrium, so that the magnetization ( $M$ ) is described by the formula:

$$M_Z(t) = M_0(1 - e^{-\frac{t}{T_1}}), \quad (2.2)$$

where  $M_0$  is the equilibrium magnetization.

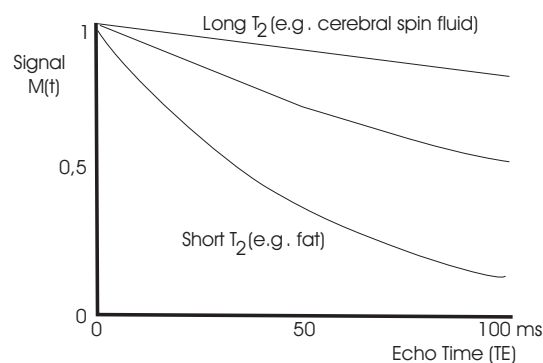


**Figure 2.2:** The spontaneous decay of a signal from the transversal magnetization is characterized by  $T_2$ .

In biological tissues,  $T_1$  for the proton is quite long: from tens of milliseconds to seconds. Differences in the  $T_1$  of tissues are one of the primary bases of contrast in clinical MRI. A second time constant ( $T_2$ ) describes the decay of the MR signal. Small variations in the local magnetic field, for example those induced by neighboring magnetic nuclei, cause the protons to precess at slightly different rates and therefore to get out of phase with one another. Interactions among the magnetized protons, and motion in inhomogeneous fields, e. g. due to diffusion, also result in signal dephasing. The observed  $T_2^*$  decay is the net effect of all the dephasing terms [BS99]:

$$\frac{1}{T_2^*} = \frac{1}{T_2} + \frac{1}{T_2^{inhom}} + \frac{1}{T_2^{suscept}}, \quad (2.3)$$

where  $T_2^{inhom}$  represents the dephasing due to magnetic field inhomogeneities and  $T_2^{suscept}$  is the diffusion-related signal loss.  $T_2^*$  generally ranges from a few milliseconds to tens of milliseconds. The MR signal,  $S(t)$ , decays according to the formula [CB02]:

$$S(t) = S_0(1 - e^{-\frac{TR}{T_1}})e^{-\frac{t}{T_2^*}}, \quad (2.4)$$

where  $S_0$  is the signal strength immediately following the excitation pulse. Like  $T_1$ , the  $T_2$  signal decay times differ among body tissues. For most current fMRI,  $T_2$  is the dominant contrast mechanism. Echo Time (TE) is a short pause (in the order of 10 ms) after sending the r.f. pulse to let the signal decay (see figure 2.2). TE has to be long enough to let the differences in  $T_2^*$  or  $T_1$  evolve before detecting the resulting signal.

### 2.2.1 Spatial Decoding

The signal detected from an anatomical region is the sum of the signals from dipoles all over the region. In order to form an image, the dipoles must somehow be spatially resolved. This is usually a two-step process: (i) exciting the magnetization into the transverse plane over a spatially restricted region. (ii) encoding spatial location of the signal during data acquisition. This is done by using

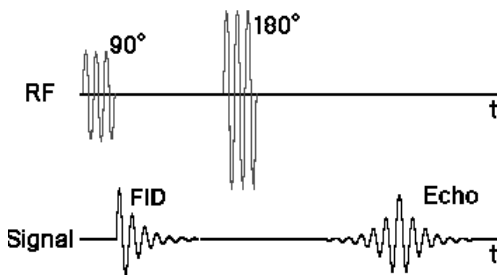


**Figure 2.3:** The signal of a spin-echo sequence [Hor02]; FID = Free Induction Decay.

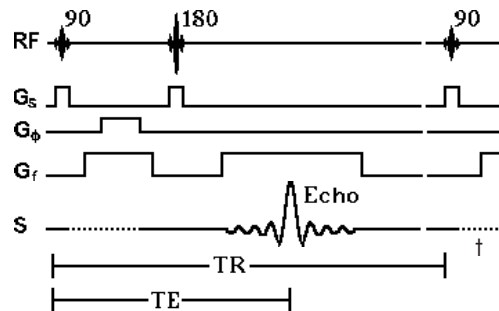


**Figure 2.4:** The time scheme of a spin-echo sequence [Hor02].

in xyz linearly varying magnetic fields to separate the signal from different locations according to frequency. With a sample placed within a linear magnetic field gradient, for example, the Fourier transform of the signal shows its strength at each frequency, and thus at each position. Present day MR imaging instruments use three mutually orthogonal sets of electromagnetic gradient coils to obtain a 3-dimensional image. The different gradients required are: *slice selection*  $G_s$ , *frequency encoding*  $G_f$  and *phase encoding* gradient  $G_\phi$ .

### 2.2.2 Echo-Planar Imaging

In conventional imaging, the frequency domain, referred to as k-space, cannot be sampled completely after a single excitation. This is because of a variety of physical limitations (finite relaxation time of the dipoles and SNR limitations) and technical limitations. Thus, k-space is sampled in a sequence of  $n$  excitation-acquisition cycles with the repetition time (TR). MR imaging times have traditionally been extremely long: from 3 to 15 min for an imaging series. **Echo-Planar Imaging** performs all required spatial encoding during the several tens of milliseconds that the MR signal is present. Thus brain slices with a resolution of  $4\text{ mm} \times 4\text{ mm}$  and thickness of  $4\text{ mm}$  can be obtained in less than  $100\text{ ms}$ . EPI is characterized by a series of very rapid gradient reversals in the frequency encoding direction. In contrast to conventional imaging it measures all lines of k-space in one slice in a single TR-period. The time scheme of the gradients is illustrated in figure 2.5. Finally, with these acquisition rates the limiting factor is the physiological response time of the brain.

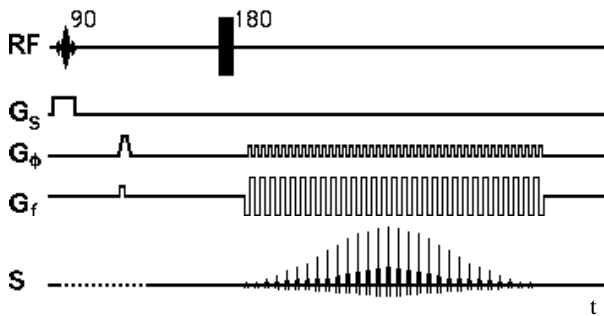


Figure 2.5: The time scheme of an EPI sequence [Hor02].

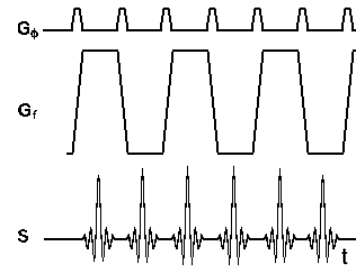
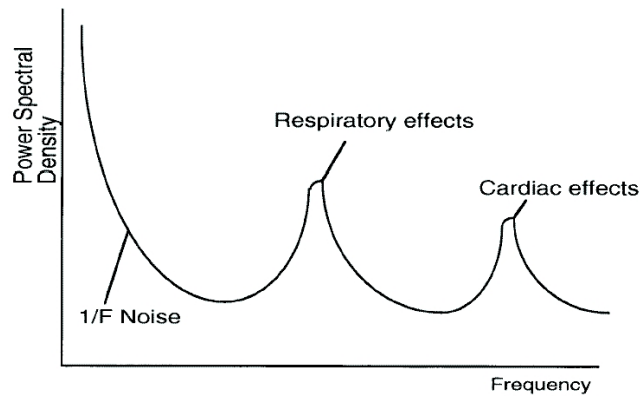


Figure 2.6: Zoom into the time scheme of an EPI sequence [Hor02].

### 2.2.3 Signal-Variations and Noise

Increased variance with random amplitude in a measured image is interpreted as noise. There are two different types of noise in an fMRI image: low-frequency and wideband noise. The wideband noise is for most MRI systems dominant. It originates in the r.f. coil and is caused from thermal sources. Low-frequency noise typically exhibits a  $1/f$  characteristic as can be seen in figure 2.7. This is composed by non-periodic, slow variations. In addition, periodic physiological noise can appear as peaks in the frequency spectrum. Cardiac and respiratory cycles exhibit frequencies of about  $\sim 1$  and  $\sim 0.2\text{ Hz}$  respectively. For TR of 2 seconds the Nyquist cut-off [Nyq28] is with  $0.25\text{ Hz}$  below the cardiac frequency and thus aliasing will occur. The respiratory cycle can result in head movement and due to its periodicity create an artificial peak in the frequency spectrum (see figure 2.7).

Any source of fluctuation such as head movement, behavioral variations, spontaneous neural and vascular fluctuations contributes to the fMRI noise and can decrease the SNR. The noise can effectively be reduced by reducing the coil volume. This is already considered in constructing the fMRI instruments by choosing a special coil for every part of the human body (brain, knee, shoulder, etc.). The experimenter has to choose carefully the acquisition time ( $T_{aq}$ ) as the SNR is proportional to the square root of  $T_{aq}$  [Wri02]. A contrary effect has the head movement which



**Figure 2.7:** Typical power spectrum of an fMRI image with noise only.

increases with time until the measurements are not reasonable anymore. Typically, the signal in an fMRI system of 2 Tesla reaches between 1-10 %. The signal intensity furthermore can change with age, vascular tone and atmospheric  $CO_2$ . [EZAR99, CDR02].

## 2.2.4 Artifacts

The most common artifact in fMRI measurements is called the Nyquist ghost or  $\frac{N}{2}$  ghost. This arises because odd and even echoes are acquired under opposite read gradients, and the data requires reversal prior to image reconstruction. Inaccurate timing of the sampling relative to the switched gradient causes a modulation of alternating lines in k-space.

This leads to a ghost image shifted by  $\frac{N}{2}$  pixels in the phase encoding direction. A simulation of this effect is shown in figure 2.8. Due to the low frequency per point encoding direction, EPI images are very sensitive to magnetic susceptibility inhomogeneities. They can cause geometric distortions of the images.

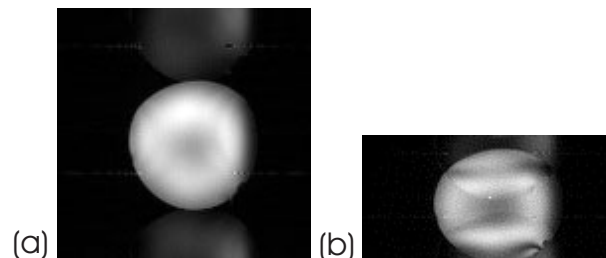


**Figure 2.8:** Examples for the effect of the  $\frac{N}{2}$  ghost on phantom images, (a) where ghost and image do not overlap and (b) where ghost and image overlap [Stu97].

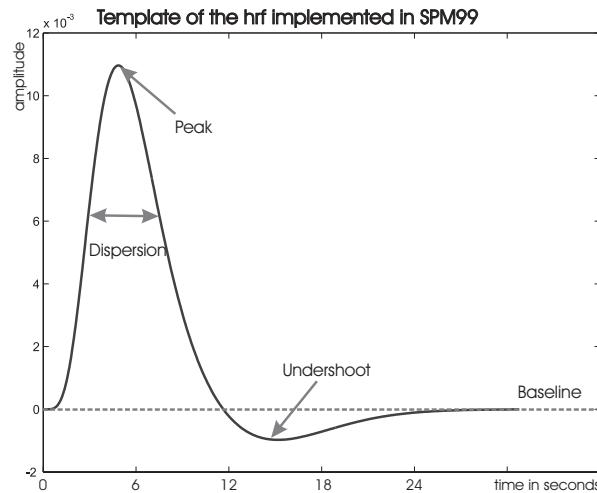


**Figure 2.9:** The *hrf* template within *SPM* composed of two Gamma density functions.

### 2.3 The Hemodynamic Response

The contrast in fMRI images is generated by the **Blood Oxygenating Level Dependent** effect. BOLD was introduced by Ogawa *et al.* 1990 [Str00] with the help of in vivo experiments with animals. There are two physiological principles responsible for the effect:

(i) Activated areas of the human brain show localized increases in blood flow.

(ii) Hemoglobin exists in an oxygenated and deoxygenated state. Oxygen binds to iron which is a constituent of the haem component of haemoglobin. When haemoglobin has no oxygen bound, each haem group has a net magnetic moment because of iron's four unpaired electrons. As soon as oxygen is bound, the net magnetic moment disappears.

The increase in blood flow seems to outstrip increases in oxygen utilization [FR86]. Thus, the oxygen content of venous blood increases during brain activation, resulting in increased MR signal intensity. Thus, large vessels will dominate the signal from a region in the brain. Signal changes due to the BOLD effect are expected between 5 and 10%. There are different approaches to model the hemodynamic response. One possibility is to use a canonical *hemodynamic response function* to model the occurrence of each event [FFTF95]. The model assumes a peak at about 6 s after the stimulus, followed by a smaller undershoot at about 15 s, returning to baseline at about 25 s. Mathematically, it is composed of two Gamma density functions.

Previously made assumptions that the magnitude of the BOLD response is linearly related to the underlying neuronal activity were to a degree confirmed in studies made by Boynton *et al.* 1996, Dale & Buckner 1997 and Pollmann *et al.* in 1998. That the linearity is not given for all parameters, especially not for short inter-stimulus times, was demonstrated by Vasque & Noll and Friston *et al.* in 1998 [JH99]. It is not yet clear to which degree these results effect from nonlinearity at the neuronal level or at the hemodynamic level.

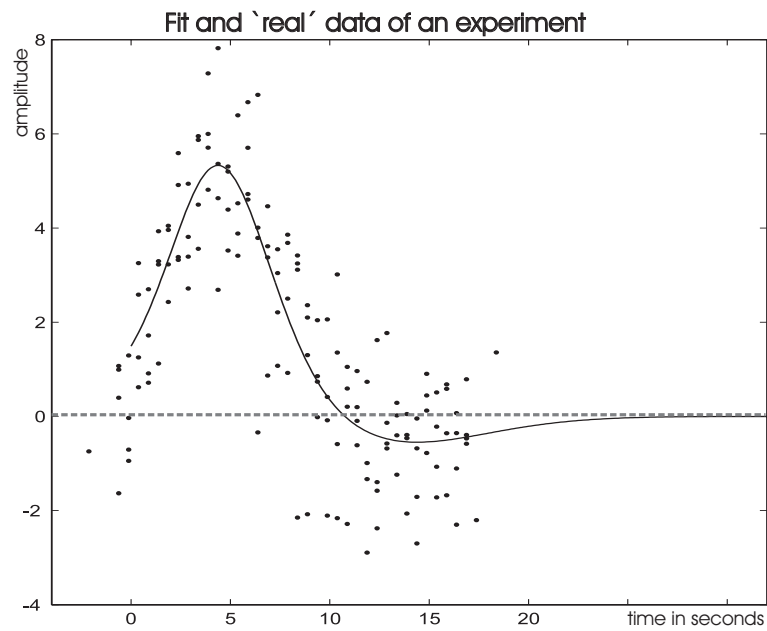


**Figure 2.10:** Data from an activated volume element (voxel) which is located in V1 overlaid with the *SPM* template. The signal recorded over 280 s is back-folded on the period of one response (20 s).

## Chapter 3

# Analyzing Methods

An average brain mapping experiment with fMRI produces around 32 million signals (16 bit integer) that need to be processed. One of the challenges for early neuroscientists using fMRI was to gain reliable and presentable results from such an amount of data. There are several fundamentally different approaches to evaluate fMRI data. Karl Friston created the basis (SPM Classic) for *Statistical Parametric Mapping*<sup>1</sup>, the most established analyzing tool currently used. *SPM* (open source code) is based on Matlab and accepts the fMRI-data in a special *Analyze*-format<sup>2</sup>. The raw data has to be Fourier transformed into the xyz-space and converted from the four dimensions (xyz and time) file into twice the number of scans. For each scan one file exists to describe the signal as a gray-value in each acquired voxel (the \*.img file). Additionally, a header describes global variables for *SPM* as the coordinates of the origin, scaling values and a short description including the filename (\*.hdr). The \*.hdr is not essential since *SPM* has an (editable) default header included.

*SPM* integrates several modules in one software. First, the preprocessing steps can be applied to improve the detection of activation events. Next, the statistical analysis, which detects the voxels in the image which show a response to the stimulus, is carried out. Finally, the activation images are displayed and probability values are quoted, which give the statistical confidence.

### 3.1 Preprocessing

The preprocessing steps consist of various spatial transformations that are concerned with mapping of one or more images to a reference image:

1. Realignment is done to correct for subject movement during the experiment.
2. Coregistration allows the scans recorded in one modality to be transferred to another modality. This can include PET and fMRI as well as a series of  $T_2$  weighted scans to be mapped onto a  $T_1$  weighted image with a higher resolution.
3. Normalization can be performed to map an individual brain to a reference coordinate system.
4. Smoothing ensures the validity of inference and generally enhances the signal to noise ratio.

---

<sup>1</sup>The current version is called *SPM99*. In the following text this version is referred to with *SPM*.

<sup>2</sup>The *Analyze*-format is introduced by The Biomedical Imaging Resource at the Mayo Foundation for a software called *Analyze*.

Realignment, normalization and smoothing is applied to the performed experiments. To differentiate preprocessed images from the original *SPM* adds to the original filename a prefix like *s\** (smoothing), *n\** (normalization), *r\** (realignment) referring to the order in which the steps have been performed.

### 3.1.1 Realignment

One fMRI session has an average length of 30 *min*. During this time the subject performs unconscious small head movements of  $\sim 1$  *mm*. This can create two unwanted effects which are not mutually exclusive:

- If the movement is random, the movement-induced signal changes behave like extra noise and will reduce the efficiency of the signal. This usually means that the areas of activation shrink.
- If the movement is correlated with the stimulation (e. g., the subject flinches when the stimulus arrives), the movement-induced signal changes will be correlated with the stimulus. Thus false areas of activation can occur. This is indicated through strong activation areas at the periphery of the brain (where small motion has a big effect on the voxel contents).

An additional reason for performing the realignment is that it increases the sensitivity of detecting induced activation. *SPM* attempts to correct for motion by ‘registering’<sup>3</sup> the image series to the first scan of each session. The images will be realigned back to what they would have been if the subject had not moved.

*SPM* writes a *\*.mat* file for each scan including the matrix for the motion correction of this scan. The matrix includes 3 variables for translation and 3 variables for rotation. For details concerning the realignment matrix compare [FFF<sup>+</sup>97]. Furthermore, a *realignment\_parameter\*.txt* which has the estimates of movement in the x, y and z direction is written.

After the realignment the graphic display of *SPM* shows the transformation and rotation amplitude versus scans (see figure 3.1). Acquisitions with more than 1 *mm* of absolute movement have to be discarded [HJ02]. For details on the implementation of realignment compare [FWR<sup>+</sup>96].

### 3.1.2 Normalization

In order to compare the results from different subjects it is necessary to warp the corresponding images into a standardized coordinate system. Since individual brains vary in both, shape and size, the normalization is not a rigid body transformation. The first step is to correct for the variations in position and size of the image compared to a template image of the same modality. This includes a resampling of the images on a voxel of  $2 \times 2 \times 2$  *mm*<sup>3</sup> in size. The second step corrects more subtle differences by means of a non-linear registration. The algorithm used minimizes the residual squared difference between the image being normalized and the template image.

*SPM* utilizes the MNI template which is created by members of Montreal Neurological Institute based on 152 averaged MRI scans. The coordinate system adopted by *SPM* is introduced by Talairach and Tournoux in 1988 [TT88]. It uses the **A**nterior **C**ommissure as the origin. Its axes are defined by the line through the superior edge of the AC and the inferior edge of the **P**osterior

<sup>3</sup>The first scan of the functional image series is chosen as the reference image that the other images are realigned to.

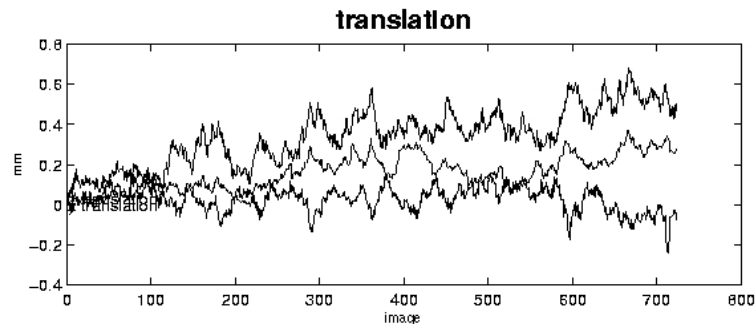


**Figure 3.1:** Visual illustration of the motion correction for a session with 724 scans. It is part of the output file `spm.ps` created for each realignment.

*Commisure* - the AC-PC line - and the interhemispheric, sagittal plane. For more details about the Talairach and Tournoux coordinate system or the MNI brain see appendix C.1 and C.2.

Unfortunately, it is not possible to perform a proper transformation between the MNI and the Talairach space since the brains vary significantly in shape. This makes it difficult to compare *SPM* results to results reported in Talairach space.

### 3.1.3 Smoothing

The smoothing is done in two steps. Some smoothing of the raw data is intrinsically introduced by resampling the images. The main part of the smoothing is done by convoluting the data with a Gaussian kernel of variable width. In addition to the smoothing which is done within *SPM*, spatial smoothing can be performed during the earlier Fourier transformation.

Smoothing also potentially increases the SNR according to the matched filter theorem ([RK82]). This theorem states that the filter that will give optimum SNR is a filter that is matched to the signal. Usually, neither exact size nor shape of the signal are known. A rule of thumb for fMRI signals is to try a Gaussian kernel of FWHM of about 2 to 3 times the voxel size.

## 3.2 Statistical Analysis

One of the basic decisions when analyzing fMRI data is which *a priori* knowledge to assume. The problem with fMRI data is that a slice cannot be interpreted on its own. Only relative conclusions can be drawn from comparing slices acquired under differing circumstances.

The most simple evaluation-method would be to apply a boxcar activation with an *ON* and *OFF* state and to subtract the average from all *ON* images from the *OFF* images. One of the disadvantages of this method is that it is very sensitive to head movement leading to many artifacts in the images. Thus, the software *SPM* is used for the evaluation using a more sophisticated method.

*SPM* is a model-based approach which assumes the time course of the haemodynamic response to be known except for variations in onset and dispersion. Contrary to this, data-driven methods such as principal component analysis [MS91] and independent component analysis [MJ98] exist.

In this chapter an overview on the principles of evaluating and presenting fMRI data with *SPM* is given (for statistical fundamentals of *SPM* compare the book [FFF<sup>+</sup>97]).

### 3.2.1 The Principles of SPM

SPM treats every voxel as an independent data point. It is based on the **General Linear Model** to calculate parameter estimates between the expected time series (called regressors) and the time course of each voxel.

This is done in three steps. First a model (design matrix) is generated including the prediction of the physiological responses as column vectors. Hence, the design matrix is the basis of the experimental design and the nature of hypothesis testing. Second, fitted parameters are estimated for these predictor vectors using a least squares approach to (multi) linear regression. Finally, one uses these parameter estimates for statistical inferences about a single subject or group level hypotheses. The results are presented as gray-level maps on a sagittal, coronal and axial sliced glass brain (the MNI template).

### 3.2.2 The Design Matrix

The design matrix includes the regressors that are the basis for the GLM. The regressors are created by convoluting the time course of the task variation (or in simple cases the **Stimulus Onsets**) with the *hrf*. The experimenter can choose between three different basis functions: Fourier Basis Sets, Finite Impulse Responses, and the Canonical *hrf*.

For the Fourier Basis sets, the response is broken down into different frequency components and for the Finite Impulse Responses it is broken down into different post-stimulus time windows. The most popular method is the Canonical *hrf*. This is a single regressor which captures the stereotypical BOLD response to an impulse of neural activity - the assumed *hrf*.

The minimum amount of necessary regressors is two: a baseline condition and the convolution of the SOTs. To be able to cope with a spread of the SOTs and peak dispersion over the whole brain two additional regressors can be included into the model: (i) the derivative of the canonical *hrf* with respect to time (ii) the derivative with respect to dispersion. In addition to the regressors correlated to the time course of the stimulation, movement-related regressors can be included as well.

It is important to note that the regressors of the design matrix have to be independent. If *parametric* design is chosen, the regressors will be orthogonalized before estimation. *Parametric* design is a possibility to give an additional parameter to a regressor which only includes the onsets of a stimulus. This can be used to investigate whether the voxel-based activation is correlated to any polynomial order of the parameter. E. g. the first regressors includes the timing of a vibrational stimulus and in the second regressors is defined with which frequency the stimulus has been applied.

### 3.2.3 Estimation

Before estimating the parameters two filters can be applied. Both, a high-pass filter and a low-pass filter are included in SPM. The high-pass filter is reasonable to remove possible alterations in the magnetic field or temperature shifts. With the low-pass filter physiological effects such as breathing or the heart rate can be excluded. It is possible to give the option *hrf*, which filters out all frequencies lower than the haemodynamic response function.

The aim of the estimation is to specify a statistical model that describes, as accurately as possible, how the time-series of each voxel varies over time. Once the statistical model is specified, SPM applies the GLM to estimate the parameters (called  $\beta$ ) of the model, using the collected and

preprocessed volumes as input data. It is important to note that the same statistical model is applied for each voxel and a different set of  $\beta$ s is computed for every voxel.

There are several partitions of variance modelled, the two most important being the *effects of interest* and *confounds* (effects of no interest). The variance remaining after these partitions have been accounted for is the error term (or noise). The amount of noise has to be minimized while keeping the simplest possible model. Adding regressors to the model reduces the degrees of freedom, but can as well decrease the error term.

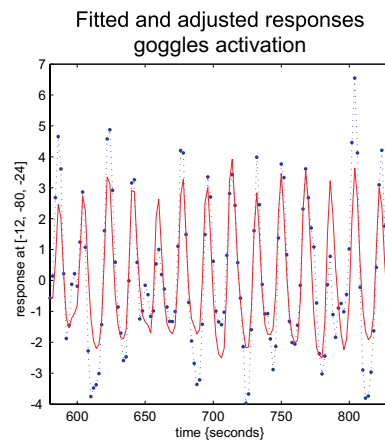


**Figure 3.2:** Plot of the fitted and adjusted response (red line) and the time course (dashed blue line) for a highly significant voxel in VI.

### 3.2.4 Contrasting and the Students t-Test

Statistical contrasts are set up and tested once the parameters of the statistical model have been estimated. There are two possibilities to conduct the statistical inference: a one-sampled t-test or the two sided F-test. The major difference is that t-tests are uni-directional while F-tests are bi-directional. This means that F-test only calculate the distance between the parameter estimates, while t-test differentiate between positive and negative distances. F-tests can be applied if testing the model and especially if searching for the minimum amount of necessary regressors. The following section is focused on t-test since it is the most commonly used for determining the significance of activation.

To understand contrasting in *SPM* it is important to note that the software distinguishes between ‘effects of interest’ and ‘effects of no interest’. The effects of interest comprise only those parameters that describe the ideal signal, e. g. the timing of the stimulus. For the t-test one weight vector (called contrast) defines which are the ‘effects of interest’. Either the test can be a real contrast in the sense of weighting one effect of interest versus confounds. In this case the sum of the vector has to be zero. Or the vector can be interpreted as a comparison of different regressors, then the sum can differ from zero. Contrast weights are requested only for the parameters of interest, weights for other parameters are set to zero. Regressors included in the model with their weight set to zero are modelled as confounds. This is mostly the case for movement-related regressors, if not the activation due to movement is part of the investigation. Artificial activation that may origin

from the process of realignment can be excluded by including the movement-related regressors with zero weight.

Regressors are given a positive weight for constructive interference and negative value if they are assumed to model confounds. A typical example is a boxcar function (E1) as the first vector and its inversion as the second vector. The corresponding contrast would be  $\vec{c} = [1 \ -1 \ 0]$  for searching the voxels that are activated during E1 and  $\vec{c} = [-1 \ 1 \ 0]$  for searching the voxels that behave the opposite.

Having chosen an appropriate contrast and calculated the corresponding t-value for every voxel separately, the result is a statistical parametric map of t-values. *SPM* creates an image of every  $SPM\{t\}$  called `spmT_000i.img` where *i* corresponds to the numbering of the contrast. The contrast values are also saved in `con_000i.img`. To every t-value corresponds a p-value, whereas the t-statistic has a probability *p* to have occurred by chance and of (1-*p*) to reflect a real event. Thus a threshold of  $p = p_0$  needs to be applied to a collection of t-scores in order to filter those values that have a probability of (1-*p*) to be false positives.

### 3.2.5 Thresholding

Before mapping the results on the glass brain a spatial extent (*k*) and statistical height ( $p_0$ ) threshold has to be entered. With the spatial extent threshold a minimum cluster size *k* (in voxels) is defined [FWF<sup>+</sup>94], i. e. only clusters that consists of at least *k* voxels above  $p_0$  survive the threshold.

Spatial extent thresholding is important for the significance of the activation. Since voxels are treated independently, the appearance of a cluster strengthens the confidence in the validity of the activation caused by stimulation.

For the statistical height thresholding an additional correction can be applied for the following reason. In a typical statistical parametric map of t-statistics ( $SPM\{t\}$ ) there are about 100 000 values, one for each voxel. Now, even if the Null Hypothesis testing is true, some t-scores will appear to be significant at a standard statistical threshold, e. g.  $p = 0.05$  simply because there are so many. The multiple comparison problem is the question of how high the threshold needs to be to ensure reasonable confidence in the significance of the residual t-scores. An appropriate correction for spatially correlated data requires an estimation of the degree of correlation. The approach adapted by *SPM* is to use *Random Field Theory* for correction.

Thus, *SPM* prompts for corrected or uncorrected threshold. In practice it is recommendable to choose uncorrected threshold when testing the data for the first time without knowing what kind of activation to expect. For final presentation corrected threshold is generally preferred. The corrected threshold  $p_{corr}$  defines the rate of false positives one is prepared to accept.

## Chapter 4

# Devices and Developments for the fMRI Environment

### 4.1 The Pneumatically Driven Tactile Display (PTD)

There are only few investigations on the processing of tactile stimulations in the human brain with fMRI technique. This is due to the difficulty of giving a reproducible and thus automated, well-defined stimulus in an fMRI environment. The device for such a stimulation cannot rely on electronic currents as they may locally change the magnetic field which inevitably leads to image distortion. All electronic frequencies can interfere with the image acquisition of the r.f. coil and produce artifacts. Ferromagnetic materials have to be avoided for security reasons. Furthermore, the devices are very limited in size as the tube of the MRI system is 55 cm in inside diameter. Some experiments have been performed to examine shape discrimination [Bod00] by manually applying non-magnetic objects in the fMRI. This is always a unique event and cannot be exactly reproduced several times within one session. For good statistics more than one run under comparable conditions is necessary. Existing automatic stimulators rely on two principles: either they are driven by piezo actuators [Ing00] or by air flow elements. The air flow is either used directly [BS01] or by moving a rubber diaphragm. These methods create reproducible surface features that can vibrate and move, but only at small skin areas. With an air flow element the stimulus is extended, but is not well-defined enough to give distinct images. In the frame of the *SenSub* project a new **P**neumatically driven **T**actile **D**isplay has been developed by T. Maucher<sup>1</sup>.

#### 4.1.1 Description of the System

The PTD is designed to present two-dimensional patterns to the skin of a blind or blindfolded proband. The display consists of non-ferromagnetic and non-electronic parts which do not interfere with the image acquisition of the fMRI as it was proved by Stefanie Runde [Run00]. The display is made up of modules (see figure 4.2), each one consisting of four tactile elements (taxels). The modules can be arranged to different shapes and sizes. Within the *SenSub* project a regular square matrix and a concave surface were built (e. g. to fit the arm). Both consist of 64 taxels, which can be addressed individually with frequencies of up to 6 Hertz. All experiments in this study were performed with a flat design (shown in figure figure 4.1). A variety of tactile stim-

---

<sup>1</sup>Ph.D. student at the Kirchoff Institute for Physics of the University of Heidelberg

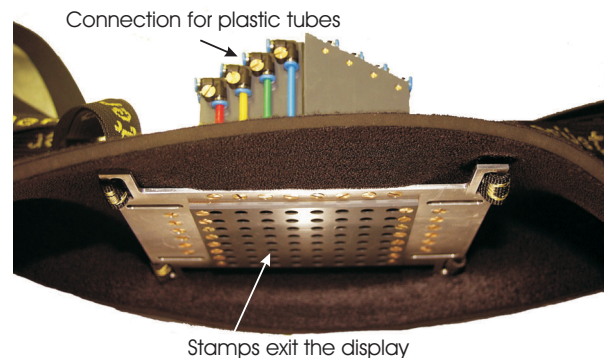


**Figure 4.1:** Picture of a flat PTD. It is produced to be mounted on the abdomen of a subject.

ulation comprising both, static and vibrational patterns of variable frequencies can be performed on the display. The experimenter controls the display from a PC placed outside the Faraday cage. Electronic signals are converted to pneumatic pulses by an *Electronic Pneumatic Interface*<sup>2</sup> which is placed in a shelf near the tube of the fMRI.

#### 4.1.2 The Way from Pattern to Perception

The PTD control unit consists of a PC with an I/O interface card for a CAN-bus and a dedicated software (*TVSSCS*), the *Trigger and Input/Output Transforming Unit* and the *EPI* with pneumatic switches. The patterns are generated in three different input modes: with a camera, by a paradigm script or interactively on the PC. A special software (*TVSSCS*) has been developed by Thorsten Maucher [Mauet] for controlling the TIOTU. The PC communicates with the TIOTU and the pneumatic valves through the CAN-bus. The PC and TIOTU are placed outside the Faraday cage of the fMRI. Only a small tube interrupts this shielding. A twisted pair cable for the CAN-bus connects TIOTU and *EPI* through this tube and provides power and control-signal for the pneumatic switches. This allows the main electronic device to be away from the fMRI-magnet. The pressure from an external compressor is reduced to a working pressure of 3-5 bar before connecting the *EPI*. Since the acoustic level of the pneumatic switches is high, the *EPI* can be covered by a sound shielding. The *EPI* distributes the air flow onto 64 plastic tubes which are connected to the taxels of the PTD. Each taxel consists of a stamp of 1 mm in diameter covered by a plastic cap which contacts the skin. The stamps are driven by a piston (see figure 4.2). A silicon pad can be placed between surface of the display and the proband's skin to control and change the distance between skin and surface of the display.

#### 4.1.3 Specifications of the PTD

All taxels of the PTD have a pitch of 10 mm. Each taxel has a diameter of 4 mm. This gives the possibility to perceive single taxels as separated points. The resolution of a pattern is limited to 8 × 8 taxels. A larger setup would be unpractical to handle. The force on the skin is adjustable between 1.3 and 2.3 N. The stamps are free to move 10 mm in vertical direction. A taxel is ON

<sup>2</sup>Not to mix up with the *Echo Planar Imaging*.

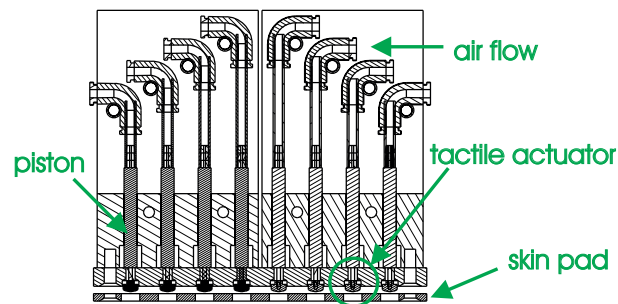


**Figure 4.2:** Schematic drawing of two modules of the PTD.

when the stamp exceeds its shaft and OFF when it is completely inside. Each taxel has a maximum temporal resolution of  $50\text{ ms}$ . Only frequencies up to  $6\text{ Hz}$  assure a constant force on the skin. For higher frequencies the force decreases and the vibration cannot be resolved clearly and distinctively enough.

## 4.2 Visual Stimulation Device

The fMRI in Strassbourg has a visual stimulation system already in place. It is based on laboratory safety glasses with LEDs<sup>3</sup> attached. The signal is created by a frequency generator outside the Faraday cage and is amplified inside the cage. The LEDs are connected to the amplifier by a coaxial cable. The experimenter controls duration and frequency of the LEDs from a PC near the fMRI control station. This system has several disadvantages: The rectangular geometry of the goggles does not fit all probands when inside the narrow headcoil ( $25\text{ cm}$  inside diameter) of the fMRI.



**Figure 4.3:** Photo of an experimental set-up with the goggles put on (covered by a blindfold).

The software for the temporal control of the flashing LEDs is developed for transmission of complex patterns which makes it not well suited for simple stimulations. Since the LEDs are fixed to

<sup>3</sup>Light Emitting Diode

the glasses, they are exposed to the strong magnetic field of 2 Tesla. To progress experiments involving both tactile and visual stimulations a new goggle system needed to be developed. Optical fibres are used to avoid electronic signals within the gradient coil. A smaller design is accomplished by conventional goggles as used by swimmers.

#### 4.2.1 Construction of a New Visual Stimulation Device

The main demand for the system is to generate light pulses inside the r.f. coil. The pulses should be easily adjustable in length and intensity whilst the wavelength is of no concern. During the experiment the subject should distinguish brightness (goggles ON) versus a dark background (goggles OFF).

The new system is integrated in the already existing PTD system. Temporal controlling is programmed as an additional feature into the *TVSSCS* software. The code for tactile and visual stimulation can easily be combined in one paradigm. This simplifies the temporal correlation of two different modalities within one session. The left and right eye can be stimulated independently in contrast to the existing setup where both sides were connected. The PC communicates via a CAN-bus with the TIOTU. The TIOTU is extended by one amplifying component to supply the goggles with a maximum current of 60 mA (for the circuit diagram see figure D.2).

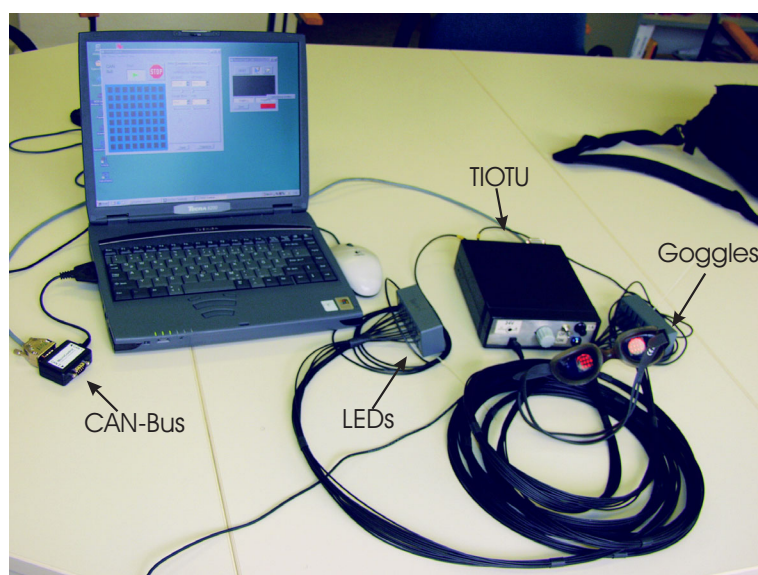


**Figure 4.4:** The fully equipped goggles system.

The TIOTU is equipped with two outputs where the left and right side of the goggles are connected with a *lemo*<sup>4</sup> style connector. The intensity can be adjusted between 20-60 mA with a knob on the front panel of the TIOTU. Twelve LEDs<sup>5</sup> providing the light for one side are combined within a hard plastic box. Six of them are connected in series and two bunches in parallel. Each LED has an optical fibre attached to it. The optical fibres are fixed with optical glue to provide for optimal performance. The 3 m long fibres are bundled for each side and lead to a plastic prism. The goggles

<sup>4</sup>Trademark for connectors which are commonly used in high-energy physics.

<sup>5</sup>red light, 5 mm diameter, ultra-bright

have countersinks on each side where the prisms are half buried. Since the fibres should not be bent, the light finds its way to the subject's eye by total reflection within the prism. This allows to lighten an area of  $2 \times 2 \text{ cm}^2$  with an adequate intensity. The dark tinge of the goggles prevent stimulations from the surrounding to be perceived. For details compare the technical drawing of the goggles in figure D.1.

In May 2002 the goggles were delivered to the fMRI system in Strassbourg and have since been used for experiments.

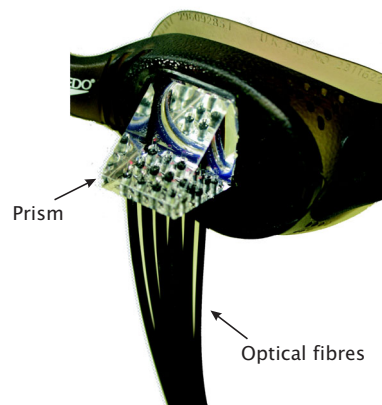


**Figure 4.5:** Photo of the interconnection between fibres, prism and goggles.

### 4.3 Software-Development for Faster Evaluation of fMRI Data

The evaluation of raw data from a fMRI session includes several steps as it is explained in section 3. Previously, the Fourier transform was performed locally on the fMRI control computer. Before the data can be copied to any other hard disk which can be reached through the network the reconstruction of the images has to be finished. The experimenter has to wait for about one day before starting with further evaluation. Thus, data handling in an optimized and manually way was required.

#### 4.3.1 Preprocessing with *SPM*

Approximately 20 parameters have to be specified in order to perform the preprocessing with *SPM*. This can be done either interactively with input boxes or in advance by special scripting language called batching. The interactive way is less vulnerable to errors but more time consuming. Batching of *SPM* is introduced as 'crash mode' by Matthew Brett [Bre02], who maintains one of the best explanation sites for batching.

It is important not to get confused by the way the terms 'scan', 'session' and 'subject' are used within *SPM*. One scan includes all slices that are obtained from the brain during one TR. Typically, the subjects remains in the scanner during the run of several paradigms. The scans from each paradigm are called sessions for the preprocessing in *SPM*. When one subject exits the scanner and returns after a break, the coming sessions are declared to be from a new subject (even it is the same person), since the scans from the previous run cannot be realigned to these.

The great advantage with batching is that once a set of parameters is defined and the debugging finished, the script can easily be adjusted to a similar session. Several sessions can be handled in one run, whereas different subjects have to be accounted for separately. The data from each session is stored in its own directory named with ongoing numbering (see figure 4.6). For each new subject a new ‘main data directory’ is created comprising all session from this run. Furthermore, a unix

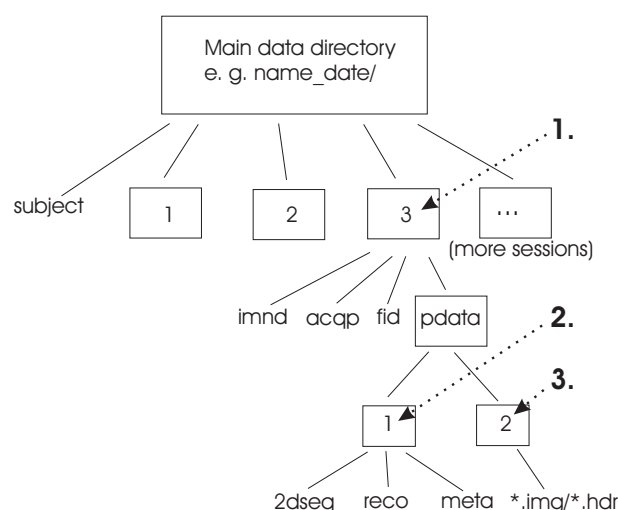


**Figure 4.6:** Data tree for storage of fMRI data and settings by Bruker.

cluster containing twelve PCs was built up in Strassbourg where Gerald Vetois developed and implemented a software to parallelize Matlab on this cluster. This saves an enormous amount of calculation time and can only be used for evaluations with batch mode.

These advantages are used for an even more automatized preprocessing where the batches for the realignment, normalization and smoothing are included into a software called *Quickshot* which is as well based on matlab.

### 4.3.2 The Script *Quickshot*

Within this thesis *Quickshot* was written to directly combine a faster Fourier transformation with the conversion and preprocessing. In addition it makes the handling of several sessions and subjects in one procedure possible. Altogether the work that had to be controlled by usually two persons and could take a two day effort is now summed in *Quickshot* with only some hours duration. *Quickshot* consists of twelve Matlab scripts and a Manual text file (printed in the appendix E) with instructions on the functionality and usage.

*Quickshot* allows all steps from the raw fMRI data to `snr*.img` and `snr*.hdr` to be done on the unix cluster which is called *tregorrois*. The Fourier transform and conversion is now done by the experimenter itself and not by the fMRI administrator anymore. The great improvement is that input boxes only occur in the beginning of *Quickshot*. Once the files and the desired job are selected, the same parameters are applied to all sessions and subjects with no further interaction necessary (see the comparison in figure 4.7).

Though it is more automatized than the previous batching, *Quickshot* can be applied to raw data as well as to already converted files (where only the preprocessing is necessary). The choice of files

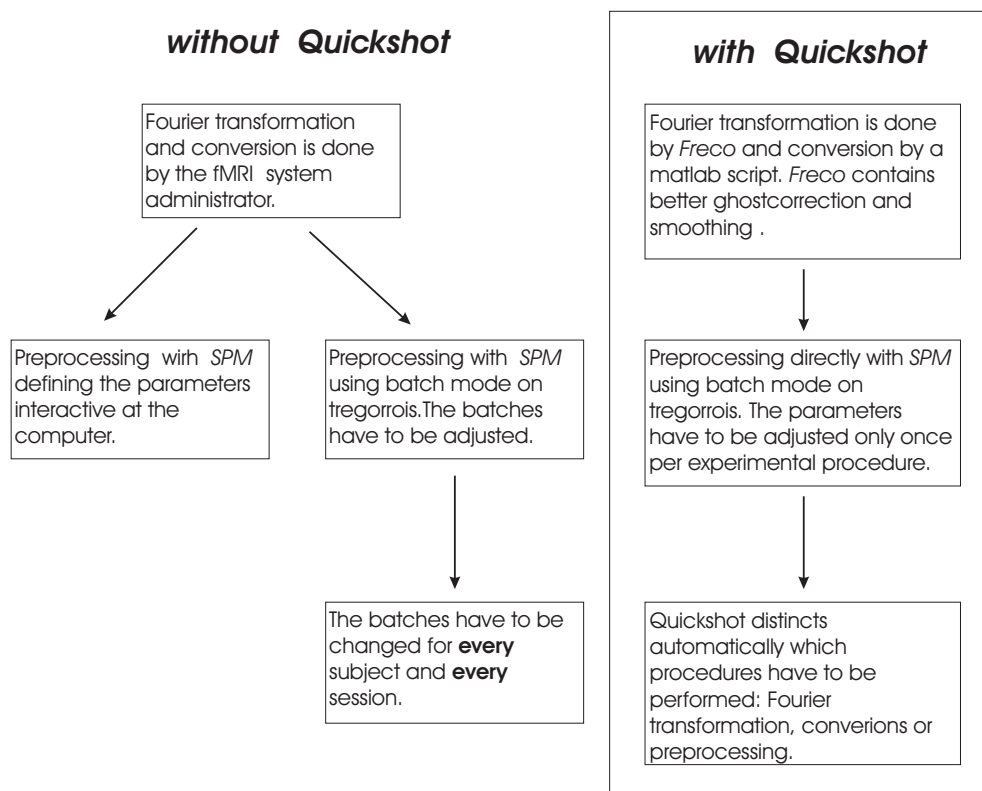


**Figure 4.7:** Comparison of the fMRI data handling without *Quickshot* versus with *Quickshot*.

helps to select which jobs have to be performed. For the file selection the graphical user interface from *SPM* is implemented.

The imaging software *ParaVision 2.0* writes the data in a special format which is called Bruker<sup>6</sup>. For illustration of the file order of the Bruker format see figure 4.6. There are three possibilities by which a directory can be selected as shown in figure 4.6, where the bold letters indicate the possible selections.

For the Fourier transformation a new version of the program called *Freco* is used. *Freco* implements correction for possible Nyquist ghosts including a rough smoothing.

Before *Freco* is launched a question window appears including three input boxes (see figure E.2). The questions allow three options:

- (i) to choose overwrite security, (if it is chosen *Quickshot* will pause every time that data already exists in the relevant directory)
- (ii) to specify the origin of the scans by a user-defined file
- (iii) to specify which preprocessing steps are performed. This is in more details explained in the Manual.

The default parameters for preprocessing with *SPM* are specified in *Quickshot*. Only this guarantees equal processing parameters on every computer. The parameters for the realignment, normal-

<sup>6</sup>Bruker is a company who builds fMRI systems.

ization and smoothing can only be changed in the source code, which in this case is a batch file. The parameters in the original version are shown in the Manual.

## Chapter 5

# Experiments

All presented experiments were conducted in the period from September to October 2002 in Strassbourg at the fMRI of the Biological Physics Institute at the Université Louis Pasteur in Strassbourg, France. Some previous measurements have been performed to test the experimental setup and to optimize the stimulation patterns and timing. There are two points of interest for the conducted measurements: (i) To perform tactile stimulation with different frequencies. (ii) To investigate the variability of the *hrf* in different areas of the cortex, different subjects and within an activation cluster. For both investigations event-related designs are chosen as explained in 5.3.1. For the entire study seven volunteers were recruited from the academic environment of the Biological Physics Institute in Strassbourg and Kirchhoff Institute for Physics in Heidelberg whereas only the results of six probands (four males and two females) are included in the investigations. One session shows large movement artifacts and is therefore neglected.

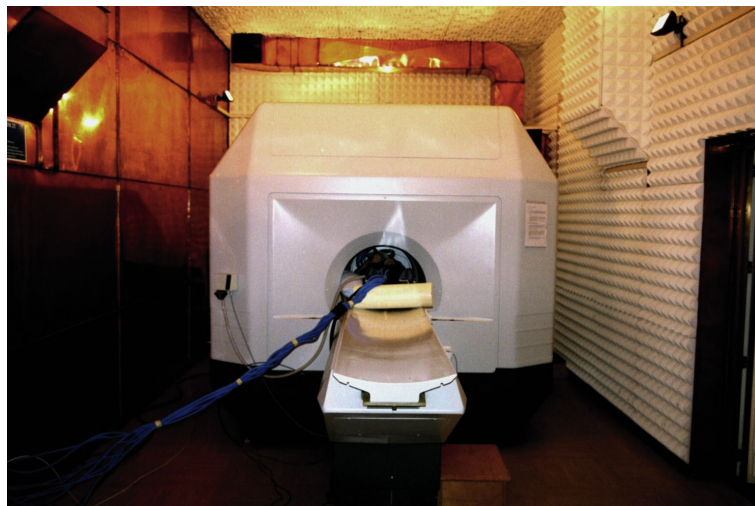


**Figure 5.1:** The fMRI in Strassbourg during an experiment with a volunteer. The pneumatic tubes connecting the PTD and the *EPI* are visible.

## 5.1 The fMRI-System in Strassbourg

The fMRI system (shown in figure 5.1) is a research-only facility affiliated to the Université Louis Pasteur. The superconductive MoTi magnet (Oxford Co, weight = 2 t) produces a magnetic field of 2 Tesla. The homogeneity is 0.1 ppm in a 40 cmsphere centered in the magnet. The inside diameter of the tube is 55 cm with gradients and body coil inserted and reduced to 33 cm by the EPI gradient coil. Maximum gradient strengths are  $30 \frac{mT}{m}$ .

Data acquisition is performed with the NMR spectrometer software *tomikon* and the imaging software *ParaVision 2.0* (Bruker). The images are initially stored in Bruker format on the local hard disk.

## 5.2 Experimental Setup

For tactile stimulation in all experiments the PTD is used. A flat version of the PTD (described in chapter 4.1) is mounted to the waist of the proband with its display contacting the abdomen. This setup was chosen because of practical reasons. The somatotopic representation of the fingertips and the foot are larger than the representation of the abdomen. But the diameter of the concave-shaped PTD cannot be adapted individually to each subject and the stimulus does not have the same intensity for everybody. Thus inter-subject comparisons would lose significance. The fingertips are not chosen for stimulation because the pneumatic controlling does not allow designs in the millimeter range.

For visual stimulation the goggles are worn the same way as swimmers do and are fixated by a silicon strap. During the experiment the proband keeps the eyes shut because it is more comfortable during the rather long acquisition time. The goggles provide such strong lights, that they are well perceived even through closed eyes. The visual activation is chosen due to its high and reproducible activation in the primary visual cortex. The activation is used as a reference signal to



**Figure 5.2:** A subject fully equipped for an experiment with the PTD mounted to its abdomen and headphones covering the ears.

the tactile activation. Previous studies have shown that the amplitude of the fMRI response in V1 peaks at a flickering frequency of approximately 8 Hz [OLC<sup>+</sup>01]. This frequency is used for all visual stimulations.

As the coils of the magnet cause a lot of noise, the subjects are equipped with ear plugs and headphones. The headphones can also be used to talk to the subjects. Visual stimulation from the environment is restricted to a minimum by the goggles.

In order to minimize movements a head foam is used and the volunteer's head is taped to the head restraint. Figure 5.2 depicts a volunteer with his head fixed to the head restraint and equipped with the headphones. Every subject holds a so-called 'panic ball' while it is in the MRI tube. When the subject squeezes the panic ball an emergency light turns on and the subject is immediately pulled out of the tube.

The activation pattern is controlled from a laptop in the fMRI control room. During the experiment a log-file is written by the TVSSCS which protocols the relative timing of the fMRI trigger and the applied pattern.

## 5.3 The Design of the Experiments

In the experiments a brief stimulus with a duration comparable to the TR of the fMRI (2 s) is applied. If the applied stimulation is of the same or shorter length as the TR, the design is called event-related. The research in the last years focuses on the optimization of event-related stimulation. Event-related stimulation has its major problem with a low SNR. The boxcar stimulation is the more conservative alternative, which is still used in many classical experiments such as the experiments of the *SenSub* project.

### 5.3.1 Event-related Stimulation

The interest in event-related designs is increasing strongly [JH99] since it has several advantages towards boxcar stimulation. Event-related stimulation can be split up into single trials with randomized order and timing. This allows to exclude any systematic influence from previous trials or cognition effects of the subject [JH99]. The single trials can be categorized individually according to the subject's performance such as reaction time and can be related to a single stimulus.

Everyday life includes events that cannot be blocked such as recognition or if the event of interest includes reactions such as astonishment. For an event-related paradigm the stimulation time is close to the recognition time. There are indications that tactile perception will change due to familiarization effects and the attention of the subject decreases if the stimulus remains constant longer than a couple of seconds. Furthermore, there are events that occur unpredictable and they can only be modelled by an event. An example for this is the spontaneous transition in the perception of ambiguous figures ([And01]).

The reason why event-related designs are chosen for the current study is mainly because they made it possible to extract and model the *hrf*. And to improving the SNR of tactile, event-related experiments by finding a better fit for the 'tactile' *hrf* than the general template implemented in *SPM*.

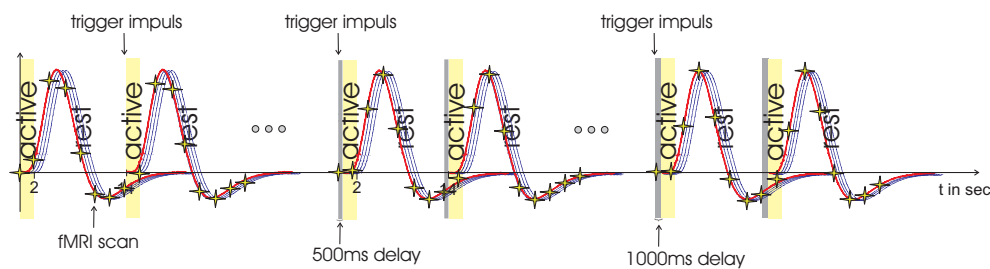


**Figure 5.3:** Schematic drawing of stimulation timing with hemodynamic response. The SOTs are variable delayed versus the measurement. Thus, different points on the curve are scanned and can be superimposed for fitting. With the same number of total scans the individual *hrf* can be fitted at more distinguished points

### 5.3.2 Paradigm Design

Two sessions have been carried out with each volunteer. The first session includes 438 scans (14.6 *min*) and the second session lasts for 724 scans (24.1 *min*). Both sessions utilize the PTD and the goggles in a vibrating mode whereas the aim differs between sessions.

In the first session the two stimulation devices are applied with equal length of active and rest phases in order to receive a comparable activation pattern for visual and tactile perception. The PTD and the goggles are only activated exclusively, with the goal to compare the shape of the hemodynamic response for both modalities.

The second session modifies the PTD vibration frequency to search for dependencies of the hemodynamic response on the tactile vibrating frequency.

In both sessions a variable shift of the activation versus the fMRI trigger is applied (see figure 5.3). If the stimulus onset is shifted for a fraction of TR the scans will take different measure points of the hemodynamic response. This simulates a higher temporal resolution of the fMRI without decrease of spatial resolution [BZH<sup>+</sup>99].

For all tactile stimulation the PTD is operated at 5 bar displaying repeatedly the same pattern which is shown in 5.4. The stimulation timing in the paradigm is given relative to the trigger of the fMRI.

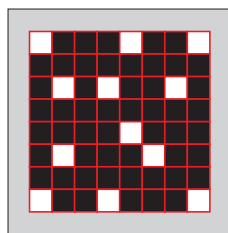


**Figure 5.4:** Pattern displayed by the PTD. The black/white squares depict taxels that are OFF/ON.

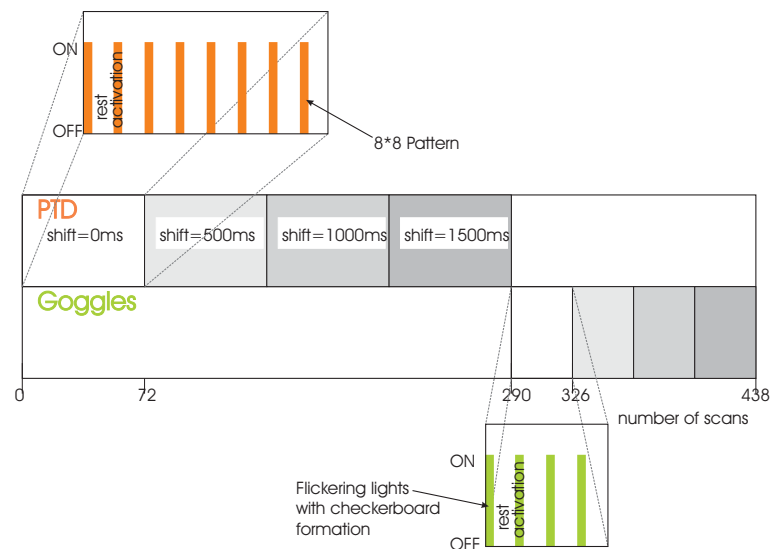


**Figure 5.5:** Design of the first session: the PTD activation is illustrated with orange and the goggles with green bars. The PTD vibrates during 2.5 s with 4 Hz, the goggles flicker for 2.5 s with a frequency of 8 Hz.

### Design of the Paradigm for Modelling the *hrf*

Since the activation in the primary visual cortex is much stronger compared to activation in the primary somatosensory cortex, the tactile stimulation is applied twice as often as the visual stimulation.

The 10 min of PTD stimulation consists of 32 epochs (18 s each) beginning with 2.5 s active and 15.5 s rest phase. The trials can be divided into four sets of 8 activations whereas between each set 500 ms pause are inserted. This delays the activation in the second (third/fourth) set with 500 ms (1000 ms /1500 ms) towards the fMRI trigger. On the PTD a randomly chosen constant pattern (see figure 5.4) is displayed at 4 Hz vibration frequency.

In the second part, 8 Hz flickering lights with checkerboard formation are used to trigger the hemodynamic response in the visual cortex of each subject. The timing is similar to the previous part with the goggles active instead of the PTD and every set consisting only of four trials (see figure 5.5).

The PTD and goggles are combined into one session to exclude any inter-session differences for the comparison of the response [MHA<sup>+</sup>00].

### Design of the *Parametric* Paradigm

To investigate a rate dependency of the human somatosensory cortex due to vibrational tactile stimulation the vibration frequency of the PTD is varied. Since the frequency of the stimulation can be added in the design matrix of *SPM* as an additional regressor the according paradigm is called *parametric*.

This paradigm focuses completely on the tactile stimulation and randomly adds goggles activation of varying duration during the whole session. This is done to maintain the attention of the subject during the rather long session of 25 min.

In the analysis the response which is evoked by the activation is compared with the response to the rest phase. The rest phase is always modelled by a constant baseline. When no task is applied, the response in rest phase can shift due to spontaneous brain activation. Thus, the goggles activation is placed in the 15.5 s rest phase of the PTD to create a better defined baseline.

In order to get sufficient statistics 16 trials were performed with five frequencies. Only for frequencies up to 6 Hz the force on the skin is comparable. Thus 2, 3, 4, 5 and 6 Hz are chosen and applied in a random order to exclude recognition or habituation effects. The session contains altogether 80 trials with each consisting of 2.5 s active and 15.5 s rest phase.

### 5.3.3 Experimental Procedures

For every subject a series of functional EPI-scans is recorded with an echo-time  $TE = 40\text{ ms}$  and a repetition time of  $TR = 2\text{ s}$ . To reduce TR no fat suppression was performed and only 20 slices with a thickness of 4 mm have been acquired. The slices cover the area from superior edge of the cortex (SI) to caudal edge (V1). The field of view of 25 cm and a slice resolution of  $64 \times 64$  voxels yield a voxel size of  $1\text{ vx} = 4\text{ mm} \times 4\text{ mm} \times 4\text{ mm}$ .

To account for saturation, three dummy images are made before the first image is taken. In case no earlier session existed, a structural, high-resolution  $T_2$ -weighted scan (structural image) with a resolution of  $128 \times 128 \times 80\text{ vx}$  and a voxel size of  $1\text{ vx} = 2\text{ mm} \times 2\text{ mm} \times 2\text{ mm}$  is taken for each subject.

For every proband the same paradigms were prepared, but not always completed. This was due to trigger errors by the TVSSCS in two cases and for proband the last 54 scans had to be discarded because of a sudden translation that leads to linear correlation of the movement regressors. If a trigger error occurred the acquisition was finished without stimulation.

For this set of experiments no Fourier filter was applied during the acquisition since this is not necessary when *Quickshot* is utilized for the conversion into the *Analyze*-format.

## 5.4 SPM Analysis

All preprocessing is done with *Quickshot*, the parameters are shown in the Manual in appendix E. For the first session,  $\text{snr}^*$  as well as  $\text{sr}^*$  images are created and estimated with a similar design matrix. For the second session, only  $\text{snr}^*$  images are needed. For both sessions a high pass filter is applied with a cutoff at 60 s. *SPM* accounts for low frequency confounds by including them in the model with zero weight.

### 5.4.1 Design Matrix for the Session: Modelling the *hrf*

The design matrix includes ten regressors plus the baseline. The first (third) vector gives the SOTs (convoluted with the *hrf*) for the PTD (goggles). To account for variations in response onset the derivative in respect to time is added as the second and fourth regressor. This increases the amount of regressors and decreases the degrees of freedom. The Plot of the ‘contrast of parameter estimates’ after having performed an F-test with the effects of interest for the PTD as contrast is shown in figure 5.6. The high amplitude for the derivative shows that including the derivative as regressors outstrips the reduction of the degrees of freedom. The full design matrix is shown in figure 5.7.

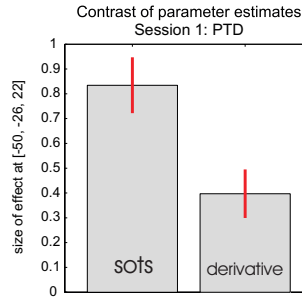


**Figure 5.6:** Contrast of parameter estimates of an F-test at an highly significant voxel in SI. Applied contrasts are  $\vec{c}_1 = [1 \ 0]$  and  $\vec{c}_2 = [0 \ 1]$ . The contrast for the derivative is almost as high as for the SOTs.

### 5.4.2 Design Matrix for the *Parametric* Session

*SPM* allows to test for dependencies between fMRI response and any polynomial order of a stimulation parameter. This is realized by additional regressors in the design matrix. In a *parametric* design matrix the first vector includes all SOTs, the second vector relates every onset to a value of the parameter (which is equal to first polynomial order). For every additional polynomial order another regressor is added, starting with the quadratic term. For the following evaluations the terms up to third order are included.

To explicitly test for the different frequencies a second design needs to be specified and the model estimated. In this design the SOTs of each frequency are written into its own regressor. The temporal derivative is again added for each frequency.

For exclusion of movement-related artifacts the translation and rotation vectors are added into both models.

### 5.4.3 Contrasting

For the first session two contrasts are applied. If testing for activation due to PTD stimulation, the contrast  $\vec{c}_{ptd} = [4 \ 1 \ 0 \ 0]$  is applied. For regressors that no weight given (here the movement and baseline regressors) *SPM* automatically applies zero weight. The factor of 4 to 1 between SOTs and derivatives origins from plotting the ‘contrasts of parameter estimates’ and averaging their amplitudes for several voxels in the **Region Of Interest** (see figure 5.6).

Activation due to goggles stimulation is tested for by applying the contrast  $\vec{c}_{gog} = [0 \ 0 \ 4 \ 1]$ . The factor between SOTs and derivative is kept constant. An example for visualizing goggles activation is shown in appendix C.4.

The contrasts for the second session are not as straight forward. Again, the factor between a regressor and its time derivative is kept 4 to 1. With the contrast  $\vec{c}_1 = [4 \ 0 \ 0 \ 0 \ 1 \ 0 \ 0 \ 0]$  only the SOTs have a nonzero weight and thus the t-test is estimated for. A second contrast  $\vec{c}_2 = [0 \ 4 \ 4 \ 0 \ 0 \ 1 \ 1 \ 0]$  searches for voxels that show a high correlation to combinations of first and second order. These contrasts are illustrated in figure 5.7. In the same way, first, second and third can be tested separately or in any combination.

When weighting the second model with the contrast  $\vec{c}_3 = [4 \ 1]$ , only voxels that exhibit correlation to the SOTs of 2 Hz will show significance (see figure 5.7(d)).

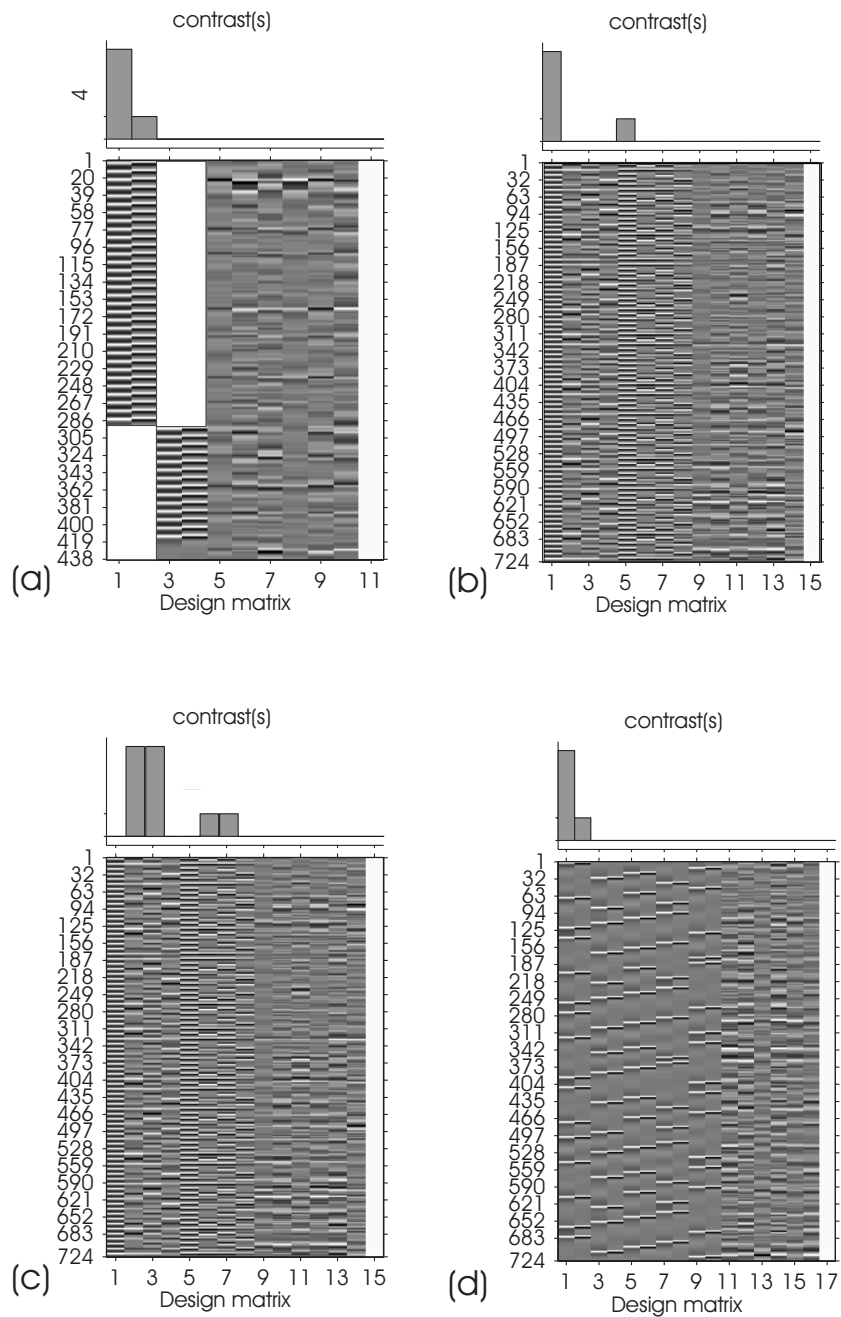


**Figure 5.7:** Design matrix and contrasts for the two sessions: (a) first session; testing for goggles activation, (b) second session; testing for SOTs, (c) second session; testing for first and second polynomial-order of stimulation frequency, (d) second session; alternative design, weighting the SOTs of 2 Hz.

# Chapter 6

## Results

### 6.1 Localization of the Observed Activity

#### 6.1.1 Experiments in Literature

Vibrational tactile stimuli have been examined on humans with fMRI technique before using various stimulation techniques. All experiments presented below utilize boxcar design for their stimulation timing. So far no publications on event-related experiments with tactile stimulation could be found.

Joseph A. Maldjian *et al.* [JM99] performed an fMRI study on seven subjects using a 15-30 Hz vibrational stimulus to the finger. They demonstrate robust bilateral activation in SII and contralateral activation in SI. The area of activation in SII is larger and has greater t-values than the observed activation in SI. Activation in SI and SII is not observed for all subjects.

Gregory S. Harrington and J. Hunter Downs [HD01] tested eight subjects for response differences due to vibration (150 Hz) and flutter (35 Hz) stimulation which was applied to the fingertip. The result for activation dependencies on the stimulation frequency is inconclusive for the different subjects. Consistent to other studies large activation is visible in bilateral SII and contralateral SI.

Elizabeth Disbrow *et al.* [DRK00] recently published a study about the somatotopic organization of cortical fields in the lateral sulcus. Eighteen subjects were stimulated with a sponge rubbing different parts of the body (face, hand, shoulder, foot, hip and leg). Focusing on the area around the lateral sulcus, the most consistent locus of activation is on the upper bank of the lateral sulcus continuing onto the operculum. Two adjacent areas are smaller and are activated less consistently. These are indications of somatotopic organization of SII and parietal ventral areas.

Stefanie Runde [Run00] performed first experiments with a  $4 \times 1$  version of the PTD stimulating parts of finger, foot and arm of three subjects in a boxcar design. The results are inconsistent and the statistics are too low to draw conclusions. Both, contra- and ipsilateral SI and SII are involved in most sessions.

#### 6.1.2 Mapping the Activation on MNI Template

To get a first impression of the strength and location of the measured activation, the normalized data is presented on the glass brain (compare appendix C.4). The data from all six subjects has undergone the same processing steps and is thresholded in exact the same way within one set. The amount of colored voxels indicates the expansion of activation and can be compared for the

different subjects within one set. Conclusions on the significance of a voxel or cluster can only be drawn by stating the t-values.

In figure 6.1 the results from the goggles measurement are presented. This experiment has been performed as a reference to the tactile activation and to extract the visual *hrf* for comparison with the tactile *hrf*.

The activation induced by the flickering goggles is recorded over 149 scans if not stated differently in the text below the glass brains. The thresholding of the t-maps, which are referred to as SPM{t}s, is done at a  $p_{corr} = 0.001$  and a spatial extent  $k = 10$  vx. All activities withstanding this threshold can be said to have a probability of less than 0.1 % to have occurred by chance.

Four of the six subjects show large and well localized activations in V1. E. g. for *lemla* the main active cluster covers with 2047 voxels and a maximum t-value of 15.6 Brodman area 17 and partially 18 and 19 (see figure 6.1(c) and figure C.4 in the appendix for the t-values). With a voxel size of  $1vx = 2mm \times 2mm \times 2mm$  the cluster size accords to  $16.4cm^3$  or a cube of  $2.5cm \times 2.5cm \times 2.5cm$ .

During the fMRI session with *heina* accidentally only one side of the goggles were connected properly and thus only one eye was stimulated. Since the optical pathway from one eye is split up in the optical chiasm (see section 1.3), the signal from one eye is spread on both sides of the sagittal fissure in V1 (see figure 6.1(a)).

For *lelet* eight smaller clusters with eleven to fifty-seven voxels are located superior and anterior to the lateral sulcus.

Although only a maximum of 149 scans (e. g. 95 scans for *mauth*) have been recorded, the activation for all subjects is localized within the visual cortex.

This is not the case for the tactile activation as elicited by the PTD in the first session during 288 scans. The thresholding of the SPM{t}s is done at a  $p_{uncorr} = 0.001$  and a spatial extent  $k = 10$  vx. All subjects exhibit several small activation clusters in mainly four regions. Two regions are located bilateral in SI, caudal in the cortex, some voxels lateral from the sagittal fissure. E. g., for *pauca* it exhibits a size of 68 voxels (as indicated in figure 6.2 (f)).

A larger activation area spreads around the lateral sulcus, reaching from lateral to some centimeter into the parietal operculum. It appears as well in both hemispheres. The biggest cluster is visible for *pauca* with 1013 voxels.

Based on the 289 scans of event-related, tactile stimulation can activation in the somatosensory cortex be seen, whereas it is not sufficiently localized. During these 289 scans the PTD is active for altogether 80 s. When applying the same threshold as previously for visual stimulation (threshold  $t = 5.1$ ) the glass brains are almost empty with exception of the **Maximum Intensity Projection** for *pauca*. Thus, the second session recorded over 724 scans is added for a more accurate activation localization.

The second session is presented with the thresholded applied at  $p_{corr} = 0.05$  and a spatial extent  $k = 10$  vx in figure 6.3. The SOTs of all frequencies are weighted equally versus the rest phase (where randomly visual stimuli are filled in).

*Heina* exhibits altogether 13 clusters in the ROI of which four consist of more than 300 voxels each. The activation can be divided into five separated regions. The four main regions (t-score of 14) are bilateral SI and bilateral around the lateral sulcus. One cluster with 98 voxels is located ventral and lateral to SI in the center between the lateral sulcus and the dorsal border of the brain (t-score of 7). It is not in the ROI.

*Kelge* is the only subject where the two most significant clusters are located in SI with 345 voxels in the left and 305 voxels in the right cortex, both containing a t-value of 14. Seven smaller cluster

		<i>heina</i>	<i>kelge</i>	<i>lelet</i>	<i>lemla</i>	<i>mauth</i>	<i>pauca</i>
SI	left	306	345	15	15	67	53
	right	257	305	–	–	89	60
SII	left	378	206	99	144	1051	170
	right	571	46	–	10	776	509
$\frac{SII}{SI}$		1.7	0.4	6.6	10.3	11.7	6

**Table 6.1:** Number of active voxels that are observed in the somatosensory cortex for the second session at given threshold ( $p_{corr} = 0.05$ ,  $k = 10$  vx). Left and right denotes the hemispheres in the brain and not the side in the glass brain.

(24 to 90 voxels) are spread bilateral at the height of the lateral sulcus some centimeters deep in the cortex.

*Lelet* shows only two small cluster, containing 15 and 99 voxels. These are both located in the left hemisphere. One appears in the dorsal cortex, close to the sagittal fissure. The other one lies in the center of the ventral-dorsal axis in the lateral cortex, ranging several centimeters medial into the cortex. It is similar for *lemla* where three of four clusters are distributed in the left hemisphere in just the same two regions. The fourth and smallest cluster lies mirrored to the ones in the lateral cortex.

The MIP for *mauth* is comparable to *heina*'s. It is discussed in detail during the next section. For *pauca* are altogether thirteen clusters detected. One big cluster containing 370 voxels is located lateral on the left side in the ventral-dorsal center. The biggest cluster in the left SI covers 53 voxels, whereas in the right SI two clusters of 25 voxels each are active. Several clusters lie in the dorsal-ventral center of the brain, two of these dorsal from the central sulcus stretching into the occipital lobe.

The amount of all activated voxels that clearly could be assigned to be located in SI or SII are listed in tabular 6.1. This was done to examine the ratio between the extension of activation in SI versus SII. It is striking that for all subjects but *kelge* the activation in SII covers a several times larger area than in SI. Calculating the mean of  $\frac{SII}{SI}$  without taking *kelge* into account gives a ratio of  $\frac{SII}{SI}_{mean} = 7.3$  with a variance of  $\frac{SII}{SI}_{var} = 3.9$ . This means that the tactile activation covers an approximative seven times larger area in SII than in SI.

The motivation to exclude *kelge* from the calculation of the mean value derives from the lack of fMRI experience of this proband. All other probands have participated in several other studies and are used to the special environment of the fMRI. An easy explanation to an over-average activation in the dorsal cortex would be that the motor cortex is involved as well. Stefanie Runde has observed activation in the motor cortex for experiments with the PTD mounted at the proband's finger, foot and arm [Run00]. She claimed this to be due to a non-comfortable positioning of the PTD which can invoke the proband to think about moving. Another possible explanation is that the proband jerks at each onset of the PTD. This activation cannot be distinguished by the analyze, it has to be excluded by cause of the localization. The most reliable way to confirm the activation is a new session with *kelge* because the circumstances and the performance of the PTD are now familiar.

When allocating activation into a certain area or when comparing results between subjects for normalized data the quality of normalization has to be noted. In all sessions only 20 slices were

recorded for each subject. Dependant on the size of the proband's head this volume can be a sufficient or not to perform an reasonable good coordinate transformation. Even if more slices (e. g. 32 slices) are acquired the normalization can contain variances in the order of 10 *mm* especially in the outer region of the brain. For a poorer normalization the localization can vary up to some centimeters from one subject to another.

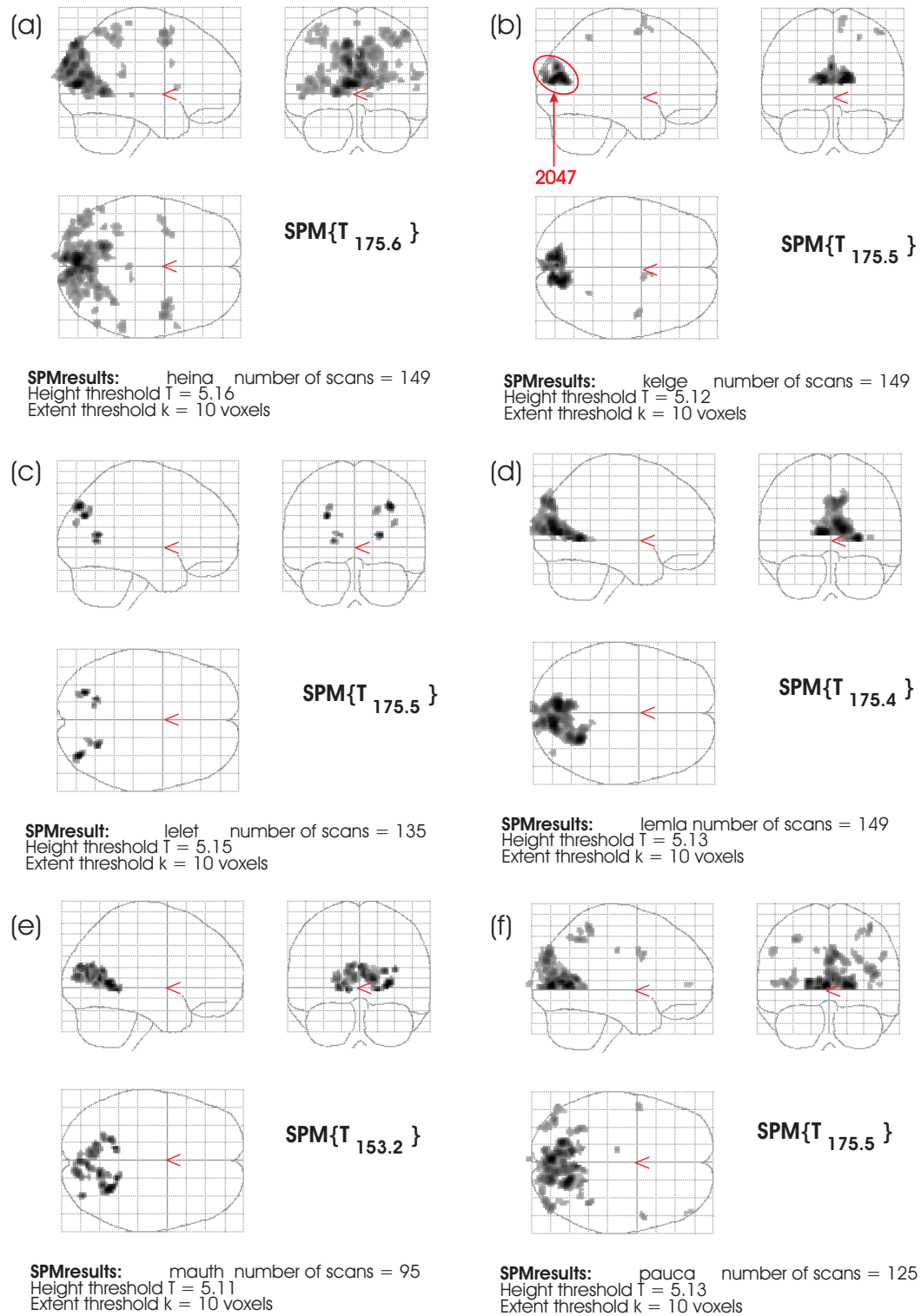


**Figure 6.1:** Set of  $SPM\{t\}$ s shows the activation induced by visual stimulation for six different subjects. The contrast  $c_{gog}^{\rightarrow} = [0\ 0\ 4\ 1]$  (see figure 5.7 for the corresponding design matrix) has been applied to the first session. The red number specifies the size of a separated cluster in voxels.

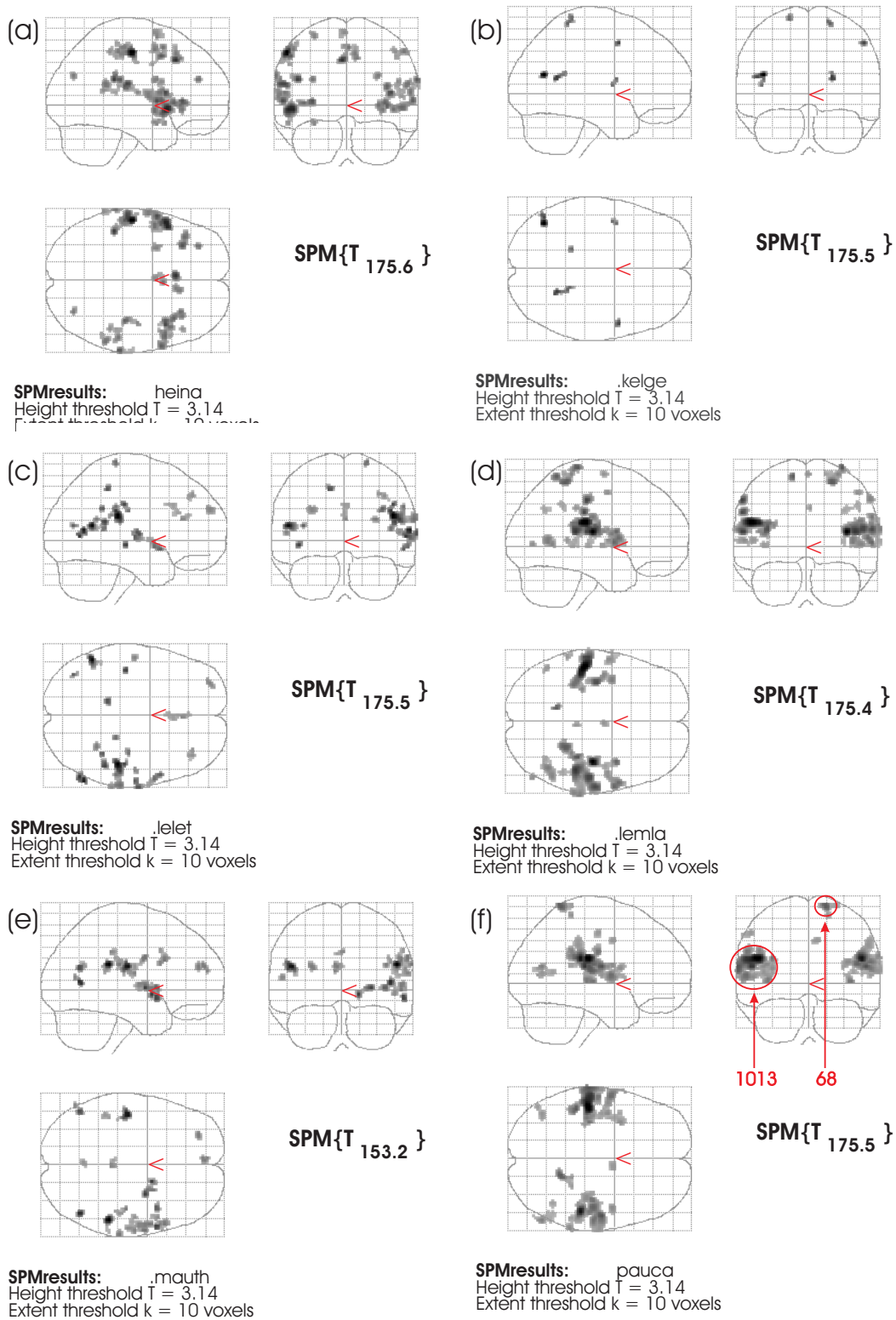


**Figure 6.2:** Set of SPM{t}s shows the activation induced by tactile stimulation for six different subjects. The contrast  $\vec{c}_{pid} = [4 \ 1 \ 0 \ 0]$  (see figure 5.7 for the corresponding design matrix) has been applied to the first session. The red numbers specify the size of separated clusters in voxels.

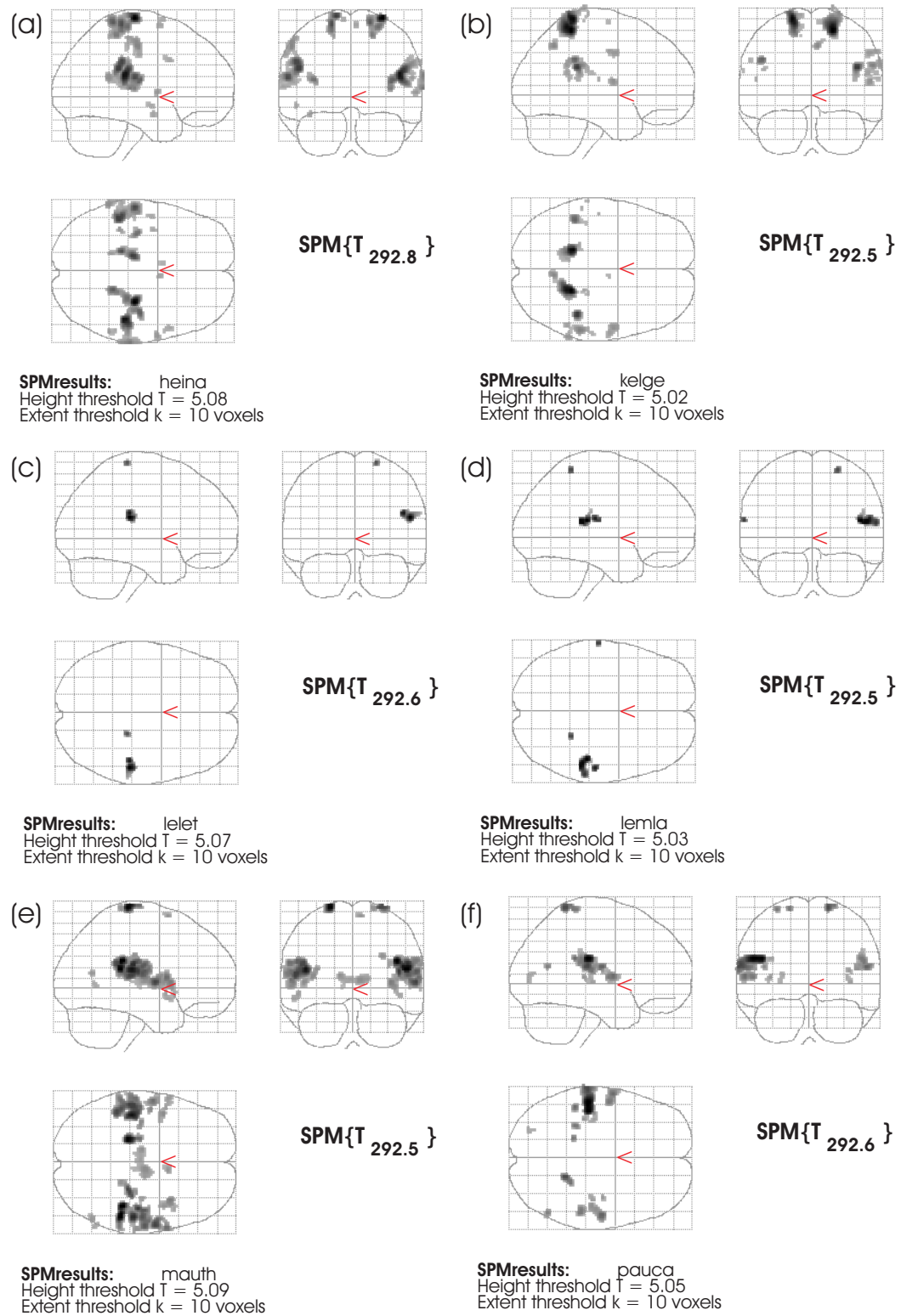


**Figure 6.3:** Set of  $SPM\{t\}$ s for the second session showing the activation induced by tactile stimulation for six different subjects. The applied contrast is  $\vec{c}_1 = [4\ 0\ 0\ 0\ 1\ 0\ 0\ 0]$ , see figure 5.7 for the corresponding design matrix.

### 6.1.3 Precise Localization of the Activation for one Subject

Only superposition of the thresholded SPM{t}s onto a coregistered structural scan of the subject can accurately localize the activated clusters of non-normalized data. This is done for the first the visual activation from the first and the tactile activation from the second session of the study. This section presents series of coronal and sagittal slices of the coregistered structural scan of subject *mauth* with superimposed SPM{t}s from visual and tactile stimulations. The lateral and central sulci were localized by visual inspection through comparison to a brain atlas ([JN95]).

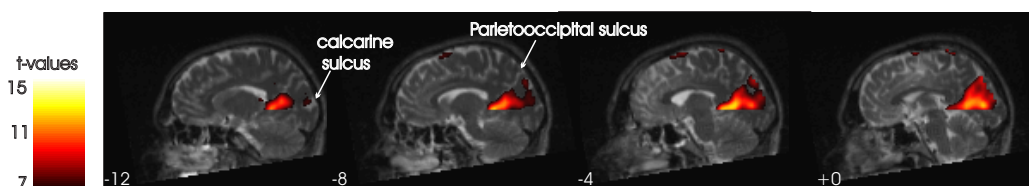


**Figure 6.4:** Sagittal slices of the structural scan of *mauth* with superimposed SPM{t}s showing activation induced by the visual stimulation. The number on the scan denotes the x coordinate, which is as well the distance to the middle slice in millimeters.

With the applied threshold of  $p_{\text{corr}} = 0.001$  and  $k = 5 \text{ vx}$  several clusters with altogether 880 voxels are visible in the visual cortex (see figure 6.4). The activity is located around the calcarine and preoccipital sulcus. The area around the calcarine sulcus defines the primary visual area (Brodmann area 17). Rostral to the primary visual cortex are the visual association regions located such as Brodmann area 18 and 19. Both are involved to some degree in the task. In figure 6.4 only the left hemisphere is presented since the right hemisphere exhibits same characteristics.

The applied threshold of  $p_{\text{corr}} = 0.001$  and  $k = 5 \text{ vx}$  yields two clusters in the dorsal cortex of the coronal slices. The smaller cluster is visible in the right hemisphere on slices  $y = -44$  to  $y = -34$  with  $t_{\text{max}} = 9$ , containing 13 voxels (number 1). Since the data which is overlaid with an structural scan is not normalized, one voxel here has a size of  $4 \text{ mm} \times 4 \text{ mm} \times 4 \text{ mm}$ . Thus, 13 non-normalized voxels assign to 104 voxels in normalized SPM{t}s as used in the previous chapter. The second cluster appears more anterior in the left brain at  $y = -32$  to  $y = -20$  and exhibits a t-value of 11.5 with an extension of 25 voxels (cluster 2). Both clusters can as well be found on the sagittal slices. The left cluster is visible on slice  $x = -20$  to  $x = -2$ , whereas the right cluster is visible on slice  $x = 28$  and  $x = 34$ . On the sagittal slices it can be distinguished that the right cluster is further anterior than the left one. Still they both lie in the postcentral gyrus at the posterior upper edge of the central sulcus. This is exactly where activation of the stomach is supposed to be projected according to the *Somatosensory Homunculus* (see figure 1.9). The asymmetry between the left and right half of the brain is a natural and direct consequence of the individual structure of the human body and brain. In sagittal slices  $x = -8$  and  $x = -2$  a third cluster appears anterior of the second one, in the medial frontal gyrus. It is visible on the coronal slices  $y = -6$  to  $y = 0$ , which are not printed here. No reasonable explanation can be offered for the occurrence of this cluster.

In the coronal slices in figure 6.5, there are three clusters active in the dorsal-ventral center (cluster 4, 5 and 6) beyond the clusters in dorsal cortex. Cluster 6 appears in the extension of the brain stem, in what can be either the thalamus or the mid brain. It covers a large area of 52 voxels, but has a low significance with  $t_{\text{max}} = 7.2$ . An active cluster in this region is not surprising and not within the ROI. The remaining two clusters are in contrast to this very interesting since their

origin is intuitively not clear. In order to localize the full extension of these rather large clusters, brain maps which show the full sagittal view of the lateral part of the left and right hemisphere are added in the appendix C.5.

Cluster 4 is located in the right hemisphere with its maximum t-value of 11.5 on the sagittal slice  $x = -36$ . It exhibits an extension of 173 voxels, i. e. an equivalent to a cube of  $11 \text{ cm}^2$ . When following the slices from lateral to medial (in figure C.6 in the appendix from top to down) the lateral activation stretches almost to the caudal cortex (slice  $x = -56$ ). It then unites with a more rostral cluster and remains active until slice  $x = -28$ . The cluster is located over the whole depth of the lateral sulcus, as visible in figure 6.5 on coronal slice  $y = -20$ . The ‘center of mass’ of the cluster is located ventral to the central sulcus, spreading both, caudal and rostral into the lateral sulcus.

In the left hemisphere cluster 5 appears almost as a mirrored image of cluster 4. It contains 167 voxels and the maximum t-value of 10.7 is visible on sagittal slice  $x = 52$ . Again the activation is located in the lateral sulcus starting from only some voxels at the lateral edge into the full depth of the groove. This cluster lies well localized at the crossing of the central sulcus and the lateral sulcus if one extrapolates the central sulcus in ventral direction (compare figure C.7, slices  $x = 60$  to  $x = 66$ ).

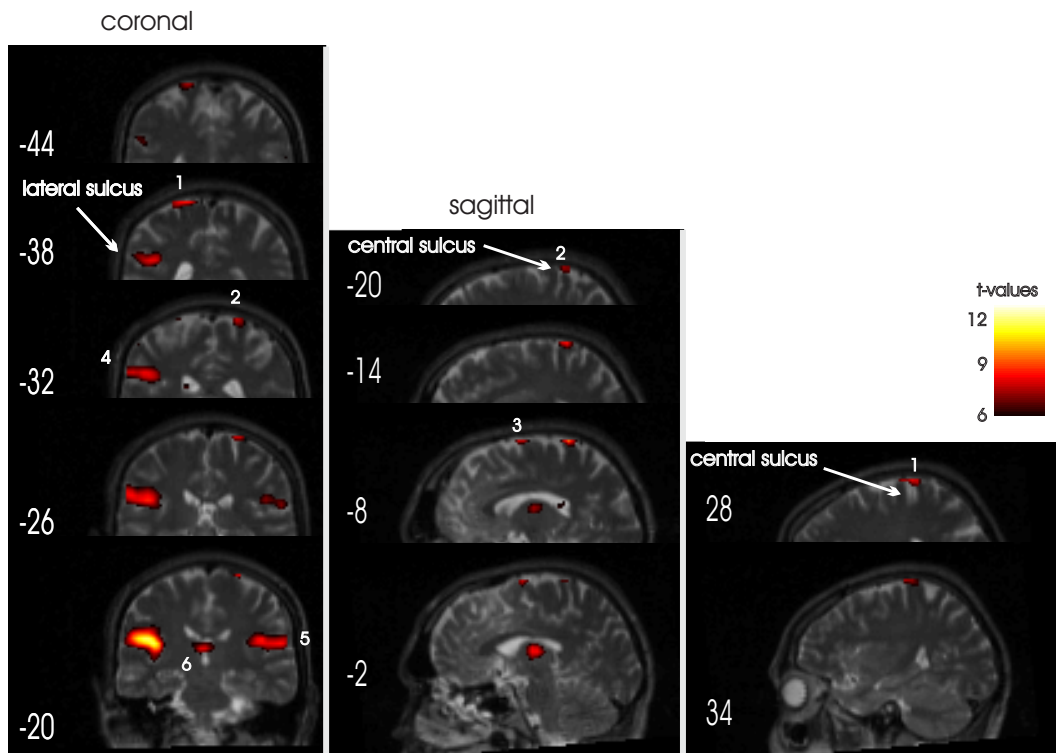


**Figure 6.5:** Coronal and sagittal slices of the structural scan of *mauth* with superimposed  $\text{SPM}\{t\}$ s weighting the tactile stimulation of the abdomen. The slices are separated by  $6 \text{ mm}$  each, the number on the scan denotes the  $y/x$  coordinate (coronal/sagittal), which is as well the distance to the middle slice in millimeters. Numbers are assigned to active clusters.

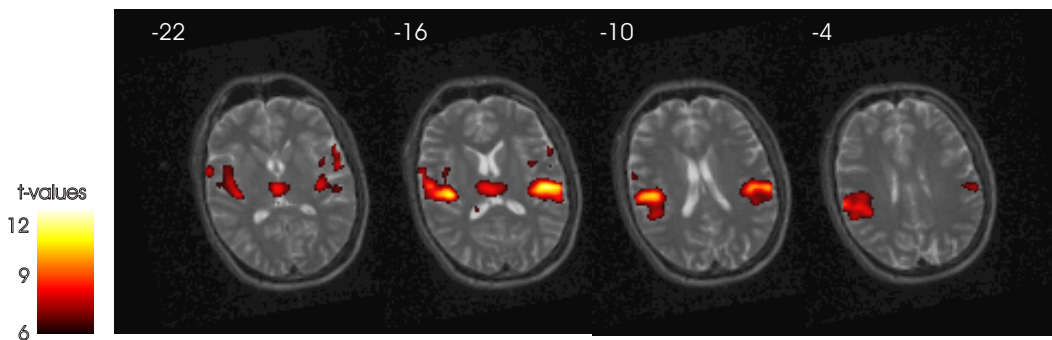


**Figure 6.6:** Axial slices of the structural scan of *mauth* with superimposed SPM{t}s weighting the tactile stimulation of the abdomen. The slices are separated by 6 mm each, the number on the scan denotes the z coordinate, which is as well the distance to the middle slice in millimeters. Numbers are assigned to active clusters.

#### 6.1.4 Summary of the Activation Localization

The activation has been discussed roughly for all subjects and sessions in section 6.1.2 and more intense for the subject *mauth* in the previous section. From the precise localization of the activation on the structural scans conclusions can be drawn for all subjects. The comparison of the normalized data shows no significant difference between the subjects. It becomes evident that 288 scans, as achieved in the first session, is not enough to accurately map tactile activation using event-related stimulation. For visual experiments utilizing a similar timing of the stimulation 149 scans are sufficient for receiving a localizable activation pattern.

The second session (724 scans in a similar design) allows a very precise localization of four activated areas in the cerebral cortex which are induced by tactile stimulation. Two areas can be identified where the bilateral representation of the stomach in the primary somatosensory cortex is expected. The activation in SI covers a rather small area of  $1 \text{ cm}^3$ . It appears on one side in all subjects and bilateral for four out of six subjects.

The stimulation is intended to be in the center on top of the stomach, therefore the onesided activation cannot be referred to as ipsi- or contralateral. A misalignment of the PTD would explain such an onesided activation in the cortex.

The remaining two clusters appear in the region where the bilateral representation of SII is expected. In the left hemisphere the activation reaches further posterior to where the primary auditory cortex is expected. The activation clusters cover a large area of up to  $11 \text{ cm}^3$  and appear in all subjects on one side and in five of six subjects on both sides. The mean ratio of the activated area in  $\frac{SII}{SI}$  calculated from five subjects is  $\frac{SII}{SI}$  of 7.3.

The activation localization is consistent with the expected activation as it has been observed in similar experiments. Most publications report a more robust activation in SII that covers a larger area as the activation in SI. J. A. Maldjian *et al.* [JM99] report a mean  $\frac{SII}{SI}$  of 5.6 in their study (see section 6.1.1). The two results are very close, especially when taking into account, that four of six subjects show a ratio of approximately this value and only *heina* and *pauca* exhibit larger values.

The possibility that activation is located in the primary auditory cortex due to acoustic stimulation from the PTD can be diminished to a very low probability. (i) The other experiments utilize totally different mechanisms, such as rubbing with a sponge or vibrations by a piezoceramic device, but

still observe a similar activation pattern in the cortex. (ii) Mapping t-values on the structural image allows a localization of the activation in the dorsal cortex, where SI is located and around the crossing of the central and lateral sulcus, where SII is expected. Only in the right hemisphere the activation leaks posterior to where the primary auditory cortex is located.

The reason for activation in the secondary somatosensory cortex in this case is not clear. SII is believed to be responsible for integrative tactile functions such as textural discrimination [JM99] and it is related to tactile learning. The current knowledge about SII comes predominantly from animal studies, because SII is relative inaccessible with its location deep within the parietal operculum. The results of this study show that vibrational stimuli induce a strong reproducible response in the second somatosensory cortex and possibly somatosensory association areas.

In this study a rather simple constant pattern was applied to the abdomen. The proband was not expected to perceive cognitive perceptions. Still the cortex related to integrative processing is strongly involved. Therefore, the activation induced by flickering lights has as well been mapped on the structural scan. And even the visual activation is not limited to the primary cortex but involves the visual association areas. With this background the appearance of activation in SII may not be surprising. The involvement of higher order cortices indicates that the brain might not experience the applied task as simple as the experimenter intuitively assumes.

## 6.2 Dependencies on the Stimulation Frequency

The initiation to investigate the frequency dependence of the tactile system derives from the behavior of the visual system. For frequencies from 1 to 10 Hz a difference of 0.3 to 1.1% of the BOLD signal has been observed by B. Ozus *et al.* [OLC<sup>+</sup>01]. The amplitude of the fMRI response increases with the frequency and plateaus at 6 Hz. The response peaks at approximately 8 Hz. They suggest that the cortical activity is related to visual processing in this frequency domain.

During the second session 144 scans are recorded for each of the PTD vibration frequencies (2, 3, 4, 5 and 6 Hz). Weighting all frequencies together gives a strong and localized signal in SI and SII as discussed in the previous chapter. It is important that each frequency itself gives a detectable and roughly localizable signal. Only if this is provided, one can search for differences of activation at different frequencies. For this reason the second session of *mauth* is modelled with the second design, where all frequencies are estimated separately. The MIPs are presented in figure 6.8 with the height threshold  $p_{uncorr} = 0.001$  and a spatial extent threshold  $k = 10$  vx.

In all five maps strong activation is visible. Due to the rather low threshold some activation is visible outside the ROI, mostly in the cerebellum and brain stem, what is not unexpected for tactile activation (compare somatosensory pathways in section 1.2). With the MIPs as presented in figure 6.8 only qualitative statements about the activation for different frequencies can be done. Dependencies on the stimulation frequency can be on the basis of voxels and are probably in images such as in figure 6.8 not visible. Visual investigations of figure 6.8 integrate over the detected activity and cannot detect the behavior of single voxels (that may even show no activity at all here). To be able to detect such dependencies the *parametric* design is estimated and contrasted for all subjects.

The strongest activation is visible in *kelge*, for whom the activation maps are presented for four different contrasts in figure 6.7. Giving a nonzero weight to all orders results in a similar MIP as figure 6.3(b), where only the SOTs have a nonzero weight. This is an indication, that the voxels are mainly correlated to the onset of the stimulus and do not distinguish between the frequencies. The test for voxels, which correlate with a combination of first, second and third order results in a small cluster in the left lateral cortex at the height of the lateral sulcus. Although the threshold is only  $p_{uncorr} = 0.001$ , no activity is located in SI as it is in figure 6.3(a). Weighting only first and second order yields a large activation in the right hemisphere around the same location as the small cluster in figure 6.3(b) is located. This cluster contains 100 voxels compared to 289 voxels for (a), where the correlation to the SOTs is weighted. One cluster is located anterior to the main activation region. In (a) no activation is visible in this area. The contrast which searches for correlations to the first order of the frequency yields twenty clusters of which not all are located in SI and SII (see figure 6.3(d)). In the right hemisphere altogether 230 voxels are active in the area of SII and 30 voxels in SI. In the left hemisphere appear 74 colored voxels. The location of the other cluster seems randomly spread over the brain. The statistical threshold is applied uncorrected, so the probability that some activity occurs by chance may not be neglected.

Because of the few scans per frequency the threshold cannot be increased. There is a second possibility to decide whether the activity, which is seen for *kelge* is due to low statistics or depicts ‘real’ frequency dependence of the somatosensory system. This would include to perform a second order analysis comparing the results of the six subjects with a ‘Random Effects Analysis’. *SPM* provides the possibility to make broader inferences or conclusions about the general population using the ‘Random Effects Analysis’. It is recommendable to do so for the (c) and (d) contrasts in figure 6.7.

The analysis has not been performed within this thesis since it appeared to extend the time frame, but will be added as soon as possible.

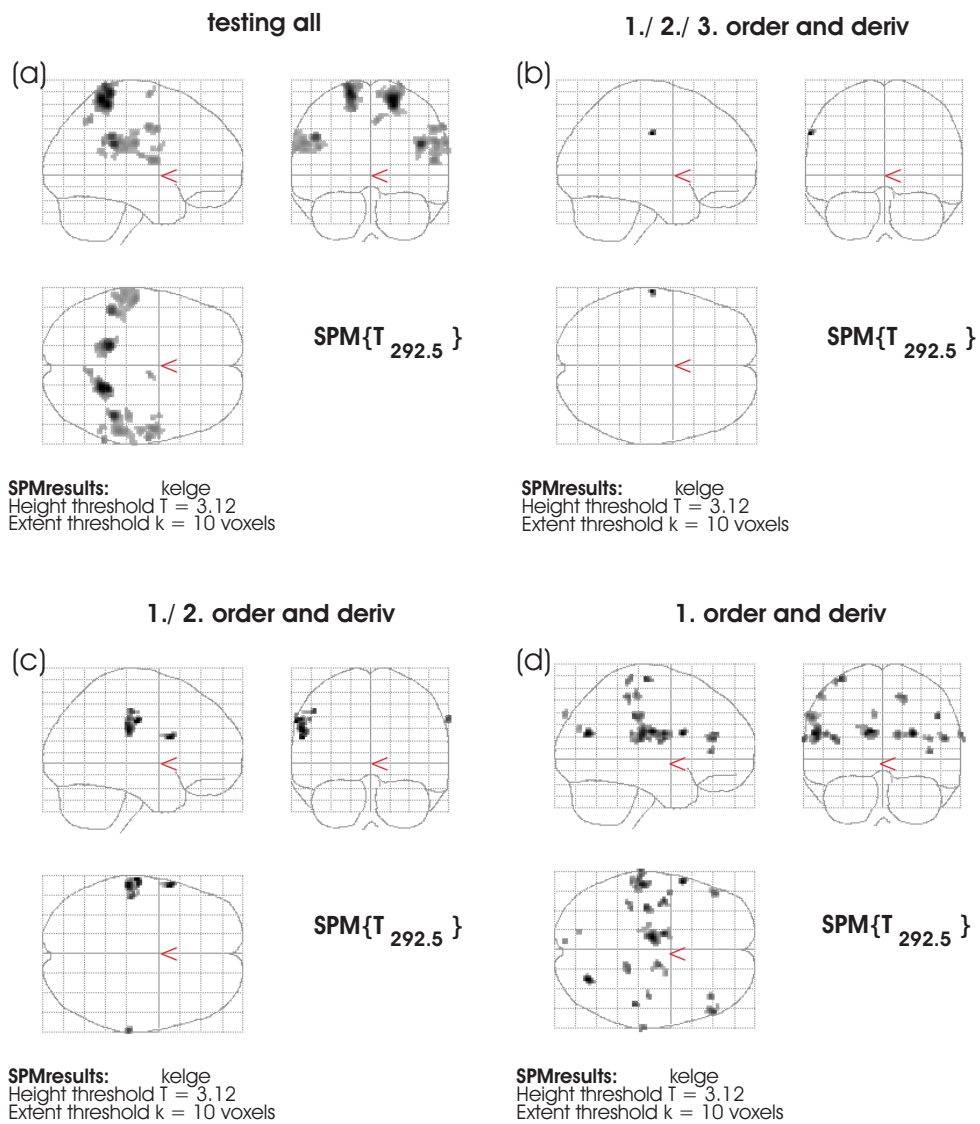


**Figure 6.7:** MIPs for the second session with *kelge* with the following contrasts applied (see figure 5.7 for the corresponding design matrix). (a) Weight on all orders with:  $\vec{c}_1 = [4\ 4\ 4\ 4\ 1\ 1\ 1\ 1]$ , (b) Weight on first, second and third plus their temporal derivatives:  $\vec{c}_2 = [0\ 4\ 4\ 4\ 0\ 1\ 1\ 1]$ , (c) Weight on first and second plus their temporal derivatives:  $\vec{c}_3 = [0\ 4\ 4\ 0\ 0\ 1\ 1\ 0]$ , (d) Weighting the first order plus the temporal derivative with:  $\vec{c}_3 = [0\ 4\ 0\ 0\ 0\ 1\ 0\ 0]$ .

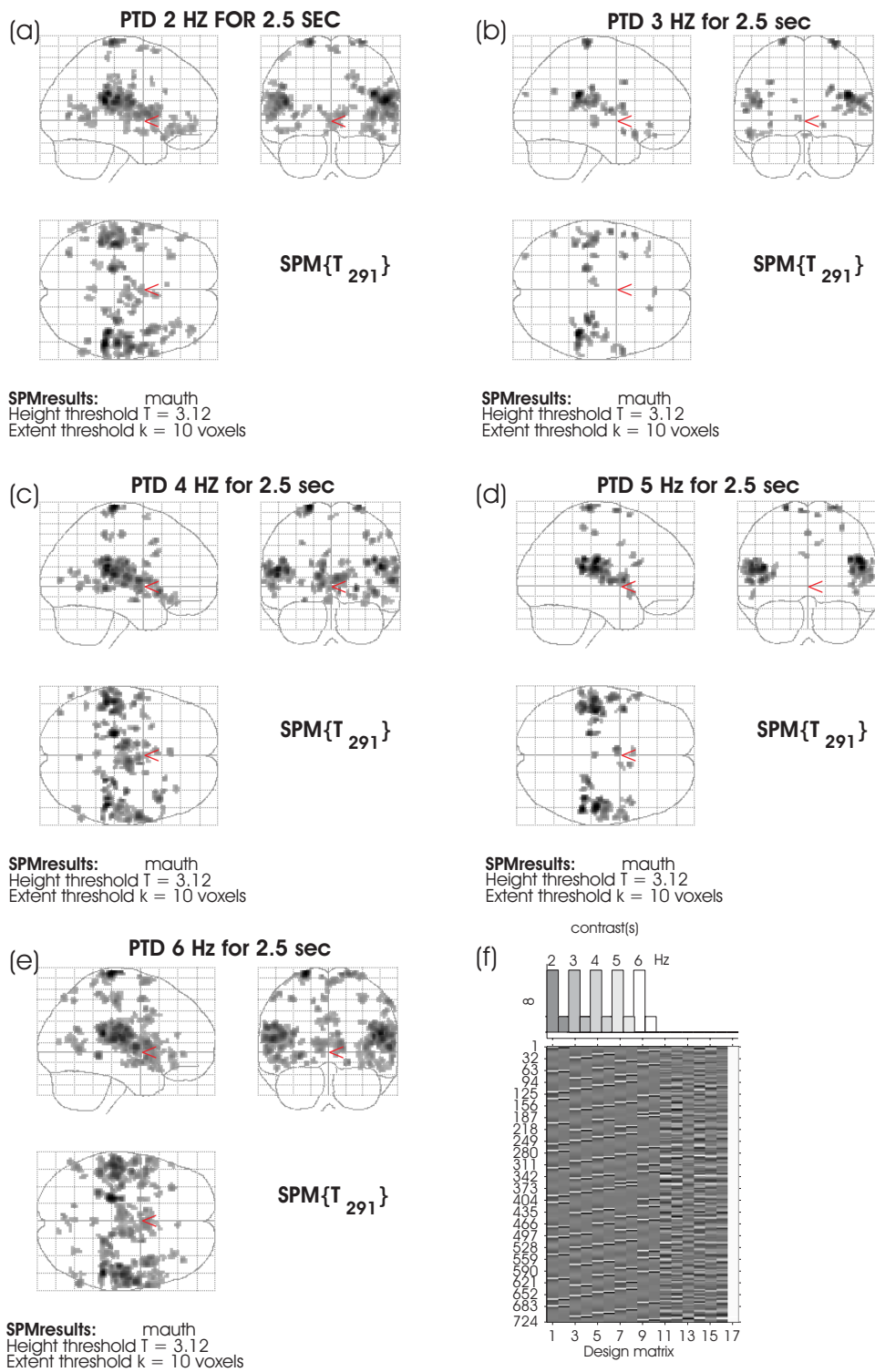


**Figure 6.8:** (a)-(e) MIPs of *mauth* induced by PTD vibration of varying frequency. (f) Illustration of the design matrix and the five contrasts for (a)-(e) overlaid in different gray colors.

### 6.3 Modelling the Hemodynamic Response

This study originates from the assumption that with each ‘stimulator-event’ an individual hemodynamic response of the brain is triggered. It seems reasonable that this response may be different for every individual, but it can as well differ between sessions [MHA<sup>+</sup>00], parts of the cortex or even within the voxels of one extended cluster. Several studies have been performed on the variability of the *hrf* induced by motor and visual activation [DJK<sup>+</sup>02, AZE97, MMO<sup>+</sup>00]. The group around G. K. Aguirre has found significant variability in the shape of the *hrf* for different subjects but responses collected during multiple scans within one subject appeared to be less variable. The interest for the *hrf* originates not only from the effort to increase the SNR, even more important is the fact that the *hrf* can be the key to the relationship between the neural activity of the brain and the measured fMRI signal [BZH<sup>+</sup>99]. This section discusses the effort to map differences of the *hrf* derived from different subjects, regions in the brain and from different voxels within a cluster. The hemodynamic response is triggered by the PTD every 18 s. This rather short inter-stimulus time was necessary for two reasons: (i) the attention of the subjects decreases over time, (ii) too long acquisition times bear a high risk for movement artifacts and trigger errors in the software. The response overlap between two sequent responses might slightly alter the shape of the response, but does not weaken or bias the test of variability in any way. The BOLD is assumed to sum two responses linear for the applied inter-stimulus time [BZH<sup>+</sup>99] (though not for very short inter-stimuli times). However, since the same inter-stimulus time is used for all subjects, the *hrf* can be compared within the series of experiments.

To model the hemodynamic response the data of the first session including visual and tactile stimulation was utilized. Two approaches were made to find characteristics of the *hrf*. The first approach tries to fit a parameterized function to the time courses of single voxels. The second approach works in the frequency space of the data, where the Fourier transform of the real signal is compared to the Fourier transform of an expected signal.

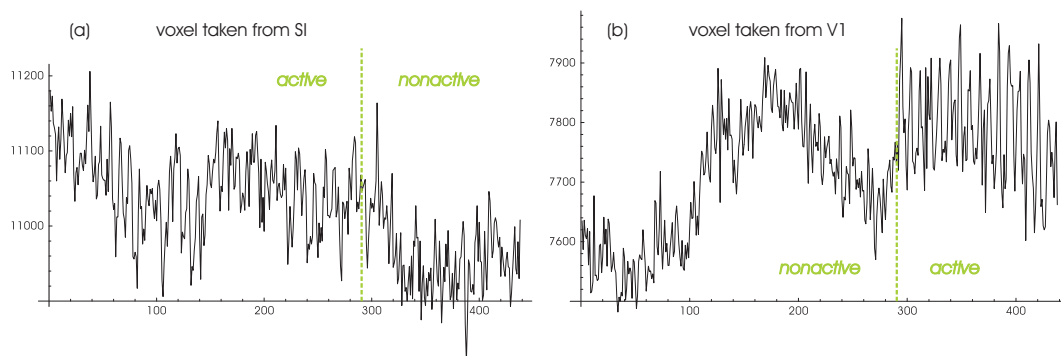


**Figure 6.9:** Two time courses of voxels that *SPM* identified as significant.

#### 6.3.1 Procedures before Fitting

*SPM* has been utilized to detect active and non-active regions in the brain (see section 6.1.2) for all six subjects. The estimation has been performed with both, normalized and non-normalized data. Normalized data on the MNI template can be used to identify the cluster in non-normalized data.

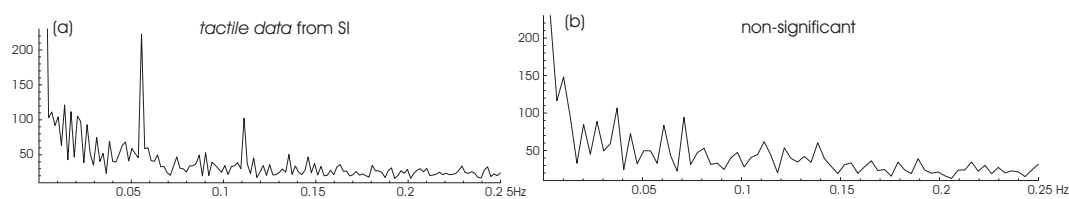


**Figure 6.10:** Averaged Fourier transformation for 23 voxels in an active cluster of SI for *kelge*. Since activation in SI is induced by tactile stimulation during the first part of the paradigm: (a) scans 1-289 are significant, (b) scans 290-438 are non-significant.

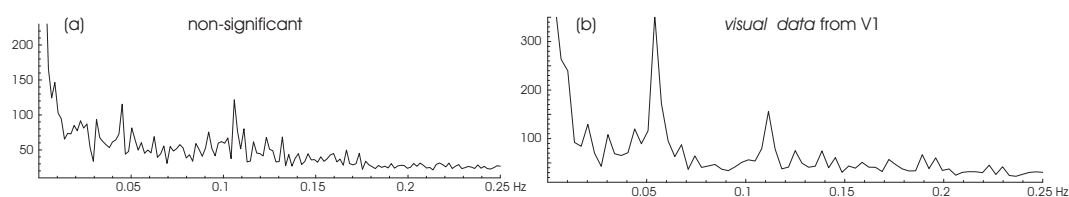


**Figure 6.11:** Averaged Fourier transformation for 181 voxels in an active cluster of V1 for *kelge*. Since activation in V1 is induced by visual stimulation during the second part of the paradigm: (a) scans 1-289 are non-significant, (b) scans 290-438 are significant.

Resulting from these observations the voxels are assigned to four categories: noise, V1, SI or SII. With the Matlab script *easyVox*<sup>1</sup> the time course of single voxels or whole active clusters can be read out from the raw `*.img` files.

Since the normalization transforms the data in a nonlinear way, the coordinates of the raw voxels cannot be reconstructed from `snr2`-data. The activation has to be allocated to coordinates in the `sr`-data from where the corresponding time courses are extracted. *SPM* is a powerful and approved tool in detecting activity, but due to its model-based principles it is not suited to find new response functions that possibly do not correspond (or are even incompatible) to its model. Thus, for all ongoing analysis Mathematica (version 4.2) is used to examine the still unprocessed, raw signal.

The extracted time course for any voxel consists of 438 integers with values that range from approximately 5 000 to 10 000. These values contain the signal of the expected 5 to 10%. Two such time courses are printed in figure 6.9. At least for the visual voxel it is obvious which part is recorded during visual activation. The tactile time course does not show as significant characteristics as the visual one.

The first step is to examine the Fourier transformation of the time courses and search for (systematic) noise frequencies as well as contributions to the signal. In this section the Fourier transform refers to the discrete Fourier transformation of a time course.

In the Fourier spectrum the absolute value of the Fourier transform is presented. Each time course has been separated into the first 289 scans and the remaining 149 scans. Only one part of these is significant, e. g. if the voxel is taken from a somatosensory region the first part will always be

<sup>1</sup>Script has been written by Thorsten Maucher based on scripts by Matthew Brett and Stefanie Runde.

<sup>2</sup>Shortcut for smoothed, normalized and realigned data as explained in chapter 3.

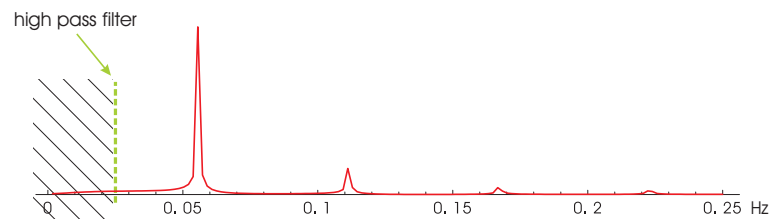


**Figure 6.12:** Fourier transformation of an ‘artificially’ created signal of how an highly significant voxel is expected to behave according to *SPM*. The green dashed line indicates where the high pass filter is applied to the real data.

significant (see figure 6.10), while the second part can only be active in a voxel from the visual cortex (see figure 6.11).

A steep increase is observed in all Fourier spectra for very low frequencies which seems independent of the category the voxel is allocated to. Furthermore, the increase for low frequencies appears as well in the significant as in the non-significant part of the time course. This indicates that low frequencies are not correlated to the signal but caused by confounds such as baseline drift due to temperature effects.

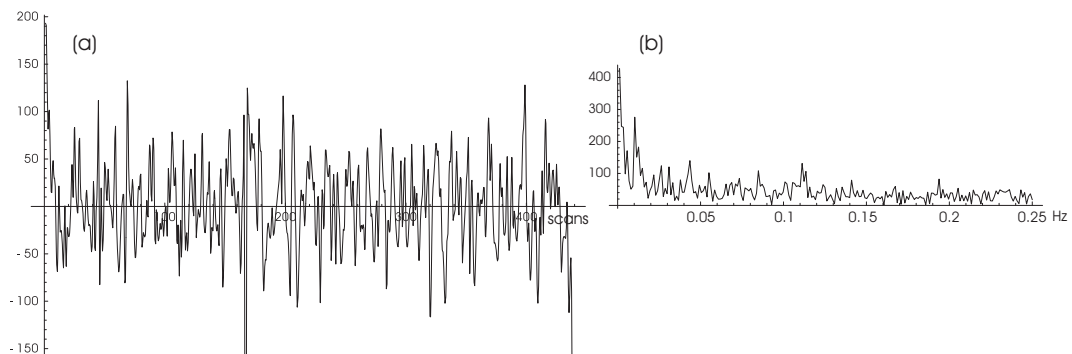


**Figure 6.13:** (a) High pass filtered time course of a non-significant voxel (noise) over 438 scans, (b) Fourier transformation of the noise time course.

Comparing figure 6.11, figure 6.10 and figure 6.12 leads to the application of an high pass filter cutting all frequencies lower than  $0.025\text{ Hz}$  (sketched in figure 6.12). The application of an high pass filter is directly motivated by the Fourier spectrum of the *SPM* template (see figure 6.12). The template’s time course is created by a 32-fold superposition of the *SPM*’s *hrf* with each  $18\text{ s}$  shift. In addition to the high pass filter the ‘zero component’ of the Fourier transformation is taken out. This centers the signal around zero instead of values in the thousands. The averaged Fourier transformation of the significant cluster in SI of *heina* resembles the Fourier transformation of the expected signal, it is only superimposed by wide-band noise.

To estimate the behavior and appearance of noise the histogram of 330 voxels located far from the ROI has been inspected. These voxels are expected to contain nothing else but noise. The time course and Fourier transformation of one of these voxels is visualized in figure 6.13. The contribution of white noise is expected to have a constant Fourier transformation. The observed Fourier transformation has a steep increase for very low frequencies and jitters around a constant

value for increasing frequency. More about the variance in the Fourier transformation of noise in section 6.3.7.

The increase for very low frequencies in the Fourier transformation confirms the application of the high pass filter for the fitting of the *hrf*. The time course remaining after the application of the high pass filter does not contain any baseline drift as seen in figure 6.13(a). Now the data jitters around zero.

The distribution of noise shows a standard deviation of  $\sigma = 67$  centered around  $\mu = 0$  (see figure 6.14). This  $\sigma$  denotes the error term of each data point in the time courses.

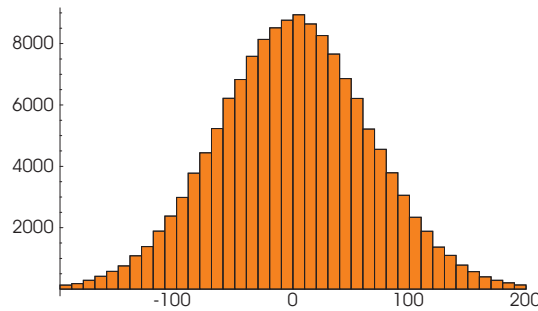


**Figure 6.14:** Histogram of 330 noise voxels (438 scans) giving a normal distribution of  $\mu = 0$  and  $\sigma = 67$ .

In the remaining text the first 288 scans of the time course that is extracted from a voxel in the somatosensory significant region are referred to as *tactile data* (see figure 6.10). The scans 290-438 of a time course that is extracted from a voxel in the visual significant region are referred to as *visual data* (see figure 6.11). Depending on whether the *tactile data* or the *visual data* is fitted, the experiment provides 288 or 149 points of measurement.

### 6.3.2 The Fitting Function

To fit the hemodynamic response several different functions are proposed in the literature: The *Poisson* function, the *Gamma* function, an overlay of two *Gamma* functions or a basis set of *Fourier* functions. For this study the overlay of two *Gamma* functions ( $\Gamma$ ) has been chosen as it is implemented in *SPM* (compare section 2.3). The fitting function  $F$  is composed as follows:

$$F(x) = \sum_{i=0}^{n-1} \left[ A_i \left( f_1(x - ix_0) - f_2(x - ix_0) \right) \right] - shift$$

$n =$  number of trials in the data

With  $f_1$  modelling the rising part and  $f_2$  modelling the post undershoot of the *hrf*. For the realization of the functions within Mathematica critical regions in the definition interval are bypassed with the *cutter* and *avoid* functions. In equation 6.1 and 6.2 the implementation of the fitting function in Mathematica is expressed.

$$f_1 = \text{cutter}(x) \exp \left[ (p_1 - 1) \ln (x + \text{avoid}(x)) + p_1 \ln \left( \frac{1}{p_3} \right) - \frac{1}{p_3} x - \ln \Gamma \left( \frac{1}{p_3} \right) \right] \quad (6.1)$$

$$f_2 = -\text{cutter}(x - d) \exp \left[ (p_2 - 1) \ln (x - d + \text{avoid}(x - d)) + p_2 \ln \left( \frac{1}{p_4} \right) - \frac{1}{p_4} (x - d) - \ln \Gamma \left( \frac{1}{p_4} \right) \right] \quad (6.2)$$

Some initial comments have to be made concerning the composition of the  $f_1$  and  $f_2$ :

- For numerical calculations it is better to implement  $\ln \Gamma(x)$  than  $\Gamma(x)$ , since the latter will easily create overflow in the computer's floating point representation [Pre86].
- The Gamma density function expands to large values in the negative domain, therefore the *cutter* function is added:

$$\text{cutter}(x) = \begin{cases} 0 & : x < 0 \\ 1 & : x \geq 0 \end{cases}$$

- The value  $x = 0$  in  $\ln(x)$  is circumvented with the *avoid* function:

$$\text{avoid}(x) = \begin{cases} 0 & : x < 0 \\ 1 & : x = 0 \\ 0 & : x > 0 \end{cases}$$

The model includes  $6 + n$  parameters that have to be fitted:  $p_1, p_2, p_3, p_4, d, \text{shift}$  and  $A_i$ , the  $n$ -amplitudes.  $p_1, p_2, p_3$  and  $p_4$  are responsible for the shape of  $f_1$  and  $f_2$ , whereas  $d$  gives the shift of the undershoot versus the rising part. The baseline can be fitted by adjusting *shift*.

The choice of parameters includes that the shape of the hemodynamic response is similar for each event, but its amplitude can differ from event to event.

The parameter  $d$  could not be adjusted with the fitting procedure because of the function's construction. Instead it was varied with 'loop' and the minimal chi-square for a wide range of  $d$ -values is selected.

The number of trial ( $n$ ) is 32 for the *tactile data* and 16 for *visual data*. Thus, the degrees of freedom for the *tactile data* is  $\nu = 250$  and for the *visual data*  $\nu = 117$ . For some of the subjects the *visual data* includes less than 149 scans (see figure 6.1) which diminishes the degrees of freedom (for *mauth*  $\nu = 78$ ).

### 6.3.3 The Fitting Routine

The fitting procedure is performed with the 'NonlinearFit' routine in Mathematica. It is included in the standard package: Statistics'NonlinearFit'. The *LevenbergMarquardt* method is used to acquire the least mean square between the high pass filtered data and the fitting function.

For visual data the significance in ways of periodicity of the time course can be distinguished by eye (see figure 6.9). After application of the high pass filter the data is centered around zero. The baseline is still uncertain and has to be fitted since it is not identical with the center of the *hrf*. The

baseline cannot be estimated from an extrapolation of the non-significant part of the time course because of strong low frequency disturbances (see figure 6.9).

To test the fitting procedure the most significant<sup>3</sup> voxel was chosen from a visual cluster for each subject. Only if the fit to such a time course provides a satisfying goodness-of-fit *tactile data* can be approached.

The choice of starting parameters proved to be critical in order to find the fit with minimal chi-square. The parameter range of the fit is not restricted, only  $d$  is restricted to 4–14. For  $d < 4$  the undershoot lies before the uprising peak. Several sets of starting parameters have been chosen and tested with the following settings:

MaximalIterations  $\rightarrow$  100–200, AccuracyGoal  $\rightarrow$  3–30, PrecisionGoal  $\rightarrow$  10–40.

### 6.3.4 Results of the Fitting

There are two parameters which describe the goodness-of-fit: (i) the value of chi-square which has been minimized by the fitting procedure and is declared in respect to the error term, (ii) the quantity  $Q$  denotes the probability that the observed chi-square is determined by chance although the right model has been chosen.

Practically spoken if  $Q$  is close to 1 the error term allows a 100% probability that the minimal chi-square has been determined by chance. The model has to be rejected for  $Q < 10^{-18}$ . For  $Q > 10^{-3}$  the model can be accepted under certain circumstances, such as non-normally distributed measurement errors.

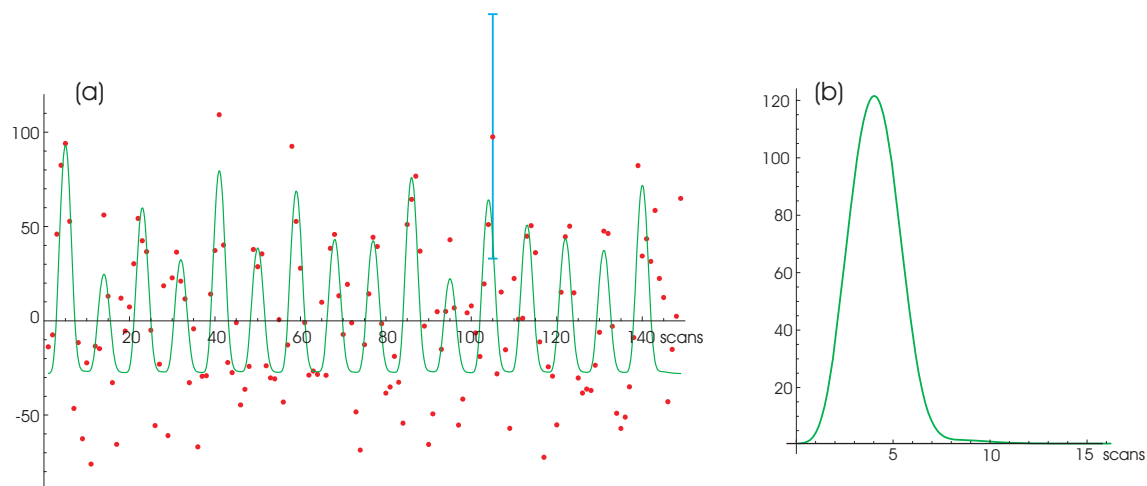


**Figure 6.15:** (a) Red dots show the high pass filtered signal. The fitted curve is colored green. For one data point the error term is added. (b) The *hrf* which has been fitted to the first trial (trials differ in their amplitude).

The following results are based on *visual data* originating from *heina*. The minimal achieved chi-square is in the order of  $\chi^2 \approx 50$ . Taking the degrees of freedom in account this gives a *quantity* of  $Q = 1 - 10^{-11}$ . The respective parameters are:

$p_1 = 11.8, p_2 = 11.2, p_3 = 0.46, p_4 = 0.32, d = 4, shift = 28$  and  $7.510^{-6} < A_i < 1.710^{-5}$

<sup>3</sup>Highest t-value in the evaluation with *SPM*.

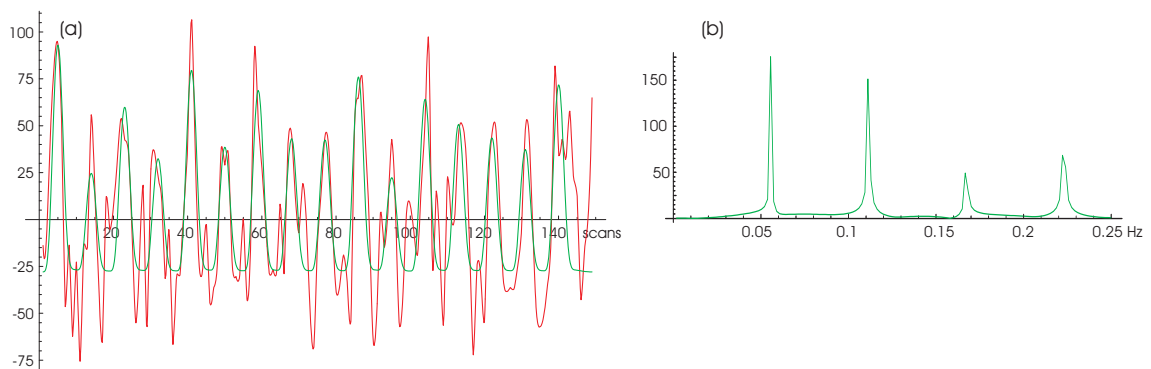


**Figure 6.16:** (a) Interpolation of high pass filtered signal (red) is overlaid with the fitted curve (green). (b) The Fourier spectrum has been determined for the fitted curve.

In figure 6.15 the fitted function is overlaid with the measured data points. The same plot shows the optimal *hrf* which does not exhibit an undershoot. Figure 6.16 illustrates an interpolation of the measured points together with the fitted curve thus allowing to easily compare the signal with the fit. The Fourier spectrum of the fitted curve can be compared to a previously presented ‘real’ spectrum (e. g. figure 6.11(b)).

The fitting was not continued because of several reasons. Most apparently it did not get obvious if the global minimal chi-square has been reached in the calculations. Different starting values lead to a very different parameter set though the chi-square only changes in the order of  $10^{-3}\%$ . The fact that  $Q$  is practically identical with 1 signifies that the error terms are assumed too large. This conclusion becomes evident in figure 6.15 where the error bar for one data point is plotted. With this error bar the model cannot distinguish between the small differences in the shape of the *hrf*. Beyond the simple determination of the hemodynamic response the initial goal was the comparison of the *hrf* for different subjects, cortices and voxels of a cluster. This is only possible if one definite set of parameters can be fitted to a selected time course.

There can be two possible reasons for not finding a global minimum. Either the starting values or the model is not properly chosen for the determination of physio. E. g. the x-translation of  $F(x)$  towards the data points could not be declined as fit parameter. Adjusting it similar to  $d$  with a ‘loop’ did not show success.

A modified fitting function has been chosen in an additional attempt to fit the data without the post undershoot. The result did not improve, instead chi-square was larger and the fitted curve does not describe the data properly.

### 6.3.5 Characterization of the Fourier Spectrum

When examining the ‘full’ frequency spectrum for one proband (see figure 6.17) it is striking that the hemodynamic response to a stimulation task is connected to two or three narrow peaks. The measured frequency spectrum has strong similarities to the ‘artificially’ created spectrum with its highest peaks at about  $\frac{1}{18} Hz$  (see figure 6.12).

The peak at  $\frac{1}{18} Hz$  has a nearly trivial explanation. The design of the experiment dictates a period of 18 s which is answered by the brain. This confirms the previously made assumption that the answer of the brain is related to each ‘stimulator-event’. Thus, the peak’s location refers only to the period of the paradigm and not to the shape of the hemodynamic response.

For a categorization of the spectrum the exact position and the amplitude of the three main peaks is determined and listed in table 6.2. The third peak could not be resolved in every spectrum.

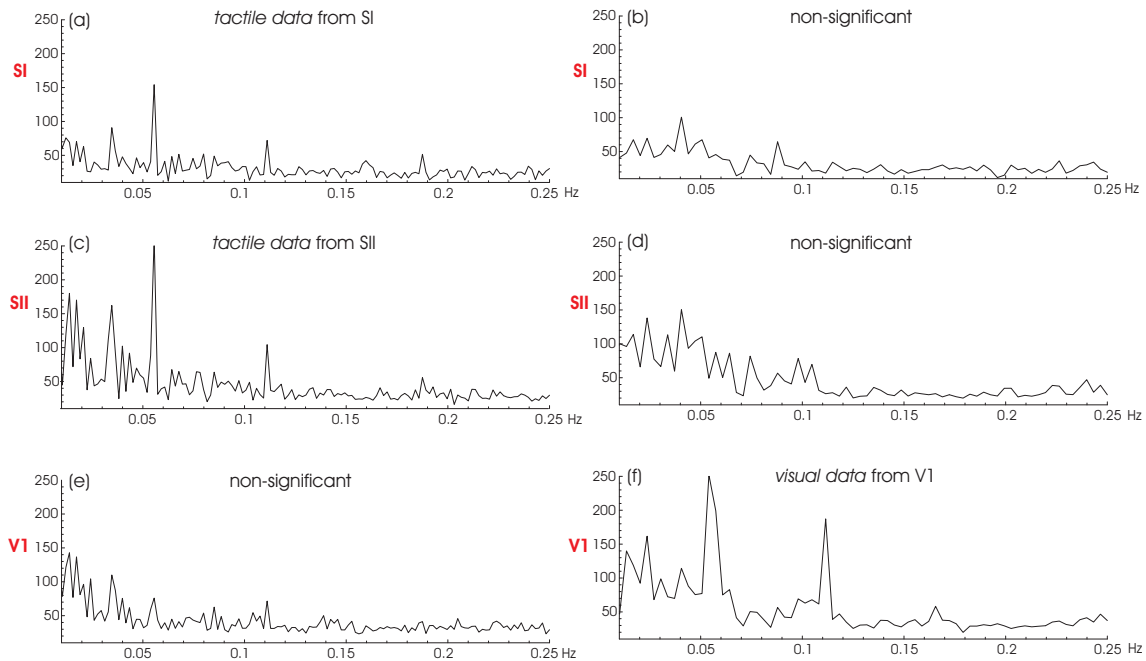


**Figure 6.17:** Fourier spectra of three clusters of *lemla*, with the data averaged over SI, SII and V1 separately. X-axis is not plotted for frequencies below 0.01 Hz for better resolution of the peaks (see figure 6.11). Figures (a), (c), (e) are derived from scans 1-289 and (b), (d), (f) from scans 290-438.

### 6.3.6 The Fourier Coefficients

The resolution of the x-axis is limited by the number of scans (minimum distance between two points  $\Delta x = (2 \times \text{number of scans})^{-1}$ ). Because of the very narrow peaks the peak detection is kept simple. The maximum value within a defined window is selected and its coordinates are recorded in table 6.2.

Only peaks that lie within a field of view of  $fov = 0.03 Hz$  around the expected position are taken into account. A window with this width is centered around 0.05, 0.11 and 0.16 Hz. The maximum amplitude within the window determines the Fourier coefficient and its x-coordinate denotes the peak position. The Fourier coefficients are equal to the y-coordinates in the table.

The position of peak1 and peak2 is identical for all subjects and clusters. Peak1 appears at  $\frac{1}{18} Hz$ , while peak2 is located at  $\frac{1}{9} Hz$ . Since the number of scans for visual data is lower than for tactile data, the x-coordinates are not identical. Taking into account the minimum distance of two points the closest possible data point for the peak position is chosen. The position of the third peak is not as similar within the different subjects. It is located at  $\frac{1}{6} Hz$  with maximal variations of  $\pm 0.01 Hz$ . The three peaks can be identified as a harmonic series, with the position of peak2 and peak3 being the double and triple of peak1's position. This explains the extremely small variations in the peak position.

	peak1 {x [Hz], y}	peak2 {x [Hz], y}	peak3 {x [Hz], y}	Base- line	$\frac{A_2}{A_1}$	$\frac{A_3}{A_1}$	No voxels in cluster
<i>heina:</i>							
SI	0.0555, 196.4	0.1111, 111.4	0.1666, 98.3	72	0.314	0.21	16
SII	0.0555, 185.9	0.1111, 113.7	0.1684, 94.9		0.362	0.203	150
V1	0.0541, 216.1	0.1115, 127.4	0.1554, 89.2		0.382	0.119	743
<i>kelge:</i>							
SI	0.0555, 222.7	0.1111, 102.2	0.1632, 35.9	32	0.368	0.021	23
SII	0.0555, 194.1	0.1111, 136.6	0.1666, 71.2		0.645	0.241	19
V1	0.0541, 354	0.1115, 156	0.1723, 56.9		0.385	0.077	181
<i>lelet:</i>							
SI	0.0555, 305.6	0.1111, 186.9	–	65	0.507	–	7
SII	0.0555, 174.2	0.1111, 109.5	0.1666, 75.1		0.408	0.093	63
V1	0.0541, 291.3	0.1115, 136.3	–		0.314	–	78
<i>lemla:</i>							
SI	0.0555, 154.2	0.1111, 72.0	0.1597, 42.2	30	0.282	0.082	20
SII	0.0555, 262.4	0.1111, 104.3	0.1666, 40.8		0.321	0.046	119
V1	0.0541, 252.3	0.1115, 187.2	0.1655, 58.3		0.709	0.122	466
<i>mauth:</i>							
SI	0.0555, 177.6	0.1111, 99.3	0.1701, 63.9	28	0.476	0.24	16
SII	0.0555, 148.1	0.1111, 75.3	–		0.394	–	147
V1	0.0532, 141.4	0.1117, 85.2	0.1702, 31.0		0.505	0.027	465
<i>pauca:</i>							
SI	0.0555, 126.8	0.1111, 77.2	–	30	0.578	–	8
SII	0.0555, 134.9	0.1111, 74.5	–		0.424	–	163
V1	0.0541, 182.2	0.1115, 118.1	0.1689, 38		0.450	0.077	605
<i>errors:</i>							
SI, SII	$\pm 0.0009, \pm 20$			$\pm 10$	$\pm 0.17$	$\pm 0.2$	
V1	$\pm 0.002, \pm 20$						

<i>Sinus:</i>	0	0
<i>SPM template:</i>	0.16	0.04
<i>Fitted curve:</i>	0.86	0.28

**Table 6.2:** Position and amplitude of three peaks in the Fourier spectrum of all subjects. ‘–’ denotes that in this case no peak could be resolved.  $A_1$  is the amplitude of peak1,  $A_2$  is the amplitude of peak2 and so on.

Information about the shape of the hemodynamic response cannot be drawn from the position of the main peaks. Instead, the Fourier coefficients have a decisive impact on characteristics of the *hrf* such as width. The absolute amplitude in the Fourier spectrum is only significant to a certain degree therefore peak2 and peak3 are normalized to peak1. The ratio of the amplitudes are listed in table 6.2 and are illustrated in figure 6.18. For the calculation of  $\frac{A_2}{A_1}$  and  $\frac{A_3}{A_1}$  a baseline has been subtracted from the amplitudes. The baseline is the mean value of the non-significant part of the Fourier spectrum. It has been achieved for one modality of each proband. Assuming white noise the baseline is equal in both, the significant and the non-significant Fourier spectrum. Since the noise is not perfectly white noise, the error term (standard deviation of the mean value) is given in the last line of the table.

For  $\frac{\text{peak2}}{\text{peak1}}$  the measured ratios are all in the range of 0.28 to 0.71 which is larger than the value of the *SPM* template with  $\frac{A_2}{A_1} = 0.16$ . On the other hand, the fitted curve exhibits a higher ratio with 0.86. All observed values lie in between the *SPM* template and the fitted curve. The mean ratio is  $M_2 = 0.43$  with  $\sigma_2 = 0.11$ .

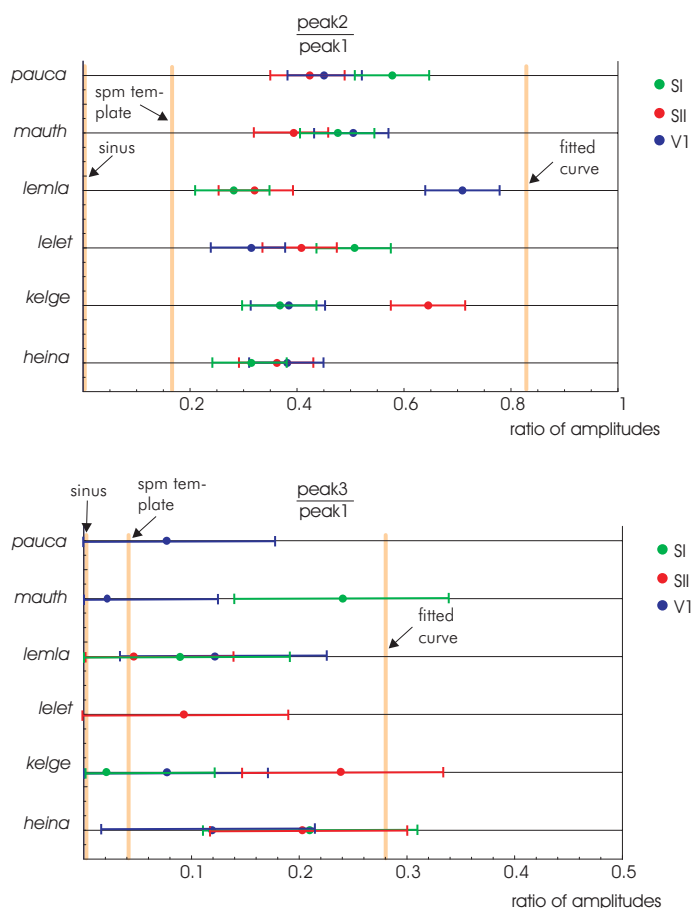


**Figure 6.18:** Ratio of Fourier coefficients:  $\frac{A_2}{A_1}$  and  $\frac{A_3}{A_1}$  for six subjects. Data achieved in SI, SII and V1 is evaluated separately and coded in red, blue and green. The values for the Sinus function, the *SPM* template and a fitted curve are added as orange bars.

The situation is similar for the ratios of  $\frac{\text{peak3}}{\text{peak1}}$ . Several of the observed values are close to the *SPM* template with  $\frac{A_3}{A_1} = 0.04$ , whereas the average value for all subjects and all modalities is  $M_3 = 0.12$ . Here the variance is larger in terms of percentage with  $\sigma_3 = 0.08$ . Again the fitted curve borders at high values with 0.28.

The interpretation of these values is not intuitively clear. By modifying the template time course the influence of the Fourier coefficients on the *hrf* shape has been tested. The increasing of the *hrf* width leads to a smaller  $\frac{A_2}{A_1}$  and a slightly smaller  $\frac{A_3}{A_1}$ . This could explain the ratios in figure 6.18. At the same time the amplitude of peak2 increases by one order if the time course is shifted to lower y-coordinates. A similar effect bears the omission of the post undershoot which results in higher amplitudes for the second than for the first peak. Only by recording the ratio of amplitudes one cannot distinguish between these effects. The interpretation of the Fourier coefficients of such a complex function calls for further and more intense investigations.

### 6.3.7 Fault Assessment

Although the error-bars in figure 6.18 have a reasonable size they do not overlap within one subject. To assure this outcome the size of the estimated error-bars has been confirmed with a detailed investigation.

In table 6.2 the different error values are added below the list of subjects. One important feature is the error of the peak's amplitude  $\Delta y$ . The contribution of noise in the fMRI signal cannot be transferred into the Fourier space easily. The impact highly depends on the characteristics of the noise such as e. g. white noise. Instead of transferring the noise of the time course into Fourier space the variance of a Fourier spectrum has been estimated. A Fourier transform of a noise time course is visualized in figure 6.13. Its histogram resembles a gaussian 'normal distribution' with a standard deviation of  $\sigma = 20$  centered around  $\mu = 46$  (visualized in figure 6.19).

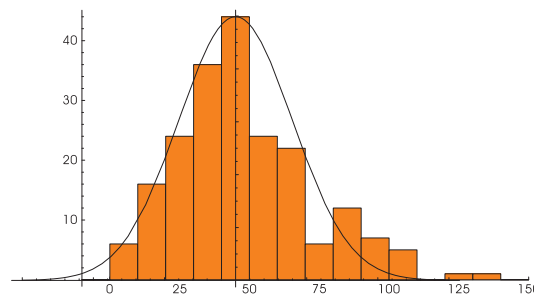


**Figure 6.19:** Histogram of the Fourier spectrum of a noise voxel (438 scans) with normal distribution of  $\mu = 46$  and  $\sigma = 20$ .

This  $\sigma$  gives an assumption about the variance of the fMRI signal if no task is induced. The variance is assumed to be overlain with the signal which corresponds to the activation task. Therefore, it is given as the error value  $\Delta y$  of the peak's amplitude.

It is though a very rough estimation for error values since the variance certainly differs between the Fourier spectra. The standard deviation cannot be estimated for every Fourier spectrum itself, since the histogram would be disturbed by the peaks. The standard deviation of the non-significant part gives only a variance of the baseline and no measure for the physiological variance which is added to the fMRI signal.

$\Delta y$  is certainly an assessment for the statistical variance of a Fourier spectrum. But it is no measure for the global error of the Fourier spectrum, especially not when comparing different spectra. For the comparison of different spectra it is necessary to record several sessions with the same proband, same paradigms and as similar circumstances as possible. With such data it would be possible to estimate the global variance and reliability of the signal.

### 6.3.8 Summary of the Hemodynamic Model

Two approaches have been traced in order to detect variabilities in the hemodynamic response. In the first attempt, a significant time course from the visual cortex has been fitted to the template that is implemented in *SPM*. The fitting has not been applied to *tactile data* since the fit on *visual data* resulted in an unreasonable *Quantity Q*.

Since single time courses did not allow for an accurate characterization of the hemodynamic response the Fourier transformation averaged over a whole cluster has been analyzed. The average includes from 7 to 700 voxels out of one area that *SPM* claims to be active. For each significant Fourier spectrum the Fourier coefficients have been extracted and compared. No systematical order could be perceived between the different categories such as V1, SI and SII.

The only statement that figure 6.18 allows is that the values from the Fourier analysis spread between the values for the *SPM* template and the result from a fitted curve. The combination of both approaches can indicate that the fitting procedure does adjust the parameters in a reasonable direction. But the proper interpretation of the ratio of Fourier coefficients has not been possible.

For both approaches one thing has to be kept in mind. The voxels are categorized on the basis of statistical inferences made by *SPM* utilizing the template to test for significance. The sensibility or probably the over-sensitivity of this inference decides over the categorization of voxels for the further analysis. With the applied threshold a probability of 5% is given that the voxels have been selected by chance. This amount of non-active voxels can have a notable impact on the average Fourier spectrum of a cluster. Although the main peaks still dominate the Fourier spectrum, the ratio of Fourier coefficients can be altered.

For the fitting procedure the most significant voxel has been selected in order to test the model. Still, the selection of the model and a successful choice of starting values included a long way of optimization. It is not only due to chance that the resulting fit resembles the template as much as possible. This is an absolutely necessary consequence of the voxel choice, since the inference test is based on the correlation with the template.

The problem of the high *Quantity Q* for the fitting could be solved with a new determination of the error term. Its fundamental would not investigate the variance of noise, but rather the variance of the response over several sessions. The assumption is that the variance should decrease with higher significance of the time course. Resulting from this the variance of the most significant voxel will be less than the determined error term.

## Discussion and Outlook

A study involving event-related visual and tactile stimuli has been performed with six healthy probands. The activation in the human brain has been investigated in respect to three aspects. The first analysis succeeded in mapping the activation induced by visual and tactile stimulation in well localized regions of the cerebral cortex.

The region activated by flickering lights has been assigned to the primary visual cortex as well as to visual association areas. The localization of activation from vibratory tactile stimulation of the abdomen turned out to be more difficult. Two distinguished and separated cortical areas are involved in the processing of such stimuli. In SI the region responsible for the representation of the abdomen could be identified. Furthermore, a large area in the somatosensory association area, most probably SII, exhibited activation.

The reliable identification of these areas could only be done by visual investigation of the activation position within the anatomic structure. Though, the majority of activation has been registered to significant landmarks in the somatosensory cortex, the involvement of the auditory cortex cannot fully be excluded. It is now important to prove the localization of the tactile activation in an additional and independent way.

This could not yet be done since the fMRI tomograph in Strassbourg has undergone great replacements and improvements from October to January. Initially, the reconstructions had been announced for the period November to January. Therefore, the temporal schedule of the experiments was very tight in order to include at least six subjects within the analysis. It was not possible to carefully analyze the data before the fMRI had been shut down, this could first be done after the completion of all experiments. At that point of time, the fMRI had already been shut down. Thus, reference measurements or additional experiments have to be performed subsequently.

Several interesting and necessary experiments can be suggested as soon as the system is running again. For example an experiment where the PTD is activated with the same paradigm as before, but without contacting the proband could clear the achieved results.

If this shows activation in the cerebral cortex the PTD is very probable to cause noise, which the proband is not aware of but the brain does react on. In the contrary case, if no activation is visible, it cannot be concluded yet that the auditory cortex is not involved.

Acoustic stimulations could be perceived with the help of an effect which is called the *cocktail party effect*: two related stimulations support each other in lowering the threshold of perception. This is e. g. the case in a noisy room, where reading from lips can support the very selective perception of words. In our case the timing of the pneumatic switches which possibly create an acoustic stimulation is related to the tactile stimulation of the PTD.

Therefore, it is advisable to compare the activation from an acoustic experiment with the here observed activation. With such an experiment it should be easy to decide which cortical areas are involved in the stimulations induced by the PTD.

From the investigation on the frequency dependence of the somatosensory system no final conclusions could be drawn. At first the data is not fully evaluated yet. Correlations between a noteworthy number of coherent voxels and the stimulation frequency have been observed for two cases in one subject. For linear as well as linear combined with quadratic order a significant amount of voxels exhibited activation in the ROI. An inference between subjects could lead to a significant result though the activation in each subject separately is low.

A group analysis is achieved by adding all subjects into one design matrix and applying the proper contrast. Furthermore, a 'Random Effects Analysis' can be performed. 'Random Effects Analysis' assumes that the effect *per se* constitutes an independent variable and the error variance is based on the activation from subject to subject. These 'second level' analysis will be added in connection with this thesis.

Anders M. Dale [Dal99] demonstrated that the efficiency of the data increases with decreasing mean inter-stimulus time if the inter-stimulus interval jitters randomly from trial to trial. Thus, for the same duration of the session more trials can be included in the paradigm. With increasing statistical power per subject more activation can possibly be observed in all subjects at the same threshold.

The third analysis relies on the activation allocation done with *SPM* and investigates the characteristics of the fMRI signal. The signal visualizes the hemodynamic response which is expected to be linearly correlated to the neuronal activity of the human brain. Since the intention was to detect variabilities in the visual and tactile response the data for this investigation is limited to one session where both tasks have been run.

Both, a fitting of time courses and the investigation of averaged Fourier spectra have been performed. The fitting analysis failed due to a too high chi-square probability  $Q$ . The normal distribution of the measurement errors has been conformed by plotting 144 000 signals into a histogram. The model as well as the data need to be improved in order to receive conclusive results that detect even small variations in the shape of the hemodynamic response.

The model seems to be under-determined since the data does not allow a definite determination of all parameters at the same time. E. g. the baseline can be adjusted in a way that a deep undershoot is exhibited. Due to a very small difference in chi-square the 'right' fit cannot be distinguished confidently. Probably, the baseline should be determined externally from physiological features. A good way would be to calculate the baseline in the non-significant part of each time course after the elimination of all low frequency confounds. Admittedly, the effort to do so resulted in unreasonable values.

A similar argumentation applies for  $d$  which denotes the delay of the undershoot versus the rising peak. Varying  $d$  allows a strong undershoot as well as no undershoot while the chi-square remains stable within  $10^{-3}\%$ .

The Fourier analysis of different cortical areas did not give any consistent results for the six subjects examined. Since each Fourier spectrum has been averaged over a whole cluster this can imply that the cluster-variability of the *hrf* is higher than the cortex-variability. For the confirmation of such a statement non-averaged Fourier spectra have to be analyzed. The low statistical threshold applied to the data in order to categorize the voxels can as well be responsible for lowering the significance of the selected data.

However, the method to Fourier analysis event-related fMRI experiments showed to be promising for activation detection. Its capability to further investigations systematical variabilities of the hemodynamic response still has to be proved. A new approach would suggest to directly categorize the voxels by Fourier analysis and with this increase the significance of the data.

# Appendix A

## Glossary

**Anterior Commissure (AC)** A small sharply defined bundle of commissural fibres located in the dorsal-ventral center and anterior of the brain. A commonly used landmark in the brain.

**Axon** Transmitter for signals from neuron to neuron by generating and propagating action potentials. The axon extends the cell body and can be several centimeter in length.

**Bilateral** Refers to both hemispheres of the brain.

**Broca's Area** Located in the inferior frontal gyrus of the frontal lobe. This area is responsible for the motor control of speech.

**Central Nervous System (CNS)** Includes the spinal cord and the brain.

**Cerebral Cortex** Covers the entire surface of the cerebral hemispheres and is composed by layers of nerve cells.

**CerebroSpinal Fluid (CSF)** Fluid surrounding the brain and spinal cord, contains glucose, proteins and other substances, that are also found in the blood. CSF appears bright white on  $T_2$  weighted fMRI scans.

**Gray Matter** Darker-colored tissues of the central nervous system in the brain. The gray matter includes the cerebral cortex, the thalamus, the basal ganglia, and the outer layers of the cerebellum.

**Gyrus** Folds on the surface of the cerebral hemispheres.

**Ipsilateral** Refers to the hemisphere of the brain which is on the same side as the stimulation.

**Lateral Geniculate Nucleus (LGN)** Part of the thalamus which serves as a relay station for simple visual information. From the LGN signals are transmitted to the primary visual cortex.

**Lobe** Portion of the Cortex that are anatomical and functional separated.

**Neuron** Nerve cell that receives information from other neurons or sensory organs. It integrates the input from all synapses and gives a new output. The human brain consists of about 100 billions of neurons.

**Posterior Commissure (PC)** Crossing fibres interconnecting the two sides of the rostral midbrain and pretectal area. Is together with AC a commonly used landmark in the brain.

**Retina** Covers the back of the vitreous body of the eye. The retina consists of photo-receptors which come in cone and rod shape.

**Sulci** Trenches in the cortex. They can serve as division between the lobes of the cortex.

**Synapse** Junction from which information is passed from one neuron to the other. A synapse can be excitatory or inhibitory in nature.

**Tactile** Related to the sensation of touch.

**Thalamus** A major relay station between the senses and the cortex. It consists of several nuclei which differ in functionality.

**Wernicke's Area** Located at the rear of the parietal lobe (near temporal lobe). The area is important for understanding speech.

**White Matter** Nerve tissue that is pale in color because it contains nerve fibers with large amounts of insulating material (myelin). The white matter does not contain nerve cells. In the brain, the white matter lies within the gray layer of the cerebral cortex.

## Appendix B

# Atlas for the Human Brain

### B.1 Brodman's Areas

Brodman mapped 52 cytoarchitectonic different areas in the brain. He founded a school where mainly the cellular structure in the cortex was investigated. His colleagues searched for similarities in neuronal structure and characteristic cell layers to identify the areas.

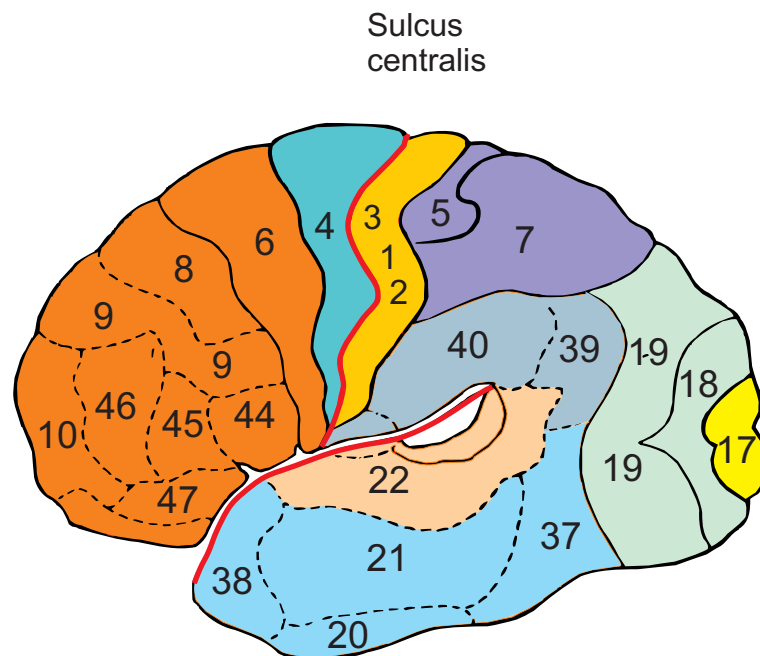


**Figure B.1:** The map created by Brodman in the beginning of the 20th century. Only areas located on the surface are numbered.

## B.2 Directions and Planes

Neuroscientists formed a new terminology to describe directions in the human brain. It is specialized in giving both, absolute positions and locations relative to e. g. the spinal cord. The terms are relatively easy to understand in a mouse. There the rostral-caudal axis runs approximately in a straight line from the nose to the tail (see figure B.2). The dorsal-ventral axis is perpendicular to the rostral-caudal axis and runs from the back to the abdomen. In the human brain the rostral-caudal axis does not follow a straight line but instead undergoes a bend (or flexure) at the midbrain (see figure B.2). The terms inferior and superior are used to describe directions pointing perpendicular to this line.

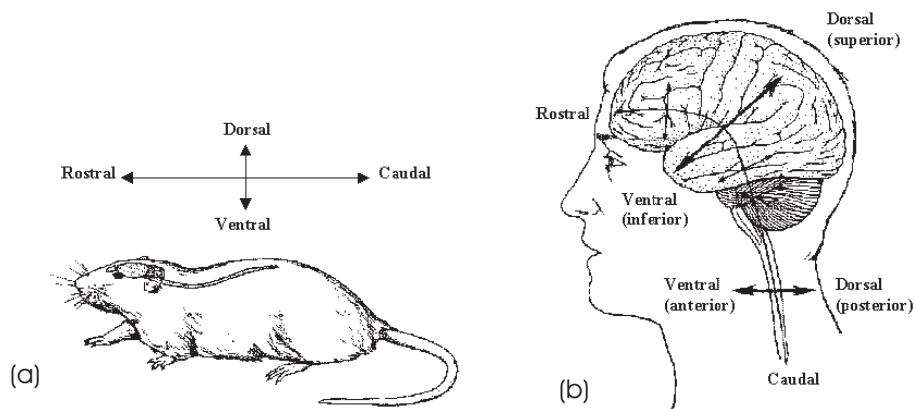


**Figure B.2:** Expressions for directions in (a) the mouse and (b) the human brain [Chr00].

To present 3-dimensional data of the human brain in a reasonable way, three anatomical slices or sections are taken. The planes are named horizontal (or axial), coronal and (para-) sagittal.

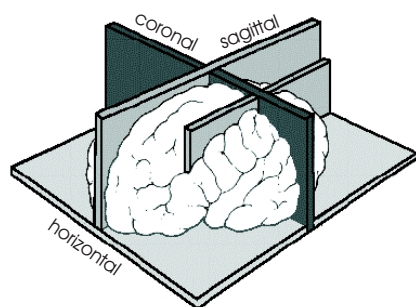


**Figure B.3:** The three planes slicing the human brain for data-presentation [Chr00].

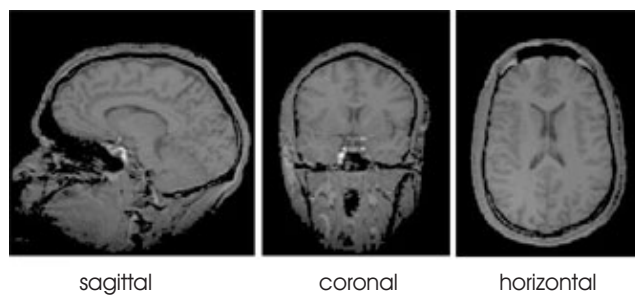


**Figure B.4:** Three magnetic resonance imaging (MRI) pictures of slices through the brain in different orientations [Chr00].

### B.3 Locations in the Human Brain

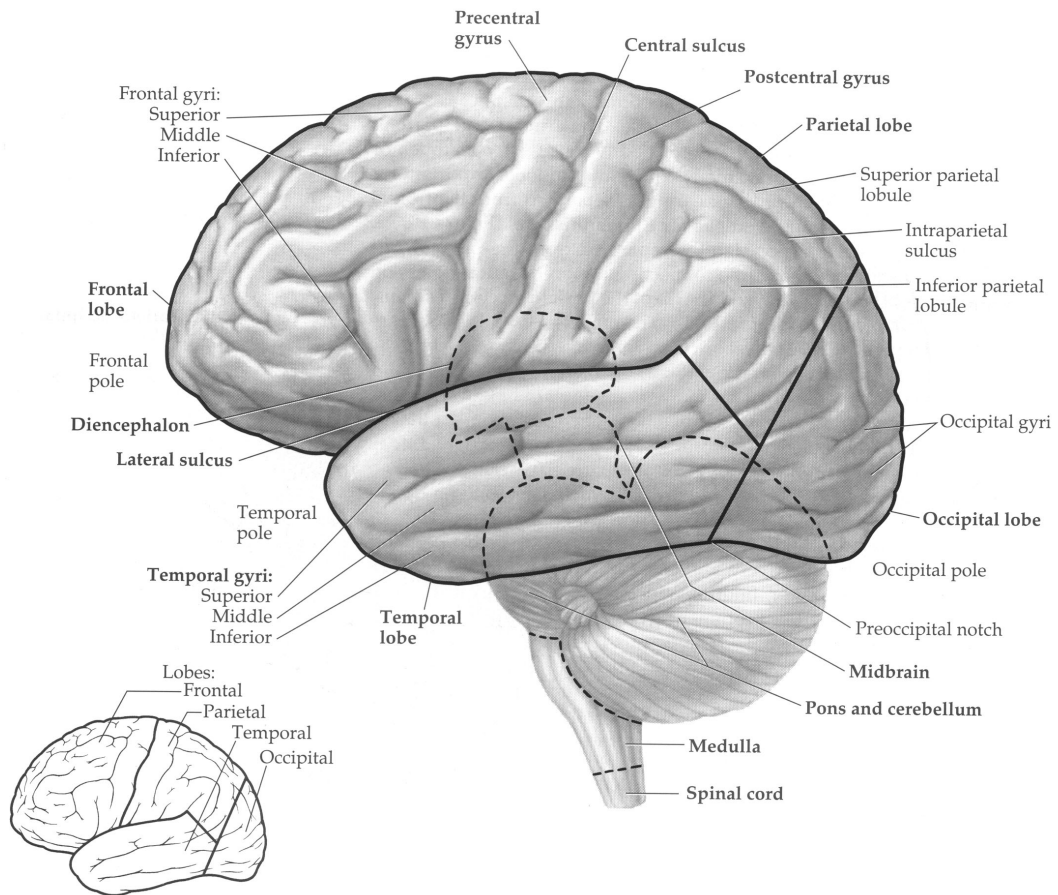


**Figure B.5:** Lateral surface of cerebral hemisphere with brain stem and part of spinal cord. In the lower left corner an overview of the four lobes of the cerebral cortex is shown [Chr00].

## Appendix C

# Ways of Presenting fMRI Data

### C.1 The Coordinate System of Talairach and Tournaux

Talairach and Tournaux tried to normalize the differences between the brains of individual subjects. They created a detailed anatomical map based on the slices from the brain of a single person. It uses a proportional grid system referring to the location of two anatomical landmarks, the Anterior Commissure and the Posterior Commissure. The Talairach Coordinate System is fully determined by a line through the superior edge of the AC and the PC and the interhemispheric, sagittal plane. The origin of the coordinate system is the AC (illustrated in figure C.2). Having identified the locations of the AC, the PC and the edges (superior, inferior, left, right, anterior and posterior) of the brain the transformation into TCS can be performed. These coordinates are rotated until the line joining the AC and PC is along the x axis, and the line joining the left and right markers is parallel to the z axis (see figure C.1).

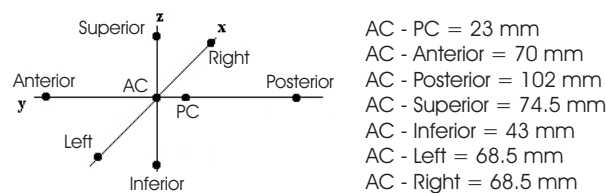


**Figure C.1:** The transformation of an individual brain into Talairach space [Stu97].

### C.2 The MNI Brain

In order to define a brain that is more representative of the population than the single brain used by Talairach and Tournoux, members of the Montreal Neurological Institute did a large number of MRI scans on normal subjects. Every brain was linearly matched to the Talairach brain with the help of 9 parameters (3 translations, 3 rotations and 3 zooms). Thus two averaged brains were created, one from 305 and one from 152 individuals. SPM99 uses the 152 average brain as a template.

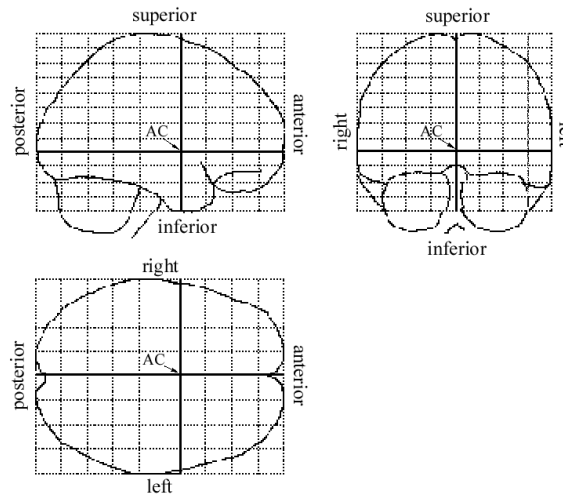


**Figure C.2:** The presentation of the TCS [Stu97].

The MNI linear transformation does not match the brains exactly to the Talairach brain, thus the MNI brain turns out to be slightly larger. The differences increase in the outer parts of the brain and are at maximum in the order of  $10\text{ mm}$ .

It is not possible to do an exact transformation from the MNI to the Talairach brain, thus some approximations have to be done (see [Bre02]). This is unfortunate since the Talairach atlas depicts the designated Brodman's areas. So far there is no published MNI atlas defining Brodman's areas on the MNI brain.

### C.3 Orientation of the Data

There are two relevant conventions for presenting fMRI data: The *radiological* and the *neurological* convention. In the *neurological* convention the activation seen left in the glass brain originates from the left part of the subject's brain. It is the same orientation as the neurologist sees the brain when standing behind a patient during surgery. Since the traditional x-ray image shows the reality mirrored, the activation in the left part of the brain is displayed in *radiological* convention on the right side of the glass brain.

*SPM* utilizes *neurological* convention for raw, realigned, and smoothed data. After the normalization the data follows the *radiological* convention.

## C.4 Results Presented with SPM

Results calculated by *SPM* are typically presented in glass brains representing the MNI coordinate system with a **Maximum Intensity Projection** displayed in three orthogonal planes. Normalized data (see section 3.1.2) does match the glass brain MNI coordinate system only to a certain degree. The more slices there are recorded the better the coordinate system transformation can be performed.

The glass brains from *SPM*'s result section are interactive, i. e. the spatial pointer can be placed on a particular cluster to help locate it in space and extract its coordinates. The red cross in the sagittal section is the origin of the coordinate system. The direction of the axes are illustrated with red, dashed arrows. Additionally, a list of the coordinates of the maximum t-scores in each depicted cluster can be printed e.g. in figure C.4.

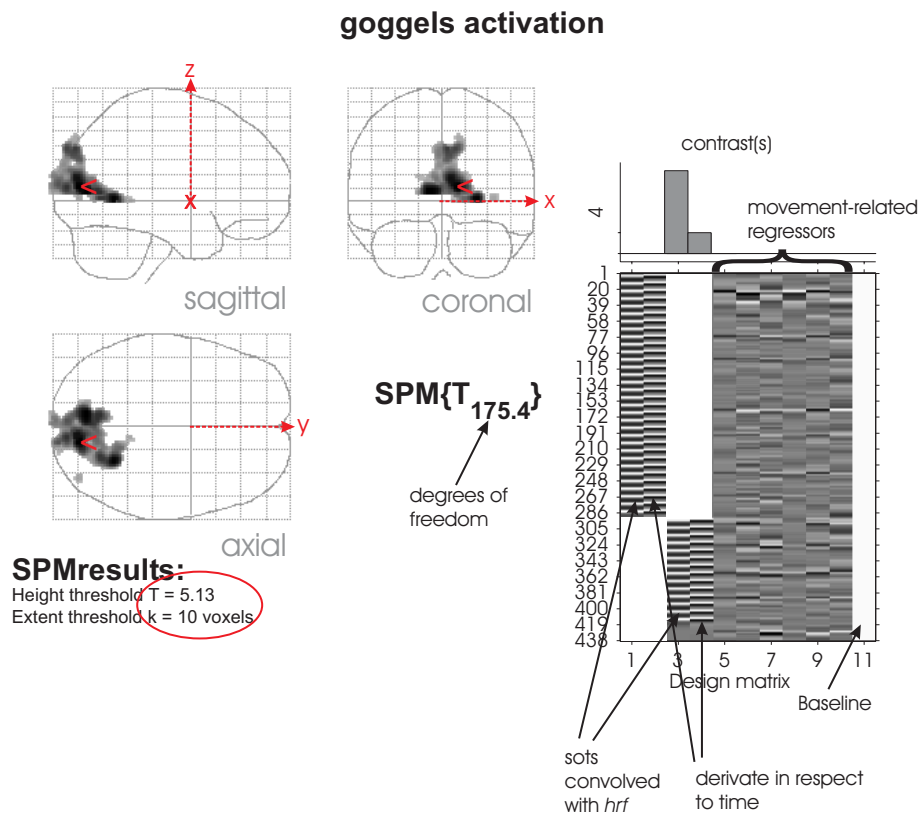


**Figure C.3:** Presentation of t-values for an experiment with flickering goggles stimulation. The data is normalized to the MNI template. The resulting height and extent thresholds values are pointed out with a red circle.

**Statistics: single cluster summary (p-values corrected for entire volume)**

cluster-level			voxel-level				x,y,z {mm}
$p_{corrected}$	$k_E$	$p_{uncorrected}$	$p_{corrected}$	$T$	( $Z_c$ )	$p_{uncorrected}$	
<b>0.000</b>	<b>2047</b>	<b>0.000</b>	<b>0.000</b>	<b>15.61</b>	<b>( Inf)</b>	<b>0.000</b>	<b>12 -80 10</b>
			0.000	15.52	( Inf)	0.000	-8 -76 6
			0.000	15.00	( Inf)	0.000	26 -56 0
			0.000	14.31	( Inf)	0.000	6 -82 16
			0.000	12.67	( Inf)	0.000	-8 -68 6
			0.000	12.37	( Inf)	0.000	8 -90 10
			0.000	12.30	( Inf)	0.000	24 -64 2
			0.000	12.08	( Inf)	0.000	4 -84 38
			0.000	11.55	( Inf)	0.000	10 -90 38
			0.000	10.73	( Inf)	0.000	-4 -90 8
			0.000	10.67	( Inf)	0.000	12 -96 12
			0.000	9.49	( Inf)	0.000	2 -82 6
			0.000	8.92	( Inf)	0.000	-4 -98 16
			0.000	8.75	( Inf)	0.000	-2 -88 36
			0.000	8.61	(7.84)	0.000	-2 -98 12
			0.000	7.69	(7.13)	0.000	-2 -92 26
			0.001	6.16	(5.85)	0.000	8 -44 0
			0.002	5.87	(5.60)	0.000	-10 -102 8
			0.003	5.82	(5.56)	0.000	18 -94 16
			0.008	5.55	(5.32)	0.000	-16 -80 18

table shows all local maxima > 4.0mm apart

Height threshold:  $T = 5.13$ ,  $p = 0.000$  (0.050 corrected)      Degrees of freedom = [1.0, 175.4]  
 Extent threshold:  $k = 10$  voxels,  $p = 0.004$  (0.000 corrected)      Smoothness FWHM = 7.1 7.0 6.6 {mm} = 3.6 3.5 3.3 {voxels}  
 Expected voxels per cluster,  $<k> = 1.042$       Search volume:  $S = 1096000 \text{ mm}^3 = 137000 \text{ voxels} = 3073.2 \text{ resels}$   
 Expected number of clusters,  $<c> = 0.00$       Voxel size: [2.0, 2.0, 2.0] mm (1 resel = 40.80 voxels)

**Figure C.4:** Coordinates of the active clusters with the global maximum (red) and several local maxima (black).

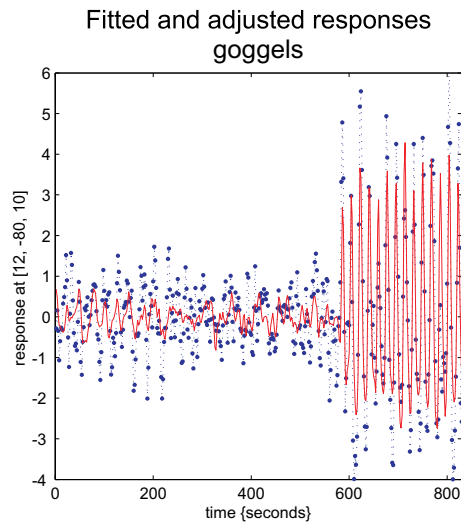


**Figure C.5:** Plot of the fitted and adjusted response (red line) and the measured time course (dashed line) for a highly significant voxel ( $T=15.61$ ) in VI (12,-80,10).

## C.5 Brain Maps of Tactile Activation

The t-values that have been determined by *SPM* can as well be rendered on a structural, high-resolution scan of the subject. For this the localization of the activation, which is stored in the

xCon.mat file, is overlaid with a coregistered  $T_2$  weighted fMRI image. The results can be thresholded in the same way as for presentation in the glass brain. Here the applied thresholds are  $p_{corr} = 0.05$  and  $k = 10$  vx. The morphological image can be presented in numerous slices or by six different views of the 3-dimensional, reconstructed brain. For the slices sagittal, coronal and axial orientation as well as the distance between each slice can be chosen.

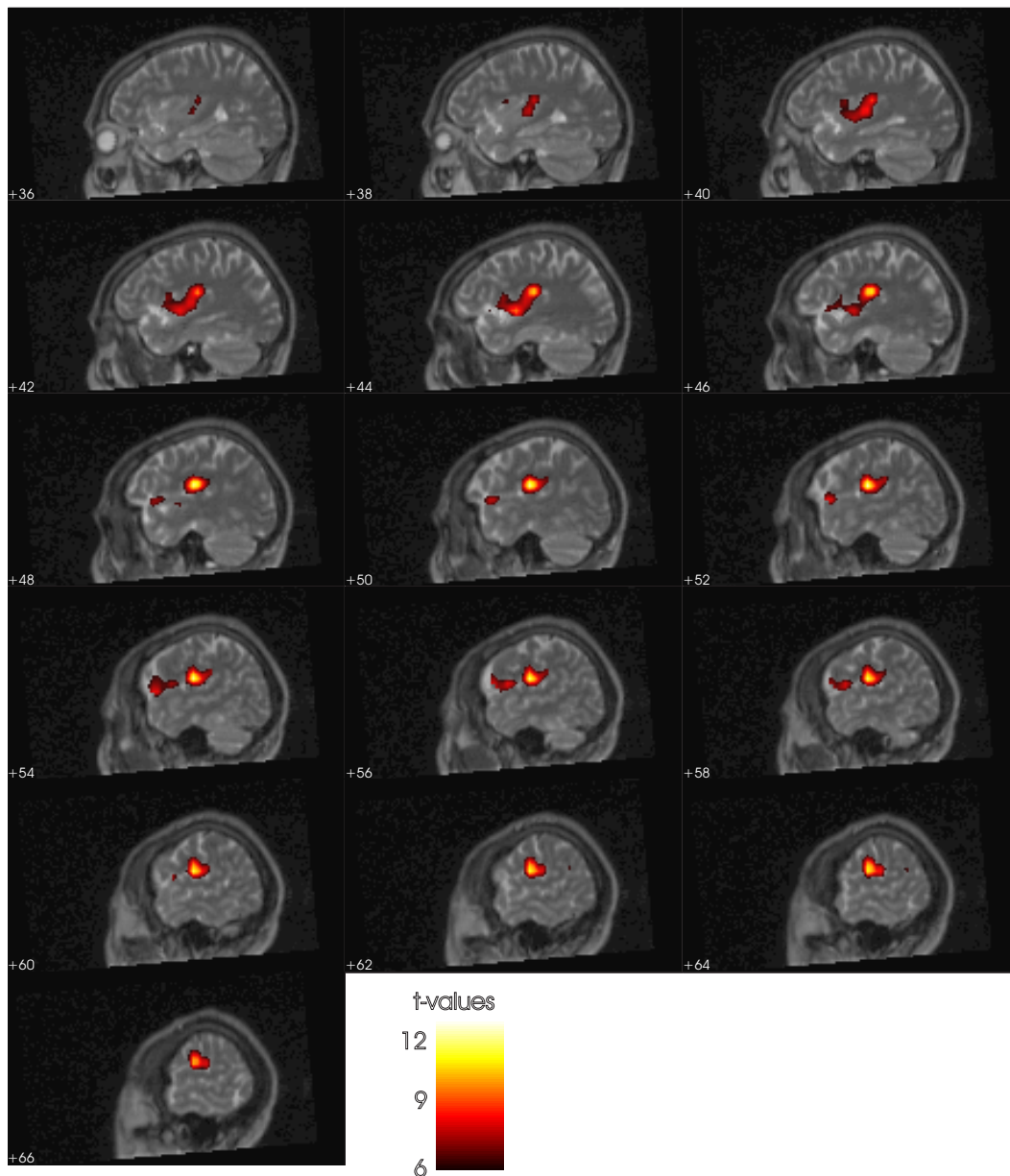


**Figure C.6:** Sagittal slices of the structural scan of *mauth* (right hemisphere) with superimposed SPM{t}s weighting the tactile stimulation (*parametric* session). The slices are separated by 2 mm each, the number on the scan denotes the x coordinate, which is as well the distance to the middle slice in millimeters.

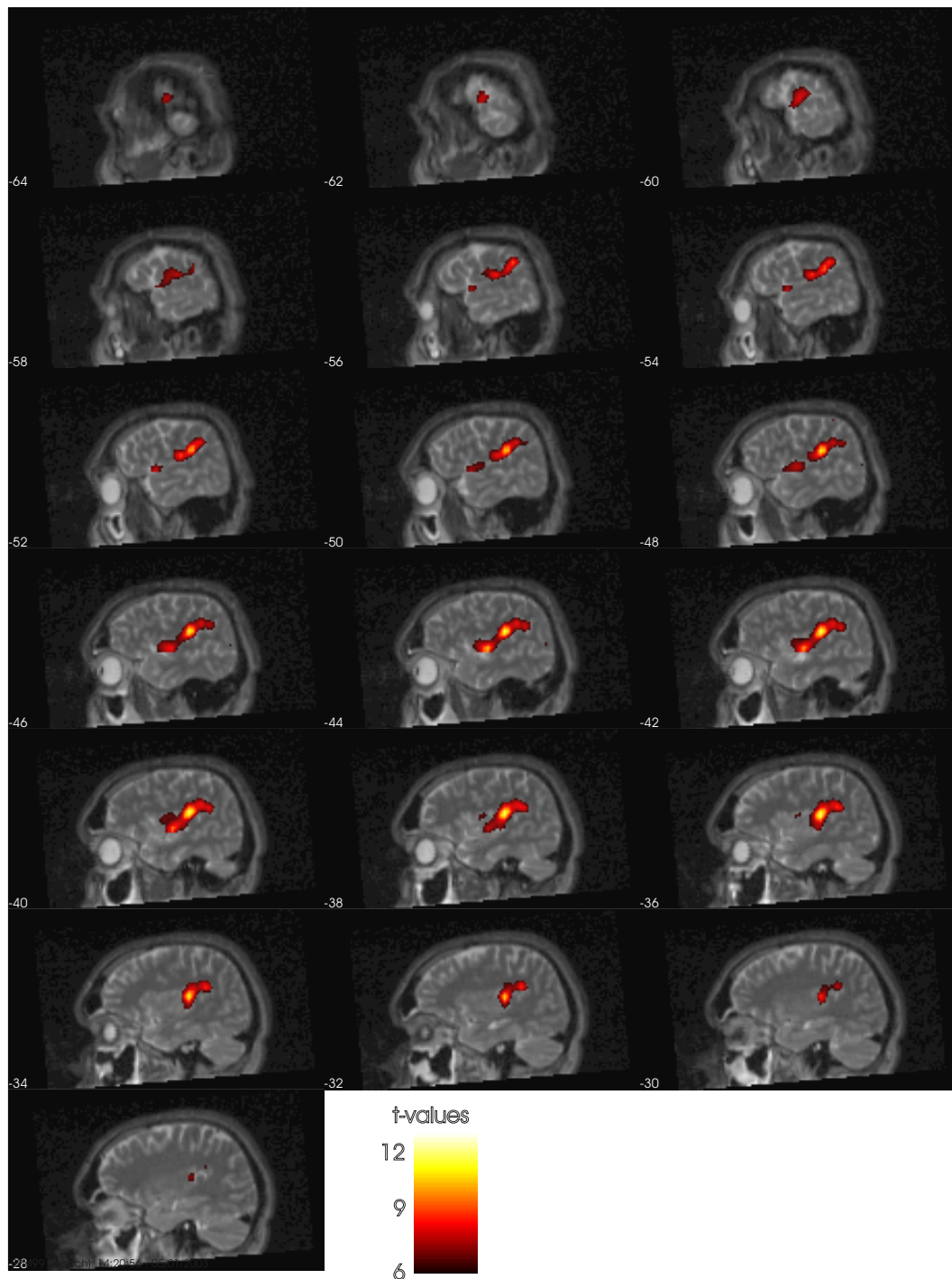


**Figure C.7:** Sagittal slices of the structural scan of *mauth* (left hemisphere) with superimposed SPM{t}s weighting the tactile stimulation (*parametric* session). The slices are separated by 2 mm each, the number on the scan denotes the x coordinate, which is as well the distance to the middle slice in millimeters.

# Appendix D

## Technical Drawings

### D.1 Technical Drawing of the Prisms

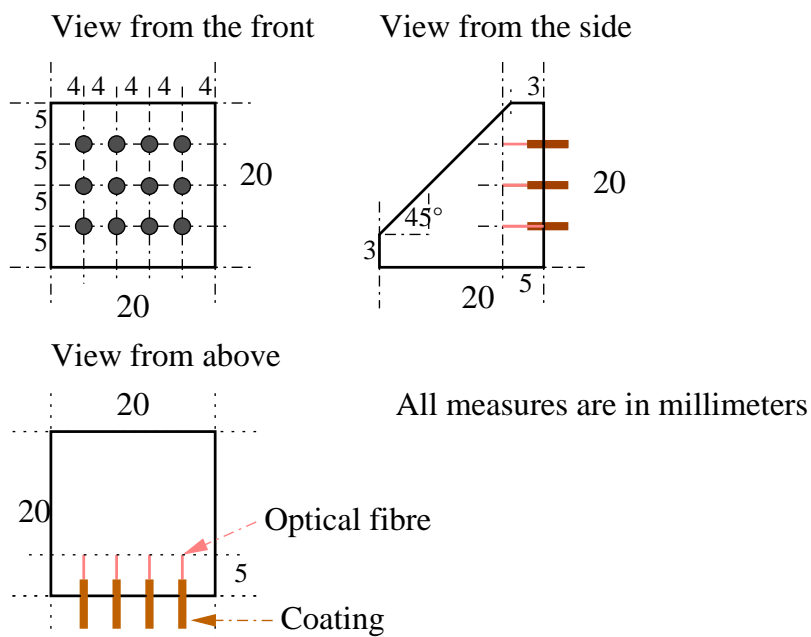


**Figure D.1:** Technical drawing provided for mechanical production.

## D.2 Circuit Diagram of Helper Electronics Added to the TIOTU

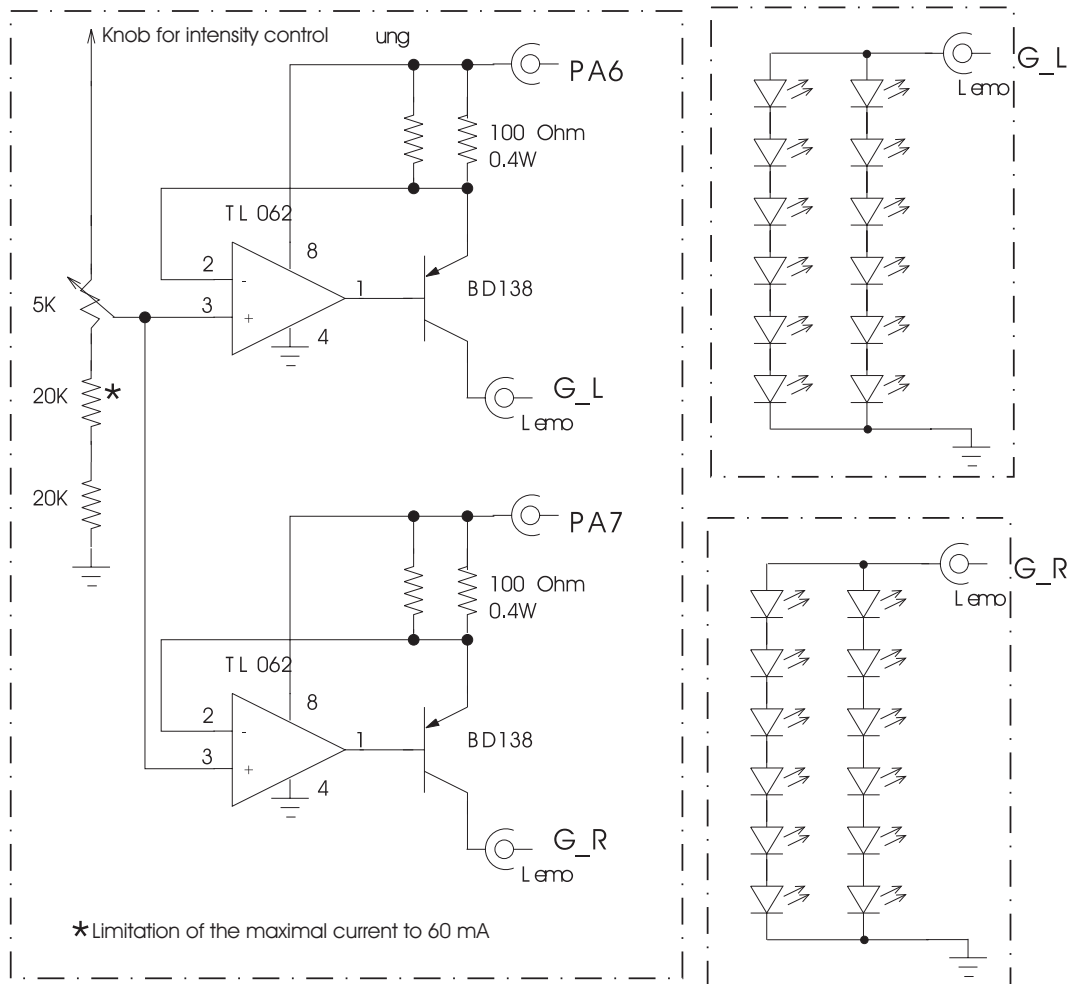


**Figure D.2:** Schematic diagram of the amplifying part of the goggles system.



## Appendix E

# Manual for *Quickshot*

TOPICS:

- **Functionality**
- **Easy Handling**
- **Adjustments**
- **Output**
- **Overwrite-security**
- **Preprocessing**
- **Usual errors sources**

### ★ **Functionality**

The Function of *Quickshot* is to reconstruct, convert and (or) batch the preprocessing of fMRI data which has been acquired with a Bruker system.

### ★ **Easy Handling**

Start Matlab, change into the *Quickshot* directory and type 'main' into the Matlab workspace.

The first question: How many subjects do you want to work on?

-Answer: A single number (in integer).

→ If you have several sessions, and you want them realigned separately, you have to announce them as different subjects.

Second question: How many sessions per subject?

-Answer: A single number (in integer).

→ Sessions will roughly be aligned to the first scan of the first session.

Example: If you have two subjects and three sessions per subject, there are two possibilities to announce them:

- Realign them separately: answer '6', '1'
- Align sessions together: answer '2', '3'

The script asks you to select a directory. This is the most important input. you have three possibilities of what to select:

1. you have the raw Bruker files and want to reconstruct, convert and preprocess.
2. you already have the 2dseq file and want to convert and preprocess the data.
3. you have the \*.img and \*.hdr files and just need the preprocessing.

In figure E.1 the numbers are assigned to the directory in the Bruker tree. The *Paravision* software of the fMRI system creates one main directory for each run.

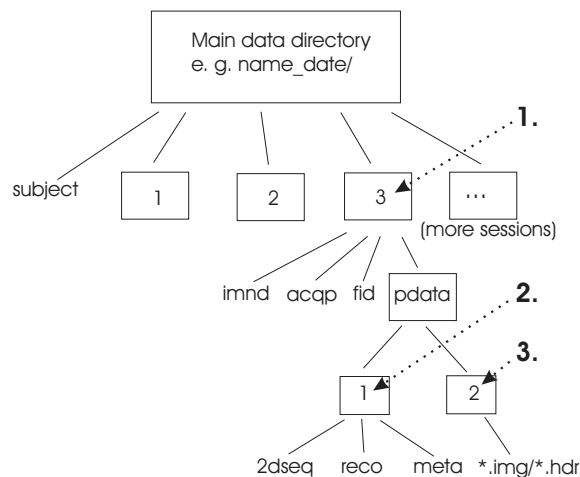


**Figure E.1:** Data format tree by Bruker with 3 directories marked for possible selection in *Quickshot*.

These are the resulting actions:

1. If you select the '3' directory, this means the 'maindatadir/3/' directory. The script will try to reconstruct the data from Bruker to *Analyze* format with the *Freco* program. That means it will write a 2dseq file in the directory under 'pdata/1' and directly go on with reading the Bruker parameter, from the acqp and imnd file. It will convert the 2dseq file in \*.img and \*.hdr files because *SPM* needs 3-dimensional files with one \*.img and \*.hdr per scan. In the last step the script launches spm\_bch to realign and normalise all files.
2. you already have the 2dseq file and want to convert and preprocess the data. Then you select the '1' directory, that means the 'maindatadir/3/pdata/1/' directory. The script will check whether the 2dseq file already exists. In this case the scripts skips the reconstruction, but does the rest (conversion and realignment).
3. If you select the '2' directory, this means the 'maindatadir/3/pdata/2/' directory. Then the script will check if the \*.img and \*.hdr files already exist. The scripts skips the reconstruction, but does the preprocessing.

Next step:

A window with three input boxes appears:

1. Do you want to overwrite any already existing data?

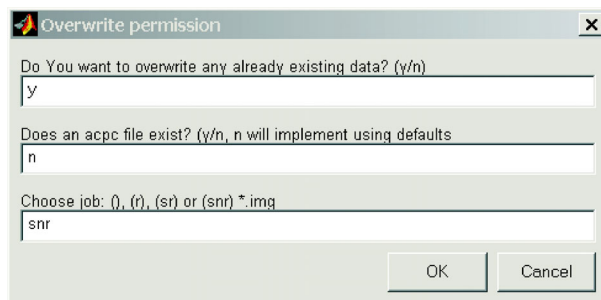


**Figure E.2:** Input box in the beginning of *Quickshot*. After pressing 'OK' the processing starts immediately.

2. Does an acpc file exist?
3. Choose job: There are following possibilities: '', 'r', 'sr', 'snr'.

These are the resulting actions:

1. If you type 'n' you will be asked before each following operation again.  
Typing 'y' allows the program to overwrite old data, but only as long as you have the owner rights of these directories. In case somebody else copied the files for you it will quit with an error message.
2. When answering 'y' *Quickshot* will search the file in './pdata/1/' and take the coordinates for the AC from this file. A typical acpc is shown below.
3. Choosing '' will stop *Quickshot* after writing the 2dseq\*.img. For selecting 'r', 'sr' or 'snr' *Quickshot* will continue until the desired images are required. For snr\*.img the r\*.img are written as well.

A typical acpc:

---

```
Position de la commissure anterieure
CX= 34
CY= 32
CZ= 9
```

---

#### ★ Adjustments

There are pathnames in the program that have to be adjusted to the current PC and directory tree: First of all *Freco* is started. This program should be implemented in '/usr/local/bin', otherwise the *Freco* pathname in line 10 of 'main.m' has to be changed. All the other Matlab scripts are in one directory given the global parameter 'batchdir'. This is the directory where you have copied the scripts of *Quickshot*. It is usually named 'quickshot'.

When getting your own copy of *Quickshot*, you need the following scripts:

- defaults.m

- read\_brukertre.m
- conv2spm(l/b).m
- preproc\_sm.m
- preproc\_rea.m
- preproc\_nor.m
- start\_dir.m
- smoothie.m
- main.m
- realignetre.m
- normalisetre.m
- /ps\_files/

Change the parameter 'batchdir' in the main.m file to the current path of *Quickshot*.

#### ★ Output

The script saves the parameter which have been read from the Bruker file in a file called IRMf\_pars. The file is written in the same directory as the 2dseq (path: '.../3/pdata/1'). During the preprocessing stat.mat, real.mat and norm.mat files will be stored in 'batchdir' containing the parameters of the realignment, normalization and smoothing. The preprocessing writes as usual an spm99.ps into the 'ps\_files'. The file is given an individual name derived from the path and name of the selected file. As it is common for *SPM*, \*.mat, r\*, sr\* or snr\* files are written into the \*.img directory, the directory where the unprocessed files are.

#### ★ Overwrite-security

The script does search after already existing data before the reconstruction and conversion. After the preprocessing no further checks are made. The work\_dir is the 'batchdir'.

Before the reconstruction *Quickshot* tests if the 2dsec already exists. Before the conversion of 2dsec into \*.img files the script only checks if the directory '2' already exists.

#### ★ Preprocessing

you should always check if the settings are the right ones. Here are the current settings:

```
realign = struct(...
'subject_nb', nsubs, ...
'num_sessions', nsess, ...
'sessions', [1:nsubs], ...
'option', 3, ...
'modality', 1, ...
'reslice_method', -9, ...
'create', 3, ...
'mask', 1, ...
'adjust_sampling_errors', 0);
```

```

Normalisation = struct( ...
'defaults', 1, ...
'estimates', 1, ...
'custom_estimates', ones(1,12), ...
'custom_norm', 1, ...
'nonlin_func_nb', 2, ...
'func_nb', 0, ...
'nonlin_ite_nb', 1, ...
'nonlin_regular', 0.001, ...
'mask_brain', 0, ...
'mask_object_brain', 0, ...
'bounding_box', 1, ...
'vexel_sizes', -1 ...);

```

```

Smooth = struct(
'FWHM', [8 8 8]...);

```

#### ★ Usual error sources

- The program is dependent on the Bruker data tree (see figure E.1) and the Bruker file names. you will get troubles if you copied single files and thus did not maintain the directory hierarchy. Or if non standard directory hierarchy is used.
- The program searches for a minimum of ten files with an `img` ending in `' / . . . /pdata/2 '` to test if the data is reasonable data. If you want to work with less files you will have to adjust the code in `main.m`.
- If you do not have write permission in the directory of the raw data and `'batchdir'` *Quickshot* will interrupt.
- Last but not least: There is one known bug in *Quickshot*, which still has to be fixed. When changing computer platform between reconstruction and conversion the converted images will show nothing but noisy gray. In the current version there are three variants of the `conv2spm.m` script provided: `conv2spm1.m`, `conv2spmb.m` and `conv2spm.m`. *Quickshot* will always work with `conv2spm.m`, so if the images are noisy test using little endian by changing the name of `conv2spm1.m` to `conv2spm.m` (or with big endian by changing the name of `conv2spmb.m` to `conv2spm.m`). One of them will work properly.

# List of Figures

1.1	Histological section through the human's glabrous and hairy skin . . . . .	3
1.2	Illustration of the afferent system . . . . .	4
1.3	The optical pathways . . . . .	4
1.4	Projection of the visual world onto the retina . . . . .	5
1.5	The division of the cerebral cortex into four lobes . . . . .	6
1.6	Illustration of the sensory primary areas in the cortex . . . . .	6
1.7	Functional organization of the somatosensory cortex with Brodman areas enlarged . . . . .	7
1.8	Medial slice through the human brain . . . . .	8
1.9	Functional organization of the somatosensory cortex . . . . .	9
2.1	Schematic drawing of the fMRI system . . . . .	10
2.2	The spontaneous decay of the magnetization signal . . . . .	11
2.3	The signal of a spin-echo sequence . . . . .	12
2.4	Time scheme of an spin-echo sequence. . . . .	12
2.5	Time scheme of an EPI sequence . . . . .	13
2.6	Zoom into the time scheme of an EPI sequence . . . . .	13
2.7	Typical power spectrum of an fMRI image with noise only . . . . .	14
2.8	Examples for the effect of the Nyquist ghost on phantom images . . . . .	14
2.9	The template of the <i>hrf</i> within <i>SPM</i> . . . . .	15
2.10	Data from an activated volume element overlaid with the <i>SPM</i> template . . . . .	16
3.1	Visual illustration of the motion correction with <i>SPM</i> . . . . .	19
3.2	Plot of the fitted and adjusted response for a highly significant voxel . . . . .	21
4.1	Picture of a flat version of the <i>PTD</i> . . . . .	24
4.2	Schematic drawing of two modules of the <i>PTD</i> . . . . .	25
4.3	Photo of an experimental set-up with goggles . . . . .	25
4.4	The fully equipped goggles system . . . . .	26
4.5	Photo of the interconnection between fibres, prism and goggles . . . . .	27
4.6	Data tree for storage of fMRI data and settings by Bruker . . . . .	28
4.7	Comparison of the fMRI data handling without versus with <i>Quickshot</i> . . . . .	29
5.1	The fMRI in Strassbourg during an experiment with a volunteer. . . . .	31
5.2	A subject fully equipped for an experiment . . . . .	32
5.3	Schematic drawing of the stimulation timing versus hemodynamic response . . . . .	34
5.4	Pattern displayed by the <i>PTD</i> . . . . .	34
5.5	Illustration of design of the first session . . . . .	35

5.6	Parameter estimates of an F-test at an highly significant voxel in SI . . . . .	37
5.7	Design matrix and contrasts for the two sessions . . . . .	38
6.1	SPM{t}s showing visual activation for six different subjects in first session . . .	43
6.2	SPM{t}s showing tactile activation for six different subjects in first session. . . .	44
6.3	SPM{t}s showing tactile activation for six different subjects in second session . .	45
6.4	Sagittal slices of the structural scan of <i>mauth</i> showing activation induced by visual stimulation . . . . .	46
6.5	Coronal and sagittal slices of the structural scan of <i>mauth</i> showing activation induced by tactile stimulation . . . . .	47
6.6	Axial slices of the structural scan of <i>mauth</i> showing activation induced by tactile stimulation . . . . .	48
6.7	MIPs for the second session with <i>kelge</i> contrasting different <i>parametric</i> orders . .	51
6.8	MIPs of <i>mauth</i> induced by varying <i>PTD</i> vibration frequency . . . . .	52
6.9	Two time courses of voxels that <i>SPM</i> identified as significant . . . . .	53
6.10	Averaged Fourier transformation in an active cluster of SI for <i>kelge</i> . . . . .	54
6.11	Averaged Fourier transformation in an active cluster of V1 for <i>kelge</i> . . . . .	54
6.12	Fourier transformation of an ‘artificially’ created signal . . . . .	55
6.13	Time course of noise voxel and according Fourier spectrum . . . . .	55
6.14	Histogram of 330 noise voxels. . . . .	56
6.15	High pass filtered signal and fitted curve . . . . .	58
6.16	Interpolation of high pass filtered signal with fitted curve and the Fourier spectrum for the fitted curve . . . . .	59
6.17	Fourier spectra of three clusters of <i>lemla</i> . . . . .	60
6.18	Plot of ratio of Fourier coefficients . . . . .	62
6.19	Histogram of the Fourier spectrum of a noise voxel . . . . .	63
B.1	The map of <i>Brodman areas</i> . . . . .	69
B.2	Expressions for directions in the mouse and the human brain . . . . .	70
B.3	The three planes slicing the human brain for data-presentation . . . . .	70
B.4	Pictures of slices through the brain in three different orientations . . . . .	70
B.5	Lateral surface of cerebral hemisphere with brain stem and part of spinal cord . .	71
C.1	Coordinate transformation of an individual brain into Talairach space . . . . .	72
C.2	The presentation of the Talairach Coordinate System . . . . .	73
C.3	Presentation of t-values for an experiment with flickering goggles stimulation . .	74
C.4	Coordinates of the active clusters with global and local maxima . . . . .	75
C.5	Plot of the fitted and adjusted response . . . . .	75
C.6	Sagittal slices of the structural scan of <i>mauth</i> (right hemisphere) showing tactile stimulation . . . . .	76
C.7	Sagittal slices of the structural scan of <i>mauth</i> (left hemisphere) showing tactile stimulation . . . . .	77
D.1	Technical drawing provided for mechanical production . . . . .	78
D.2	Schematic diagram of the amplifying part of the goggles system . . . . .	79
D.3	Circuit diagram for the construction of the <i>TIOTU</i> . . . . .	80

E.1	Data format tree by Bruker . . . . .	82
E.2	Input box in the beginning of <i>Quickshot</i> . . . . .	83

# List of Abbreviations

<b>fMRI</b>	functional Magnetic Resonance Imaging
<b>PET</b>	Positron Emission Tomography
<b>TVSS</b>	Tactile Vision Substitution System
<b>TVSSCS</b>	Tactile Vision Substitution System Control Software
<b>SenSub</b>	Sensory Substitution (name of EU-project)
<b>VTD</b>	Virtual Tactile Display
<b>PTD</b>	Pneumatic Tactile Display
<b>PSVA</b>	Prosthesis for Substitution of Vision by Audition
<b>LGN</b>	Lateral Geniculate Nucleus
<b>MRI</b>	Magnetic Resonance Imaging
<b>SNR</b>	Signal to Noise Ratio
<b>EPI</b>	Echo Planar Imaging
<b>EPI</b>	Electronic Pneumatic Interface
<b>BOLD</b>	Blood Oxygenating Level Dependant
<b>hrf</b>	hemodynamic response function
<b>SPM</b>	Statistical Parametric Mapping
<b>AC</b>	Anterior Commissure
<b>PC</b>	Posterior Commissure
<b>GLM</b>	General Linear Model
<b>SOTs</b>	Stimulus Onsets
<b>TIOTU</b>	Trigger Input/Output Transforming Unit
<b>ROI</b>	Region Of Interest
<b>MIP</b>	Maximum Intensity Projection
<b>FID</b>	Free Induction Decay



# Bibliography

- [And01] Timothy Andrews. Binocular rivalry and visual awareness. *Trends in Cognitive Science*, 5(10):407–410, 2001.
- [AZE97] G. Aguirre, E. Zarahn, and Mark D. Esposito. The variability of human, bold hemodynamic responses. *NeuroImage*, 8:360–369, 1997.
- [BBD00] Peter Bandettini, Rasmus Birn, and Kathleen Donahue. Background, methodology, limits and implementation. In *Handbook of Psychophysiology*, chapter 36, pages 978–1007. Cambridge University Press, 2nd edition, 2000.
- [Bod00] Anna Bodegard. Object shape differences reflecting by somatosensory cortical activation in human. *The Journal of Neuroscience*, 20(RC51):1–5, 2000.
- [Bre02] Mathew Brett. Medical research council - cognition and brain science unit - imaging. <http://www.mrc-cbu.cam.ac.uk/Imaging>, 2002.
- [BS99] M.A. Brown and R.C. Semelka. *MRI Principles and Applications*. Wiley-Liss, New York, 1999.
- [BS01] Frank Bremmer and Anja Schlack. Polymodal motion processing in posterior parietal and premotor cortex. *Neuron*, 29:287–, 2001.
- [BZH<sup>+</sup>99] P. Belin, R. J. Zatorre, R. Hoge, B. Pike, and A. C. Evans. event-related fmri of the auditory cortex. *NeuroImage*, 10:417–429, 1999.
- [CB02] Mark S. Cohen and Susan Y. Bookheimer. Functional magnetic resonance imaging. <http://fmri.ucsd.edu/fmri/FMRI-TINS.html>, 2002.
- [CDR02] B. J. Casey, Mathew Davidson, and Bruce Rosen. Functional magnetic resonance imaging: Basic principles of and applications to developmental science. *Developmental Science*, 5(3):301 – 309, 2002.
- [Chr00] Kalina Christoff. Lectures for neuroanatomy. <http://www-psych.stanford.edu/~kalina/BB/>, 2000.
- [CTAV98] C. Capelle, C. Trullemans, P. Arno, and C. Veraart. A real-time experimental prototype for enhancement of vision rehabilitation using auditory substitution. *IEEE Trans. Biom. Eng.*, 45, 1998.
- [Dal99] Anders M. Dale. Optimal experimental design for event-related fmri. *Human Brain Mapping*, 8:109–114, 1999.

- [DJK<sup>+</sup>02] J. R. Duann, T. P. Jung, W. J. Kuo, T. C. Yeh, S. Makeig, J. C. Hsieh, and T. J. Sejnowski. Measuring the variability of event-related bold signal. *NeuroImage*, 15(4):823–835, 2002.
- [DRK00] Eliyabeth Disbrow, Tim Roberts, and Leah Krubitzer. Somatotopic organization of cortical fields in the lateral sulcus of homo sapiens: Evidence for sII and pV. *The Journal of Comparative Neurology*, 418:1–21, 2000.
- [EZAR99] Mark D. Esposito, E. Zarahn, G. Aguirre, and B. Rypma. The effect of normal aging on the coupling of neural activity to the hemodynamic response. *NeuroImage*, 10:6–14, 1999.
- [FFF<sup>+</sup>97] K. Friston, R. Frackowiak, C. Frith, R. Dolan, and J. Mazziotta. *Human Brain Function*. Academic Press, 1997.
- [FFTF95] K. Friston, K. Frith, R. Turner, and R. S. J. Frackowiak. Characterizing evoked hemodynamics with fmri. *NeuroImage*, 2:157–165, 1995.
- [Fou02] American Health Assistance Foundation. Brain anatomy. <http://www.ahaf.org/alzdis/about/AnatomyBrain.htm>, 2002.
- [FR86] P. T. Fox and M. E. Raichle. Focal physiological uncoupling of cerebral blood flow and oxidative metabolism during somatosensory stimulation in human subjects. *Proc. National Academic Science U S A*, 83(4):1140–1144, 1986.
- [FWF<sup>+</sup>94] K. Friston, K. Worsley, R. Frackowiak, J. Mazziotta, and C. Evans. Assessing the significance of focal activation using their spatial extent. *Human Brain Mapping*, 1:219–220, 1994.
- [FWR<sup>+</sup>96] K. Friston, S. R. Williams, R. Howard, R. Turner, and R. S. J. Frackowiak. Movement-related effects in fmri time-series. *Magnetic Resonance in Medicine*, 35:346–355, 1996.
- [GNM02] Bradley Goodyear, David Nicolle, and Ravi Menon. High resolution fmri of ocular dominance columns within the visual cortex of human amblyopes. *Strabismus*, 10:129–136, 2002.
- [GS02] William Germann and Cindy Stanfield. *Principles of human physiology*. San Francisco: Benjamin Cummings, 2002.
- [HD01] Gregory S. Harrington and J. Hunter Downs. Fmri mapping of the somatosensory cortex with vibrational stimuli. is there a dependence on stimulus frequency? *Brain Research*, 897:188–192, 2001.
- [HJ02] Richard Henson and Oliver Josephs. Spoken cued-recall during event-related fmri. NeuroImage Human Brain Mapping Meeting, poster No. 10312, 2002.
- [Hor02] J.P. Hornak. The basics of mri, rochester. <http://www.cis.rit.edu/htbooks/mri/inside.htm>, 2002.

- [Ing00] John E. Ingeholm. The helix: an automated mri compatible tactile stimulator. Poster, 2000.
- [JH99] O. Josephs and R. N. H. Henson. Event-related functional magnetic resonance imaging: modelling, inference and optimization. *Phil. Trans. R. Soc. Lond.*, 354:1215–1228, 1999.
- [JM99] R.S. Patel J.A. Maldjian, A. Gottschalk. Mapping of secondary somatosensory activation induced by vibrational stimulation: an fmri study. *Brain Research*, 824:291–295, 1999.
- [JN95] J.B. Angevine J. Nolte. *The Human Brain in Photographs and Diagrams*. Mosby, St. Louis, 1995.
- [Kan91] E.R. Kandel. *Principles of Neural Science*. Prentice Hall International, London, fourth edition, 1991.
- [LHW75] LeVay, Hubel, and Wiesel. The patterns of ocular dominance columns in macaque visual cortex revealed by a reduced silver stain. *J. Comp. Neurol.*, 159:559–575, 1975.
- [Mar96] J. H. Martin. *Neuroanatomy*. Appleton & Lange, 2nd edition, 1996.
- [Mauet] Thorsten Maucher. *Aufbau und Test eines Taktilen Seh-Ersatzsystems*. PhD thesis, Kirchhoff Institute of Physics, Not published yet.
- [MHA<sup>+</sup>00] D. McGonigle, A. Howseman, B. Athwal, K. Friston, R. S. J. Frackowiak, and A. Holmes. Variability in fmri: an examination of intersession differences. *NeuroImage*, 11(1):708–734, 2000.
- [MJ98] McKeown and M. J. Jung. Spatially independent activity patterns in functional mri data during the stroop color-naming task. *Proc. National Academic Science USA*, 95:803–810, 1998.
- [MMO<sup>+</sup>00] F. M. Miezin, L. Maccotta, J. M. Ollinger, S. E. Petersen, and R. L. Buckner. Characterizing the hemodynamic response: Effects of presentation rate, sampling procedure, and the possibility of ordering brain activity based on relative timing. *NeuroImage*, 11(1):735–759, 2000.
- [MMS00] Thorsten Maucher, Karlheinz Meier, and Johannes Schemmel. The heidelberg tactile vision substitution system. In *Proceeding of the sixth International Conference on Tactile Aids, Hearing Aids and Cochlear Implants (ISAC2000)*, 2000.
- [MMS01] Thorsten Maucher, Karlheinz Meier, and Johannes Schemmel. An interactive tactile graphics display. In I. Kamisian M. Deriche, N. Shaikh-Husin, editor, *The Sixth International Symposium on Signal Processing and its Applications (ISSAP2001)*, 2001.
- [Mol97] Diana Weedman Molavi. Neuroscience tutorial. <http://thalamus.wustl.edu/course/basvis.html>, 1997.

- [MS91] Moeller and Strohter. A regional covariance approach to the analysis of functional pattern in positron emission tomography data. *J. Cereb. Blood Flow Metab*, 11:121–135, 1991.
- [Nyq28] H. Nyquist. Thermal agitation of electric charge in conductors. *Physical Review*, 32:110–113, 1928.
- [OLC<sup>+</sup>01] Bahadir Ozus, Ho-Ling Liu, Lin Chen, Meenakshi Iyer, Peter Fox, and Jia-Hong Gao. Rate dependence of visual human cortical response due to brief stimulation: An event-related fmri study. *Magnetic Resonance Imaging*, 19, 2001.
- [Pre86] W. H. Press. *Numerical Recipes*. Cambridge University Press, 1986.
- [RK82] A. Rosenfeld and A. C. Kak. *Digital Picture Processing II*. Academic Press, Orlando, 1982.
- [Run00] Stefanie Runde. Design and analysis of fmri experiments probing brain activity induced by tactile stimulation. Master’s thesis, Kirchhoff Institute of Physics, 2000.
- [Sho] Jamie Shorey. Foundations of fmri. <http://www.ee.duke.edu/~jshorey/MRIHomepage/fmri.html>.
- [ST87] R.F. Schmidt and G. Thews. *Physiologie des Menschen*. Springer-Verlag, 23. edition, 1987.
- [Str00] Bryan Strange. *Imaging the Functions of Human Hippocampus*. PhD thesis, Institute of Cognitive Neuroscience, 2000.
- [Stu97] Clare Stuart. *Functional MRI : Methods and Applications*. PhD thesis, University of Nottingham, 1997.
- [TM41] S. A. Talbot and W. H. Marshall. Physiological studies on neural mechanisms of visual localization and discrimination. *Am. J. Ophthalmol.*, 24:1255–1263, 1941.
- [TT88] J. Talairach and P. Tournoux. *Co-planar stereotaxis atlas of the human brain*. Thieme, 1988.
- [Wri02] Graham Wright. Mri in heart and circulation. <http://www.sunnybrook.utoronto.ca>, 2002.
- [ZBR<sup>+</sup>99] Michael Zigmond, Floyd Bloom, James Roberts, Story Landis, and Larry Squire. *fundamental Neuroscience*. Academic Press, 1999.

# Acknowledgements

I would like to express my gratitude to the following people for their support and assistance, because without, this work had not been possible neither as instructive and interesting.

Prof. Dr. K. Meier for supporting the project into ventured directions and asking the decisive questions.

Dr. C. Scheiber for many fruitful discussions and giving me a great working atmosphere in Strassbourg.

Prof. Dr. R. Fink for taking on the part of second referee.

Thorsten for great teamwork, being a patient help at any time of the day or week, and for his good humor throughout the year.

Felix for his very helpful proof-reading.

Dominik for his patient introduction into Mathematica and help with the time-consuming programming.

All members of the Electronic Vision(s) Group for their interest in the project and the good vibes within the group.

Martin for giving me strength and patience, and even in hard times bringing out the best in me.

My family for supporting whatever crazy idea I can think of.

The financial support of the European community is gratefully acknowledged.